Project name:
Integration and exploitation of networked Solar radiation Databases for environment monitoring
Project acronym:
SoDa
Contract number:
IST-1999-12245

Deliverable title:
Heliosat version 2
Deliverable number:
D3.2
Type of deliverable:
Report
Security:
Public
Author:
ENSMP / T&M (Rigollier C., Lefèvre M., Wald L.)
Contributors:

Contractual date of delivery to the Commission:
November 2000
Actual date of delivery to the Commission:
April 2001

1 ABSTRACT

The well-known method Heliosat-I converts observations made by geostationary meteorological satellites into estimates of the global irradiation at ground level. This method was implemented in many places and is routinely used to produce maps.

The method Heliosat-I suffers from several drawbacks, which come from several empirically defined parameters inside the method. These render the accuracy of the estimates very sensitive to their tuning during the implementation phase. By principle, the method cannot cope with changes in spaceborne radiometers, which occur periodically in operational meteorological programmes. Consequently, parameters have to be tuned at each change. Finally, the accuracy of the estimates may be improved.

A new method, called Heliosat-II, is developed to overcome these drawbacks. It is based upon the same physical principles, which have proved their efficiency in the method Heliosat-I as well as in others. To cope with changes in sensors, the inputs to the method are physical quantities, the radiances, instead of the digital counts output from the sensors. This is one of the major thrusts of the development of the method Heliosat-II. Beyond the new capabilities of dealing with very long time-series of observations, it opens the possibilities of using known models of the physical processes in atmospheric optics, thus removing the need for empirically-defined parameters and leading to a better accuracy of the estimates of irradiation.

Eumetsat does not perform calibration of sensors in the visible range on a routine basis for the Meteosat Operational Programme (MOP) series of satellites. Consequently, an operational method has been developed, tested and validated for the calibration of the visible channel of the series of satellites of the Meteosat Operational Programme. It performs on an automatic basis and is well suited for the processing of large volume of data. It is based upon the analysis of the content of the satellite images. Though the development took place within the development of the method Heliosat-II, we succeeded in making it an independent calibration process, which can be used for other purposes. It can likely be used for the calibration of other geostationary satellites having spectral bands similar to Meteosat, such as GOMS, GMS, Insat, and the first GOES series. Some of the methodological developments may be re-used for other sensors working in visible and near infrared bands on polar platforms, since they offer generic aspects.

Daily sets of calibration coefficients are obtained by this method, compared to the monthly or yearly sets of some concurrent methods or to the approximated analytical laws of others. The present work resulted into a time series of daily sets for the years 1985 to 1997, which constitutes a unique database. This database will be necessary for the execution of the method Heliosat-II. Beyond this, efforts were made to disseminate this database to the public (web site: *www-helioserve.cma.fr*). The developed service is unique in the world to our knowledge.

The second step in the development of the method Heliosat-II deals with the model used for modelling the clear-sky irradiation. The better the accuracy of the model, the better the accuracy of the estimate performed by the method Heliosat. Studies of several clear sky models were performed. Of particular interest are the models of the European Solar Radiation Atlas (ESRA). A published article demonstrates that these models could be used in the framework of the Heliosat method. The additional study performed within the SoDa project

strongly encourages the introduction of the ESRA models in the Heliosat-II method. The accuracies of these models are among the best, and their robustness (*i.e.*, the constancy of their performances with respect to different conditions) are a clear advantage with the aim of producing a robust method. The accuracy (RMSE) in the assessment of the diffuse hourly irradiation ranges from 11 Wh m^{-2} to 35 Wh m^{-2} for diffuse irradiations up to 250 Wh m^{-2}.

Compared to the other models used up to now in the Heliosat method, the accuracy in the ESRA model is mostly gained by the introduction of the Linke turbidity factor. From an operational point of view, the use of the ESRA model implies the knowledge at each pixel of the image, of the Linke turbidity factor and of the ground elevation. The ESRA models have been coded in language C and can be run in the web site Helioserve: *www-helioserve.cma.fr*. In this site, user can already simulate the clear-sky irradiation, given the geographical site, the elevation and the Linke turbidity factor. This service has been used as one of the essential elements for establishing the first prototype of the SoDa intelligent system.

The third step is the accurate assessment of the cloud index and, further, of the quantities ρ_g and ρ^t_{cloud}, which characterise the ground albedo and the cloud albedo. The adopted approach is based upon explicit formulations of the radiance and the transmittance. These formulations make use of the modelling of the clear sky radiation, thus offering a strong consistency. This explicit approach offers several advantages. It removes many empirical parameters, compared to the versions of the method Heliosat-I. It makes use of recognised expressions of the radiance and the transmittance. It permits to use known values of the albedo of specific objects, or to estimate such albedoes. Similarly to the method Heliosat-I, the approach does not behave satisfactorily for sun zenithal angles larger than 75 - 78°. Though applicable, it produces larger errors.

From an operational point of view, these parameterisations of ρ_g and ρ^t_{cloud} request the knowledge of the Linke turbidity factor and the elevation for each pixel of the Meteosat image to be processed. This constraint is not an additional one, since the model of the clear sky irradiation also requests these informations. The good point is that this study demonstrates that the Linke turbidity factor is sufficient to describe the optical state of the clear atmosphere in the broadband of the satellites Meteosat. The gain in operation is important. Only one map of the ground albedo will be necessary, instead of having one map per slot as presently in the most advanced versions of the method Heliosat-I.

The final step of the development deals with the relationship between the cloud index and the hourly global irradiation. The clear sky index is adopted instead of the clearness index. The relationship is modified, especially for the clear skies and for the overcast skies. It reproduces better the observations made by several independent teams. The University of Oldenburg adopted this model in their current version of the method Heliosat-I. Compared to the standard method Heliosat-I, it provides better results.

The new method Heliosat-II is applied to a limited number of Meteosat images, namely for the months of January 1995, April 1995 and July 1994. Measurements performed by thirty-five meteorological stations are used to assess the performances of the new method. The computed quantities are hourly irradiation, daily irradiation, monthly mean of hourly irradiation, monthly mean of daily irradiation, 5-days irradiation and 10-days irradiation. The results are very good, compared to objectives. The accuracy observed by comparison with

ground measurements is better than the targets set up before the development. The correlation coefficient is high in all cases. For the hourly and daily irradiation, it is possible to remove the constraint on the sun zenithal angle if necessary, still keeping an acceptable accuracy. Removing this constraint, or decreasing the threshold, leads to a larger number of estimates, which may be useful.

The same comparison is performed but using images in B2 format instead of high resolution images. These B2 images are very useful to construct climatological databases. The results are good, compared to objectives. The accuracy observed by comparison with ground measurements is better than or close to, the targets set up before the development. The correlation coefficient is high in all cases. The method Heliosat-II may apply to the images in B2 format with a satisfactory accuracy, thus opening new avenues in the climatology of the solar radiation. The B2 images may even be used to assess the hourly irradiation. However, given the poor sampling in time of these images, it may be recommended to limit their use to the assessment of daily irradiation or to the irradiation for larger periods.

The method Heliosat-II meets the objectives set up before its development. It is more physically sound than the previous one. It also presents results that are more accurate. All parameters that needed to be tuned for each implementation of the method Heliosat-I have been removed, set up to constant values, or automatically determined. The method Heliosat-II has the capabilities to process any type of data from geostationary meteorological satellites, including large time-series of images taken by different sensors. It is applicable in real-time or on archives of images, whatever their resolution. By suppressing empirically defined parameters, the implementation is the same for all cases. It facilitates exchange of knowledge and further collective improvements of the method Heliosat-II. One may use now a single map of apparent ground albedo instead of having one per slot processed, which may amount to 18 maps for high latitudes in summer for assessing hourly irradiation and 36 in the case of half-hourly irradiation.

The method Heliosat-II may be improved in several points. Of particular interest are a better modelling of the physical processes occurring at large sun zenithal angles and the identification of superimposed cloud layers with the accurate modelling of their effects in the relationship between the clear sky index and the cloud index. The snow covering periodically the ground as well as permanent cloud coverage over a site creates problems in preventing from accurate determining the apparent ground albedo. The method Heliosat-II, as well as all other known methods, cannot perform accurately in areas where the scales of variability of the irradiation are smaller than 2-5 times the size of the pixel. This holds for the mountainous areas, for example. The Swiss meteorological office uses a combination of Heliosat estimates and a dense network of ground measurements for the valleys in the Alps.

The gains in accuracy obtained are not coming from an increase of the dimensionality of the inputs originating from the satellite images, which remain the same. They come from external knowledge, that is the elevation and the Linke turbidity factor for each pixel of the area to process and some properties of the sensor for the day under concern. Thus, the implementation of the method Heliosat-II requests such knowledge.

There is presently no operational implementation of the complete method Heliosat-II. The creation of long time-series of daily irradiation is under discussion within the Consortium.

Beyond this, the development of the method Heliosat-II benefits to the project SoDa in several important aspects:

- Assessing the clear-sky models presently used by the partners Meteotest, EHF and ENTPE and those available through the commercial products ESRA and MeteoNorm,
- Developing a library in language C for the ESRA clear sky models,
- Creating a simulation tool launchable by the means of a standard web browser that simulates the hourly and daily irradiations under clear sky,
- Improving the method for satellite image processing in operational use at the EHF (University of Oldenburg)

Though the development of the method Heliosat-II was initially planned by the partner ENSMP before the decision of funding the project SoDa, its level of achievements and the rapid pace of development would have not been attained outside the framework of this project. The development clearly benefits from several resources, including scientific expertise, not available at ENSMP.

The project SoDa will benefit to the exploitation of the method Heliosat-II, its implementation and its penetration. As already seen, this method request some information that are or will be available through the SoDa service. This service will help in the implementation and further in the penetration by providing an easy access to the necessary information.

TABLE OF CONTENTS

2 INTRODUCTION

Solar radiation is observed by the means of networks of meteorological stations. Various measurements can be made: cloud coverage, sunshine duration, global irradiation, the direct or diffuse irradiation, the spectral distribution of the irradiance etc. For irradiation measurements, the relative RMSE is approximately 3 to 5 percent if the station is well maintained. Costs for installation and maintenance of such networks are very high; consequently, there are a few measuring stations in the world. In the Western Europe and Northern America, where the situation is best, the average distance between stations is approximately 100 km. In Eastern Europe, the average distance is approximately 500 km and is approximately 1000 km in Africa. The situation is worse over the oceans. In the present situation, the irradiation over a particular site in the world is performed by interpolation / extrapolation of the measurements available and closest to this site.

Anonymous (1995) performed a study of the errors resulting from interpolation techniques for the assessment of global daily irradiation for agricultural purposes (agricultural policy for Europe). Using eight neighbouring stations, the root mean square error (RMSE) was 20 per cent in relative value. Supit (1994) reported relative RMSE of 15 - 25 per cent, using several techniques and five stations. Both authors and others stress the importance of the geographical and climate parameters upon the results and the importance of the adequacy between the spatial and temporal scales of the optical state of the atmosphere, the density of the network and the quantities to interpolate. The most complete study is that of Zelenka *et al.* (1992). Various techniques were defined and applied to six very dense networks in Europe and North America. For daily irradiation, relative RMSE of 15 per cent in July up to 40 per cent in January was found. Hulme *et al.* (1995), Beyer, Wald (1996) and Beyer *et al.* (1997) computed climatological means (respectively 30 and 10 years) of monthly means of respectively sunshine duration and daily irradiation using sophisticated interpolation methods calling upon satellite-derived estimates and 800 and 600 stations in Europe. The relative RMSE ranges from 5 per cent in July up to 11 per cent in January.

Several authors (Zelenka *et al.*, 1992; Hay, 1981, 1984; Hay, Hanson, 1985; WMO, 1981; Perez *et al.*, 1997) studied the extrapolation and interpolation errors as a function of the distance to the measuring stations. The errors are very similar for both cases, though the interpolation errors are lower. The larger the distance, the larger the RMSE. For global daily irradiation, the relative RMSE is 10 per cent for a distance of 16 km, 20 per cent for 64 km and 30-40 per cent for 256 km. For the global hourly irradiation, the errors are worse: 15 per cent for 4 km, 20 per cent for 16 km, 25 per cent for 64 km and 45 per cent for 256 km.

Mapping the solar radiation by interpolation / extrapolation of measurements is possible but leads to large errors, except if the network is dense. It should be noted that a deficient station might strongly affect the final map. Finally, interpolation / extrapolation techniques cannot reproduce radiation features that are smaller than twice the average distance between stations.

Several authors have shown the potentialities of the images of the Earth taken by the meteorological satellites for the mapping of the global irradiation impinging on a horizontal surface at the ground level. One advantage is that the errors in the estimates are constant throughout the mapped area, except in areas with highly variable relief or for very large areas, where illumination and observation angles may change dramatically. Consequently, an

estimate of the quality may be provided for every site. Zelenka *et al.* (1992, 1999) and Perez *et al.* (1997) demonstrate that for the best methods, the irradiation assessed by satellite is better than that estimated from interpolation technique as soon as the distance to the stations is greater than 34 km for the hourly irradiation and 50 km for the daily irradiation.

Many methods were developed especially in the years '80s. Among them was the method called Heliosat, developed by Armines / ENSMP under the auspices of the European Commission (Cano 1982; Cano *et al.* 1986; Michaud-Regas 1986; Diabaté 1989). This method was among the most accurate methods as shown by several authors (Grüter *et al* 1986; Raschke *et al.* 1991). It was simple enough to widely disseminate in the world (Diabaté *et al.* 1988a b, 1989; Wald *et al.* 1992). It became popular and several modifications were proposed (Moussu *et al.* 1989; Obrecht 1990; Zelenka *et al.* 1992, 1999; Beyer *et al.* 1996; Fontoynont *et al.* 1997; Iehlé *et al.* 1997; Ineichen, Perez 1999).

2.1 A new method: Heliosat-II

The purpose of the present work is to create a new version, called Heliosat-II, which integrates the knowledge gained by these various exploitations of the original method and its varieties in a coherent and thorough way. The various empirical parameters should be expressed using physical laws. This new version should also be more accurate. Given the fact that the inputs should still be images taken in the visible range (broad range), this can only be attained by introducing external knowledge on the optical state of the atmosphere for each location. The major objectives of the Heliosat-II project are

- to improve the capabilities of the method to process any type of data from geostationary meteorological satellites, including large time-series of images taken by different sensors,
- to be applicable in real-time or on archived data
- to improve the implementation of the method, by e.g. reducing the number of empirical parameters,
- to improve the accuracy of the estimates of the global irradiation.

The achievements of the project will be measured against some criteria regarding applicability limits in time and space and against irradiation measurements performed by standard meteorological stations in Europe. Contrary to the previous developments in Heliosat-I, no measurements will be used for the development. The method should therefore be applicable in any part of the world. There is no direct comparison with the results that might be produced by the standard Heliosat-I method. This would have meant an adaptation of some parameters to the specific cases to be treated with some tuning because of the change in satellite using the available measurements. This would maybe lead to a lack of objectivity in the comparison of both methods.

The previous discussions on the accuracy attained by interpolation / extrapolation and the results that have been attained by standard implementations of the method Heliosat-I and that have been published or that are known through the Heliosat scientific network, provide a baseline for the accuracy presently achievable. We aim at improving this baseline by approximately 30 %. This leads to the objectives in accuracy for the new method Heliosat-II. These are presented in the following after an introductory discussion on the problems

encountered when comparing ground measurements and satellite-derived assessments of irradiation.

2.2 Comparison with ground measurements

One of the major points when validating a method which derive parameters from satellite data is the link between these parameters and the measurements of these same parameters by standard procedures at ground level (pyranometers, for example). In performing comparisons between ground measurements and satellite-derived information one indeed assumes that the ground information should be similar to the satellite-derived information in the method for processing satellite data were with no error.

An important aspect is the fact that satellite information is a snapshot over a large area (typically 30 km^2), while ground information is a time-integrated pinpoint measurement (typically 1 hour). Discrepancies between satellite and ground measuring systems partly explain why the information obtained by one system should differ from the other. Another aspect is the variability of the parameter under concern within a pixel. If the parameter is homogeneous, and more exactly has a uniform value over the pixel, then the ground measurement has the same value than any other pinpoint measurement that would be made over that pixel. That is the ground measurement is representative of the parameter.

However, uniformity is seldom encountered. Therefore, one has to deal with weaker hypotheses. Before proceeding, we have to consider also that images are not acquired in the middle of the time-lapse of the ground measurement. For example, the satellite Meteosat observes France every half-hour plus 15 minute (e.g. 1015 UT, 1045 UT...). Therefore assuming that one hour is the time-lapse that should be compared to the satellite-derived parameter, one has to construct an one-hour synthetic value by the means of interpolation using time-adjacent measurements made by the pyranometer. Indeed the justification in doing so is done exactly in the same way than for the space domain (*i.e.* the pixels). The same hypotheses are to be applied. The most common one is the stationarity of increments of the parameter in space and time.

It is assumed furthermore that the optical properties of interest are passive tracers of atmospheric velocity, and that their turbulent properties can be derived from that of the velocity. This is only partly true for clouds since they have their own dynamics, which may differ strongly from the wind dynamics. Using the hypothesis of ergodicity and the Taylor hypothesis, time-average, as performed by pyranometers, may be replaced by average in space, as performed by satellite sensor. According to the Taylor hypothesis, also called ‘frozen turbulence’, one can consider that the aggregates of turbulent eddies which govern oscillations of optical properties at a fixed point are translated without change with the mean velocity of wind. The spatially computed statistics of the satellite-derived parameter can be compared to the time-computed statistics of the ground measurements. This hypothesis is very convenient and often used. It remains a working hypothesis, which is not always verified when possible. It may be valid for very small intervals of time relative to the variation of the turbulence, which is obviously not the case here.

The size of the pixel (~ 10 km) as well as the measurement lapse time (1 hour) are well within the critical range intermediate between small-scale and meso-scale turbulence. Within this

range, there is generally no strong links between the fluctuations observed at one scale (e.g. 10 km) and another (e.g. 1 km). The statistical properties cannot be accurately transposed from one scale to another as one can do in the so-called 'inertial' ranges in small- or meso-scale turbulence. It follows that we cannot claim that the satellite-derived information, averaged over a block of pixels or not, should match the ground measurement. A discrepancy is expected because of the natural variability of the radiation, which is difficult to predict or assess in the general case.

The size of the block of pixels centred on the location of the pyranometer has a strong influence on the comparison, the magnitude of it depending upon the case. Under uniform conditions, the results are the same. In the heterogeneous case, the results may differ significantly in an unpredictable way. Pinker, Laszlo (1991) studied the effect of different spatial sampling of satellite observations on retrieved surface global radiation using two different resolutions: 8 and 50 km. They found that, on the average, the results differed by about 8 - 9 percent. Several other attempts, not published in international journals, found similar conclusions and demonstrated that there is not an unique size of pixel aggregate giving the best results. It is possible at one time to get better agreement with one resolution and at other times better agreement with a different resolution. Beyer *et al.* (1992) suggested that the local variance might be used as a measure of the spatial heterogeneity and may serve to determine the most appropriate size.

Zelenka *et al.* (1999) studied the different components of the relative discrepancy they found in comparing satellite-derived estimates and pyranometers measurements of hourly global irradiation. They share the total relative error of 23 percent as

- 12-13 percent for the method
- 3-5 percent for the accuracy of these well-maintained pyranometers
- 5-8 percent for the spatial variability of the irradiation
- 3-5 percent for the difference of types of measurements: space-integrated versus time-integrated.

Finally, Diabaté (1989) shows the limits of such validation approaches, the results depending upon the number of cases, the size of the time-series and the seasons.

2.3 Accuracy to be achieved by the method Heliosat-II

Once these preliminaries recalled, one can give some figures as objectives for the accuracy that should be attained by the method Heliosat-II. These figures are expressed as root mean square errors (RMSE), in Wh m^{-2}. They have been computed using typical values for irradiation in Europe (ESRA, 2000).

Though most of the published results are obtained after averaging the individual satellite assessments on a block of pixels, thus decreasing the RMSE observed for a single pixel, the objectives for the method Heliosat-II are set up for a single pixel. The pyranometer measurements are compared to the satellite estimates for the pixel containing it.

The reasons to do that are one the one hand not to be dependent upon the size of the block of pixels, knowing that averaging over a block decreases the error, and on the other hand, to be

able to assess the accuracy that can be attained by images of reduced resolution like those in the so-called ISCCP-B2 format. Such images are very useful for climatology. This format was set up in the framework of the International Satellite Cloud Climatology Project (ISCCP) (Schiffer, Rossow 1983, 1985), part of the World Climate Research Program (WCRP). This set is derived from the operational Meteosat images, in both visible and thermal infrared bands. The B2 reduced-resolution set is produced according to the following steps:

- first, time sampling of geostationary images reduces the frequency of observation to synoptic three-hour intervals, starting at 0000 Universal Time (UT),
- second, the higher-resolution visible-channel data are averaged to match the lower resolution of infrared-channel data (*i.e.* an image of 2500 x 2500 pixels with a resolution of 5 km),
- third, overlapping image pixels are removed,
- fourth, spatial sampling of images is performed to reduce the apparent resolution to approximately 30 km at nadir (*i.e.* an image B2 of 416 x 416 pixels with an apparent resolution of 30 km), by taking 1 pixel over 6 in each direction. The value of the corresponding B2 pixel is given by the radiance of the south-easternmost pixel in a 6x6 pixels square.

In all other respects, the satellite measurements are preserved in the reduced-resolution data set, since volume reduction is accomplished by the sampling described above (Anonymous 1996). The images B2 are formed by pixels that are effectively pixels of original size (*i.e.*, 5 km) but with a sub-sampling of 6 in each direction. This means that a B2 pixel is not an average of say, 30 km x 30 km, but is a pixel of 5 km in size, which represents an area of 30 km x 30 km. Thus a block of B2 pixels would represent a very wide area, with pending questions about its impact on the statistical quantities (average, RMSE). The homogeneity (from a statistical point of view) is far from being achieved and averaging over a block of B2 pixels may create bias, an adverse effect to increasing the quality.

Type	*Root mean square error (in Wh m^{-2})*	*Typical percentage for a given typical value*
Hourly irradiation	~ 130	~ 22 % for 600 Wh m^{-2}
Daily irradiation	~ 800	~ 18 % for 4,5 kWh m^{-2}
5-days sum of daily irradiation	~ 3000	~ 14 % for 22 kWh m^{-2}
10-days sum of daily irradiation	~ 5500	~ 12 % for 45 kWh m^{-2}
Monthly mean of hourly irradiation	~ 80	~ 13 % for 600 Wh m^{-2}
Monthly mean of daily irradiation	~ 400	~ 9 % for 4,5 kWh m^{-2}

Table 2.1 Accuracy objectives for the method Heliosat-II for a single pixel

3 NOTATIONS

The following notations are employed in this document.

The following subscripts are used

- *0*: extraterrestrial or astronomical values,
- *g*: ground related values,
- *c*: clear sky (*i.e.* cloudless sky) values,
- *b*: overcast sky values.
- λ: spectral values.

3.1 Astronomical quantities and sun angles

- *t* is the time.
- θ_S is the sun zenithal angle.
- γ_S is the sun elevation at time *t*, also called the solar altitude angle. γ_S is 0° at sunrise and sunset. $\theta_S = \pi/2 - \gamma_S$.
- I_0 is the solar constant, that is the extraterrestrial irradiance normal to the solar beam at the mean solar distance. It is equal to 1367 $W.m^{-2}$.
- $I_{0\lambda}$ is the spectral distribution of solar radiation outside the atmosphere. It is created by averaging or interpolating values read in published tables, to irradiance for 10 nm intervals centred on the indicated wavelengths. These tables are those of Neckel, Labs (1984), read from Justus (1989) and Rossow *et al.* (1992). Units are $W\ m^{-2}\ \mu m^{-1}$.
- ε is the correction used to allow for the variation of sun-earth distance from its mean value. It depends upon the day. $I_0\ \varepsilon(t)$ is the extraterrestrial irradiance for the current day observed on a surface normal to the solar beam.
- δ is the declination (positive when the sun is north to the equator: March 21 to September 23). Maximum and minimum values of the declination are +23°27' and -23°27'.
- *Dl* is the length of the day, *i.e.* 24 hours or 86400 seconds.
- the solar hour angle, ω, expresses the time of the day in terms of the angle of rotation of the Earth about its axis from its solar noon position at a specific place. As the Earth rotates of 360° (or 2π rad) in 24 hours, in one hour the rotation is 15° (or $\pi/12$ rad). Given an instant *t* in true solar time (TST) expressed in decimal hour, $\omega = (t-12)\pi/12$. If *t* is Universal Time (UT) in decimal hour, if λ is the longitude (positive eastwards) and if Δt is the correction of time (the so-called equation of time) in decimal hour, then $\omega = \pi/12\ (t + 12\lambda/\pi + \Delta t - 12)$, if λ is in radians, or $\omega = 15\ (t + \lambda/15 + \Delta t - 12)$ if λ is expressed in degrees.

3.2 Radiation quantities

The letters *L*, *G*, *D*, *I* and *B* denote the following quantities:

- *L*: radiance (W m^{-2} sr^{-1}),
- *G*: global irradiance or irradiation,
- *D*: diffuse irradiance or irradiation (diffuse component of solar radiation),
- *I*: normal direct irradiance or irradiation (beam component of solar radiation normal to the direction of the sun),
- *B*: direct irradiance or irradiation (beam component of solar radiation).

The basic time intervals to which the irradiation values refer are identified by the following subscripts:

- *h*: hourly values (e.g., the integral of the global irradiance observed during one hour, which is the hourly irradiation),
- *d*: daily values (e.g., the integral of the global irradiance observed during one day, which is the daily irradiation),
- *m*: mean monthly values (e.g., the mean value of the hourly irradiation observed during one month for the hour *h*).

Notations for the irradiances and irradiations:

- $G_0^t(i,j)$ is the horizontal irradiance outside the atmosphere for the time *t* and the pixel *(i, j)*. $G_0^t(i,j) = I_0\, e(t)\, \sin g_S(t,i,j)$. It is expressed in W m^{-2}.
- $G_{0h}(i,j)$ is the horizontal hourly irradiation outside the atmosphere for the hour *h* and the pixel *(i, j)*. It is expressed in W h m^{-2}.
- $G_{0d}(i,j)$ is the horizontal daily irradiation outside the atmosphere for the day *d* and the pixel *(i, j)*. It is expressed in W h m^{-2}.
- $G^t(i,j)$, $B^t(i,j)$ and $D^t(i,j)$ are respectively the horizontal global, beam and diffuse irradiances at ground level for the time *t* and the pixel *(i, j)*. They are expressed in W m^{-2}.
- $G_c^t(i,j)$, $B_c^t(i,j)$ and $D_c^t(i,j)$ are respectively the horizontal global, beam and diffuse irradiances at ground level under clear sky for the time *t* and the pixel *(i, j)*. They are expressed in W m^{-2}.
- $G_h(i,j)$, $B_h(i,j)$ and $D_h(i,j)$ are respectively the horizontal global, beam and diffuse hourly irradiations at ground level for the hour *h* and the pixel *(i, j)*. They are expressed in W h m^{-2}. Similar notations hold for the daily irradiations, with a subscript *d*.
- $G_{ch}(i,j)$, $B_{ch}(i,j)$ and $D_{ch}(i,j)$ are respectively the horizontal global, beam and diffuse hourly irradiations at ground level under clear sky for the hour *h* and the pixel *(i, j)*. They are expressed in W h m^{-2}. Similar notations hold for the daily irradiations, with a subscript *d*.

3.3 Notations for describing the optical properties of the atmosphere and the ground

- $KT^t(i,j)$ is the clearness index for the time t and the pixel (i, j). It is equal to the ratio of the global radiation at ground on a horizontal surface $G^t(i,j)$ to the horizontal radiation outside the atmosphere $G_0^t(i,j)$: $KT^t(i,j) = G^t(i,j) / G_0^t(i,j)$. The clearness index may be defined from irradiance or from hourly or daily irradiations: $KT_h(i,j)$ or $KT_d(i,j)$.
- $K_c^t(i,j)$ is the clear-sky index for the time t and the pixel (i, j). It is equal to the ratio of the global radiation at ground on a horizontal surface $G^t(i,j)$ to the same quantity but for clear skies $G_c^t(i,j)$: $K_c^t(i,j) = G^t(i,j) / G_c^t(i,j)$. It may be defined from irradiance or from hourly or daily irradiations: $K_{ch}(i,j)$ or $K_{cd}(i,j)$.
- $T_L(AM2)$ is the Linke turbidity factor for a relative air mass m equal to 2.
- m is the relative optical air mass. It expresses the ratio of the optical path length of the solar beam through the atmosphere to the optical path through a standard atmosphere at sea level with the sun at the zenith.
- $\delta_R(m)$ is the integral Rayleigh optical thickness.
- $L^t(i,j)$ is the radiance observed by the spaceborne for the time t and the pixel (i, j). It is expressed in W m^{-2} st^{-1}.

3.4 Notations for other properties of the site

- z is the elevation of the site above mean sea level.
- p is the pressure at site elevation and p_0 is the mean atmospheric pressure at sea level.
- φ and λ are respectively the latitude (positive to the Northern Hemisphere) and longitude of the site (positive eastwards).

3.5 Satellite (Meteosat) -related quantities

- S_λ is the sensor spectral response in the visible range, covering approximately the interval [0,3 µm, 1,1 µm] for Meteosat (unitless).
- I_{0met} is the total irradiance in the visible channel for the various Meteosat sensors (*i.e.* $\int_{0.3}^{1.1} I_{0\lambda} S_\lambda d\lambda$), in W m^{-2}.
- $\rho^t(i,j)$ is the apparent albedo observed by the spaceborne sensor for the pixel (i, j). It has no unit and is equal to the bidimensional reflectance, assuming the Lambertian hypothesis.

$$\rho^t(i,j) = \frac{\pi L^t(i,j)}{I_{0met}\, \varepsilon(t) \sin \gamma_S(t,i,j)} = \frac{\pi L^t(i,j)}{I_{0met}\, \varepsilon(t) \cos \theta_S(t,i,j)}.$$

- $\rho^t{}_{cloud}(i,j)$ is the apparent albedo observed by the spaceborne sensor over the brightest clouds for the pixel (i, j) (unitless) (a quantity specific to the method Heliosat)

- $r^t_g(i,j)$ is the apparent albedo observed by the spaceborne sensor over the ground under clear skies for the pixel (i, j) (unitless) (a quantity specific to the method Heliosat)
- θ_v is the viewing angle, equal to zero when looking to nadir.
- a^t, b^t and CN^t_{dark} are the calibration coefficients of the Meteosat radiometer at instant t.

4 THE METHOD HELIOSAT-I

4.1 Description of the method

The principle of the method Heliosat-I is the construction of a "cloud index" resulting from a comparison of what is observed by the sensor to what should be observed over that pixel if the sky were clear, which is related to the "clearness" of the atmosphere. At each pixel (i, j) of the current image at time t, a normalised count $CN^{*t}(i,j)$ is computed as:

$$CN^{*t}(i,j) = (CN^{t}(i,j) - CN0^{t}) / [I_0\, e(t)\, (\sin \gamma_S(i,j))\, (\sin \gamma_S(i,j))^{0,15}] \qquad (4.1)$$

where

- $CN^{t}(i,j)$ is the numerical count observed by the sensor at time t for this pixel (i, j), $CN0^{t}$ being what can be called the sensor zero (the numerical counts are not necessarily calibrated),
- $(\sin \gamma_S)^{0,15}$ is the clear sky transmittance (model of Perrin de Brichambaut, Vauge 1982).

This normalised count $CN^{*t}(i,j)$ is related to the apparent albedo $\rho^{t}(i,j)$ observed by the spaceborne sensor. In preparation to the determination of the cloud index $n^{t}(i,j)$, a reference map of the normalised count for clear sky is constructed (Moussu *et al.* 1989). It is also called the normalised count for ground, $CN^{*}_{g}(i,j)$. Given a time-series of images, it is evaluated at each pixel in a recursive fashion by minimising the variance between the digital counts and those resulting from the clear sky model, the cloudy cases being eliminated at each step (Cano *et al.* 1986). The cloud index is defined as a function of $CN^{*}_{g}(i,j)$, $CN^{*t}(i,j)$, and the typical normalised count of the brightest clouds tops CN^{*}_{cloud}:

$$n^{t}(i,j) = [CN^{*t}(i,j) - CN^{*}_{g}(i,j)\,] / [CN^{*}_{cloud} - CN^{*}_{g}(i,j))\,] \qquad (4.2)$$

The computation of CN^{*}_{cloud} is performed using the inverse of the algorithm used for determining the reference albedo map and retaining only the cloudy areas. The histogram of this "only cloud" image provides an estimation of CN^{*}_{cloud}.

The clearness index $KT_h(i,j)$ may be defined for the hour h centred on t as:

$$KT_h(i,j) = G_h(i,j) / G_{0h}(i,j) \qquad (4.3)$$

where $G_{0h}(i,j)$ is approximated by $I_0\, e(t) \sin \gamma_S$, where γ_S is for the middle t of the hour. Care should be taken of the sunset and sunrise. Several previous studies did show a linear relationship between the cloud index and the clearness index, where the parameters A and B are positive and have been determined once for ever (Diabaté *et al.* 1988; Diabaté 1989):

$$KT_h(i,j) = -A\, n^{t}(i,j) + B \qquad (4.5)$$

This relationship between $KT_h(i,j)$ and $n^{t}(i,j)$ leads to the computation of the global hourly irradiation $G_h(i,j)$.

The global daily irradiation $G_d(i,j)$ is computed from the set of hourly irradiations available for that day. The larger the number of images used per day, the lower the level of error. A model has been proposed by Diabaté (1989), using an analytical law fitted onto climatological hourly values. However most users adopted the following model. Let denote the horizontal

daily irradiation outside the atmosphere by $G_{0d}(i,j)$ and the daily clearness index by $KT_d(i,j)$. $G_d(i,j)$ is then computed from the N assessments of the hourly irradiation $G_h(i,j)$ made during the day:

$$G_d(i,j) = KT_d(i,j)\, G_{0d}(i,j) = G_{0d}(i,j) \sum_{h=1}^{N} w_h\, KT_h(i,j) \qquad (4.6)$$

where $w_h = \dfrac{G_{0h}(i,j)}{\sum_{h=1}^{N} G_{0h}(i,j)}$

It comes

$$G_d(i,j) = G_{0d}(i,j) \frac{\sum_{h=1}^{N} G_h(i,j)}{\sum_{h=1}^{N} G_{0h}(i,j)}$$

The method Heliosat-I is currently used by several institutes in Europe and elsewhere with geostationary satellites like Meteosat (Europe), GOES (USA) or GMS (Japan). A scientific network ensures collaboration between these institutes and improvements in the method. There is also a software, the Sun-UNIX version of it made at Armines / Ecole des mines de Paris being in public domain and available on an Internet server (*http://www-cenerg.cma.fr/tele*). A PC-based package including a satellite data receiver has also been developed and marketed by a French company.

There are several empirical parameters in the method Heliosat-I, especially in the computation of the apparent albedoes of the ground and clouds and in the follow-up of the changes of the ground albedo. The clear-sky model is also site-dependent. In this model, the optical state of the clear atmosphere is expressed by the sole exponent. As a basis, a value of *0.15* has been selected but other values may perform better. The parameters c and d in the relationship between $KT_h(i,j)$ and $n^t(i,j)$ may be adjusted by comparison with measurements made at meteorological stations. These parameters were well tuned during the construction of the method or of its varieties and this explains the good results attained by the authors when performing a comparison with ground observations. For example, according to Diabaté (1989), Diabaté *et al.* (1988) or Grüter *et al.* (1986), the typical relative error (RMSE) is about

- 7-18 percent for the assessment of the hourly irradiation,
- 10 percent or better for the monthly mean of the hourly irradiation,
- 10-15 percent for the assessment of the daily irradiation,
- 10 percent or better for the monthly mean of daily irradiation.

Rigollier (2000) performed a survey of the literature and reported the accuracy found by several authors when comparing irradiations measured by ground stations and irradiations derived from satellite data by various methods. She retained only the comparisons performed by authors, who were not the inventors of a method. Her work thus demonstrates the actual accuracy that can be attained by a naive implementation of a method. Table 1 reports her

results for the method Heliosat-I. It appears that the accuracy, expressed as bias and root mean square error, is usually lower than claimed by the inventors. This is also true for other methods and not restricted to the Heliosat method (Rigollier, 2000). This table clearly shows that modifications of the method Heliosat-I are necessary to ensure that any correct implementation should lead to similar results.

Type	*Reference*	*Bias (rel. value)*	*RMSE (rel. value)*
Hourly irradiation	Satel-Light project (CEC, DG 12) (various versions - 3 independent assessments per version) (Fontoynont *et al.* 1997)	~ 10 %	~ 30 %
	Bauer (1996) (format B2, low spatial resolution)	2 %	35 %
	Zelenka *et al.* (1999) (modified Heliosat)	1 %	23 %
Daily irradiation	Iehlé *et al.* (1997) (format B2, using 3-4 hourly irradiations only)	16 %	27 %
	Zelenka *et al.* (1992)	- 10 %	16 %
10-days sum of daily irradiation	Iehlé *et al.* (1997) (format B2)	16 %	19 %
Monthly mean of hourly irradiation	Heidt *et al.* (1998)	N/A	19 %
Monthly mean of daily irradiation	Solar Radiation Atlas of Africa (Heliosat) (Raschke *et al.* 1991)	- 8 %	10 %
	Heidt *et al.* (1998)	N/A	10 %

Table 4.1. Accuracy of some methods (relative values of bias and root mean square error RMSE) as found in the literature. A positive bias means under-estimation. Adapted from Rigollier (2000).

4.2 The improvements to be undertaken

Given the good fundamentals of the method Heliosat I with respect to the objectives, it was decided to keep its principles, that is the computation of a cloud index n from the apparent albedo, the albedo of the ground (*i.e.* without clouds or minimal albedo) and the albedo of the very bright clouds (or maximum albedo). Actually, this principle is that commonly adopted when the only inputs are images taken in the visible broad range (Pastre, 1981; Möser, Raschke, 1983, 1984; Cano *et al.* 1986; Stuhlmann *et al.* 1990; Delorme *et al.* 1992; Colle *et al.* 1999).

Four points of improvements were identified, in order to meet the objectives expressed above:

- Calibration. Values in images should be calibrated. This will permit to take into account the change of sensor or of gain or calibration, if any, in a time-series. Hence, large time-series spanning over several changes of sensors and satellites may be processed, enhancing the interest of the Heliosat method in climatology. It will also contribute to reduce drastically the number of empirical parameters since many of them would now be expressed using known physical laws and parameters.
- Modelling the clear-sky irradiation G_c. Iehlé *et al.* (1997) and Rigollier (2000) showed the importance of the model used for modelling the clear-sky irradiation. The better the

accuracy of the model, the better the accuracy of the estimate performed by the method Heliosat.

- Computation of the cloud index *n*, and especially of the apparent albedoes of the pixel under concern (ρ^t), of the ground (ρ_g) and of the very bright clouds (ρ_{cloud}).
- Relationship between the cloud index *n* and the hourly global irradiation G_h. This go through an intermediate value, the clear-sky index K_c, which is used instead of the clearness index *KT*.

Each of these points and how it has been improved, is discussed in detail. The efforts are aiming at a better quality on a global sense, which means that operational aspects and accuracy of the assessed irradiation are equally treated. A comparison between irradiation values retrieved from the processing of Meteosat images and ground measurements is performed, which permits to demonstrate the benefits of the new method Heliosat II.

5 CALIBRATION

5.1 Introduction

The method Heliosat-I was constructed to cope with various types of inputs, including analogue signal coming from the geostationary meteorological satellites, the so-called Wefax format (Weather Facsimile). A relative calibration was performed (the first equation of the Chapter 4), permitting to compare digital counts as far as the sensor or its characteristics (e.g. gain or sensitivity) were unchanged. These are strong limitations and each operation of the method Heliosat-I faces problems periodically, which are usually solved by tuning several parameters.

To avoid similar problems, the method Heliosat-II deals with physical quantities, namely radiances, expressed in $Wm^{-2}sr^{-1}$, instead of relative digital counts. It permits to better introduce known models of the atmospheric optics into the processing, thus likely increasing the quality of the estimates. Using such models also decreases the number of empirically defined parameters, leading to more stable results and an easier implementation independent of the characteristics of the images to process. Finally the absolute calibration in radiances may be the only solution to process in an automatic way long time-series of images, acquired by various sensors within the same programme, such as the series of satellites of the Meteosat Operational Programme (MOP).

The following table displays the history of changes in the operational Meteosat satellite in the MOP programme. A slot denotes the half-hour period necessary for the acquisition of an entire image. For ESA and Eumetsat, the successive operators of the series of the satellites Meteosat, the slot 1 denotes the half-hour: 0000 UT and 0030 UT, the slot 2: 0030 and 0100 UT, and the slot 48: 2330 and 2400 UT. This table shows a great variability, especially between the satellites Meteosat-3, -4, -5 and -6.

The various Meteosat sensors have different sensitivities due to their difference in the spectral band. Each of the spectral channels can be operated at one of 16 different gain levels. These gain levels are used to obtained the optimum dynamic range for each spectral channel and are adjusted as required (Eumetsat, 1996). This occurred several times within the periods given in the table. These sub-periods are not reported here. These changes in gain affect the sensitivity of a given sensor, and are to be compensated by an adjustment of the operational calibration coefficient. With this table, one may better figure out the problems encountered when using the method Heliosat-I.

Satellite	*Beginning of the period*		*End of the period*	
	Date	*Slot*	*Date*	*Slot*
Meteosat -1	9 December 1977		25 November 1979	
Meteosat -2	16 August 1981		11 August 1988	14
Meteosat -3	11 August 1988	17	19 June 1989	17
Meteosat -4	19 June 1989	18	24 January 1990	17
Meteosat -3	24 January 1990	19	19 April 1990	17

Meteosat -4	19 April 1990	19	30 October 1990	25
Meteosat -3	30 October 1990	27	5 November 1990	17
Meteosat -4	5 November 1990	19	11 December 1990	17
Meteosat -3	11 December 1990	19	13 December 1990	18
Meteosat -4	13 December 1990	20	22 January 1991	17
Meteosat -3	22 January 1991	18	25 January 1991	18
Meteosat -4	25 January 1991	19	2 May 1991	16
Meteosat -5	2 May 1991	18	3 May 1991	29
Meteosat -4	3 May 1991	30	26 November 1991	16
Meteosat -5	26 November 1991	19	29 November 1991	17
Meteosat -4	29 November 1991	18	11 February 1992	17
Meteosat -5	11 February 1992	19	5 February 1992	17
Meteosat -4	5 February 1992	19	8 September 1992	18
Meteosat -5	8 September 1992	19	24 September 1992	15
Meteosat -4	24 September 1992	16	4 May 1993	18
Meteosat -5	4 May 1993	19	7 May 1993	16
Meteosat -4	7 May 1993	18	3 November 1993	17
Meteosat -5	3 November 1993	21	18 November 1993	16
Meteosat -4	18 November 1993	20	4 February 1994	17
Meteosat -5	4 February 1994	19	21 October 1996	18
Meteosat -6	21 October 1996	19	25 October 1996	17
Meteosat -5	25 October 1996	18	13 February 1997	16
Meteosat -6	13 February 1997	18	3 June 1998	16
Meteosat -7	3 June 1998	17		

Table 5.1. History of the satellites of the MOP series

5.2 The Earth viewing calibration approach

Sensors aboard the satellites observing the Earth are measuring the energy reflected or emitted by the system ground -atmosphere. A raw image does not have any scientific or quantitative meaning value *per se* if not calibrated, since the calibration function describes the relationship between the digital count and the actual geophysical value of the object seen. Satellite images are usually calibrated. Further, when dealing with time-series of images, comparisons between images acquired at very different instants are made. These images should be well-calibrated with respect to each other, in order to ensure that any variation in time is due to change in the signal coming from the observed target, and not from a change in calibration of the observing system. However, the satellites of the MOP series have no onboard calibration system in the visible range. Added to the lack of pre-launch calibration for some of the satellites, this prevents from an accurate calibration of the digital outputs of the radiometers

into accurate radiance measurements. The European Space Agency and Eumetsat performed from times to times perfectly calibrated airborne measurements (Kriebel 1981; Kriebel and Amann 1993; Kriebel *et al.* 1996), which permits to compute accurate calibration coefficients for a limited period. The calibration coefficients of the visible channels are not dynamically adjusted within the Meteorological Products Extraction Facility (Eumetsat 1996). In its Web site (*www.eumetsat.de*), Eumetsat proposes a series of calibration coefficients on a yearly basis.

This is far from being sufficient to our opinion, especially when looking to the numerous changes occurring each year. A higher temporal sampling is needed and daily calibration coefficients should be computed using the Earth viewing approach. The method recently proposed by Lefèvre *et al.* (2000) offers the advantage of being entirely automatic, and is the only one to our knowledge. It has been proved as accurate as others using sophisticated modelling of the optical properties of the atmosphere and of the reflection properties of selected objects on the ground, such as desert or oceans.

5.3 The method of Lefèvre *et al.* (2000)

This method, also called the auto-calibration method, is based on the analysis of two quantities, which are constant in radiance over the time-series. These quantities are statistical parameters using the fact that in the entire field of view of the Meteosat sensor, the mixed presence of land, ocean, and clouds of different reflectivity over approximately one third of the Earth, whatever the day and time of the year, leads to the preservation of such statistical quantities with time. In an empirical way, Lefèvre *et al.* selected three parameters, which are the numerical counts *CN* corresponding to a dark target, and to the percentiles 5 % and 80 % of the histogram of the mid-day image. These numerical counts vary in time according to the Meteosat sensor and the date of viewing, but the two quantities that are derived in radiances (and defined in the following) were found constant for the test periods. Then it was hypothesised that any drift in these quantities should reflect a drift in the calibration of the Meteosat sensor for any period of time. The validity of this assumption for the whole time-series is demonstrated *a posteriori* by the very good results obtained in calibration when compared to other works by the authors.

Assuming a linear response of the sensor, the relationship between the emerging radiance from the atmosphere and measured by the sensor, L^t, and the numerical count, CN^t, observed at instant t is:

$$L^t = \alpha^t (CN^t - CN0^t) \qquad (5.1)$$

where α^t and $CN0^t$ are respectively the calibration coefficient of the sensor (in W m^{-2} sr^{-1} CN^{-1}) and the offset numerical count of the calibration.

Actually, the method of Lefèvre *et al.* can only perform the calibration of an image relative to another. To calibrate a series of images, the procedure is the following:

- use a calibration function found in the literature,
- calibrate the image corresponding to that day (called hereafter the reference image),

- perform the method of Lefèvre *et al.* to calibrate all the other images relative to the reference one.

The first two steps are performed only once. Once the calibration function selected for the reference day t_0, *i.e.* a^{t0} and $CN0^{t0}$, this function is applied to the corresponding images for this day noted t_0, using the above Equation.

The percentiles 5 % and 80 % of the mid-day image, when most of the field of view is illuminated, correspond to the numerical counts, respectively CN^t_5 and CN^t_{80}, for which 5 percent (resp. 80 percent) of the surface of the cumulative histogram is reached (percentile 5 %, resp. 80 %). The third parameter of interest is the numerical count CN^t_{dark} of a dark target, namely the first mode of the histogram of an image acquired at a night slot, when approximately half of the field of view is in the dark.

The radiances corresponding to the numerical counts CN^t_5, CN^t_{80} and CN^t_{dark} obey the following relationships:

$$\begin{aligned} L^t_{dark} &= a^t (CN^t_{dark} - CN0^t) \\ L^t_5 &= a^t (CN^t_5 - CN0^t) \\ L^t_{80} &= a^t (CN^t_{80} - CN0^t) \end{aligned} \qquad (5.2)$$

It comes:

$$\begin{aligned} a^t &= (L^t_{80} - L^t_5) / (CN^t_{80} - CN^t_5) \\ CN0^t &= CN^t_{dark} - L^t_{dark} (1/a^t) \end{aligned} \qquad (5.3)$$

Lefèvre *et al.* analysed the changes in time of the two following quantities: (L^t_{dark} / F^t) and $[(L^t_{80} - L^t_5) / F^t]$, where F^t is the incoming extraterrestrial solar irradiance in the visible channel for the Meteosat sensor under concern. If I_{0met} is the total irradiance in the visible channel, *i.e.* $I_{0met} = \int_{0.3}^{1.1} I_{0\lambda} S_\lambda \, d\lambda$, with S_λ being the sensor spectral response in the visible range, covering approximately the interval [0,3 µm, 1,1 µm] for Meteosat, and if $e(t)$ is the eccentricity of the Earth orbit, then $F^t = I_{0met}(t)\, e(t)$. Lefèvre *et al.* found these two quantities invariant in time.

It comes:

$$L^{t0}_{dark} / F^{t0} = L^t_{dark} / F^t \qquad (5.4)$$

$$(L^{t0}_{80} - L^{t0}_5) / F^{t0} = (L^t_{80} - L^t_5) / F^t \qquad (5.5)$$

The first equation expresses that the most frequent radiance observed by the sensor when looking at the obscurity towards the Earth is time-invariant. The second equation deals with the images of the Earth well illuminated by the Sun; the mixed presence of land, ocean, and clouds of different reflectivity over approximately one third of the Earth, whatever the day and time of the year, leads to the preservation of the dynamics of the observed signal, expressed as $[(L^t_{80} - L^t_5) / F^t]$. In both equations, the ratioing by F^t accommodates for the changes in sensor. Lefèvre *et al.* underlined the heuristic aspect of the approach. They stressed that only the percentiles 5 % and 80 % offer such invariance, while one may expect a greater stability in the selection of the percentiles.

The calibration function proposed by Lefèvre *et al.* is:

$$L^t = a^t \, (CN^t - CN^t_{dark}) + b^t \qquad (5.6)$$

with

$$a^t = [(L^{t0}_{80} - L^{t0}_{5}) / (CN^t_{80} - CN^t_{5})] \, F^t / F^{t0}$$

$$b^t = L^{t0}_{dark} \, F^t / F^{t0}$$

According to the study of Lefèvre *et al.*, the reference day will be selected as t_0 = *1 January 1985*, and the calibration values for this day will be that proposed by Moulin *et al.* (1996). Lefèvre *et al.* demonstrated that the selection of the reference date has a negligible impact on the results.

5.4 Analysis of the initial method and changes

Before applying the method, some tests have been made, which result into changes of the initial method.

5.4.1 Selection of slots

The method lies on the analysis of two specific images: one acquired when the observed portion of the Earth is mostly in the obscurity and the other one when this portion is entirely illuminated. Lefèvre *et al.* made use of the slot 11 (0530 UT) to compute CN^t_{dark} and of the slot 24 (1130 UT) to compute ($L^t_{80} - L^t_5$). These slots are not necessarily available in the whole time-series. Can another slot be used in such cases?

Figure 5.1 exhibits the series of images available in the B2 format for the 11 June 1996. One sees the variation in illumination of the portion of the Earth observed by the satellite Meteosat, located above the Equator at longitude 0 (Gulf of Guinea).

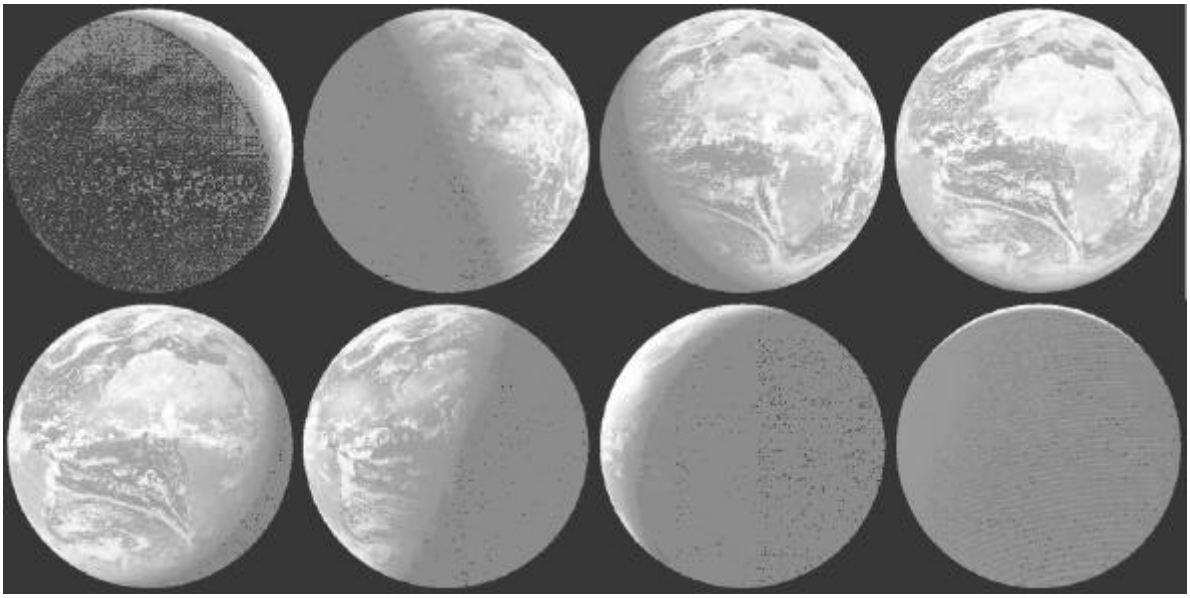

Figure 5.1. Series of images available on the 11 June 1996 in the B2 format. From left to right and top to bottom: slots 6, 12, 18, 24, 30, 36, 42 and 48.

Before the 16 November 1995, five slots only are supplied in the B2 format: slots 11, 17, 23, 29 and 35. After this date, eight slots are available: slots 6, 12, 18, 24, 30, 36, 42 and 48. After the 2 October 1996, the slot 23 replaces the slot 24. When a slot has not been acquired correctly, Eumetsat replaces it by the closest slot offering a good quality if possible. During the quality check of each image performed at Ecole des Mines, some slots have been rejected, creating gaps in the time-series.

The well-illuminated image is that of the slot 23 (1100 to 1130 UT) or 24 (1130 to 1200 UT). Figure 5.1 clearly shows that the images for the slots before (17 or 18) and after (29 or 30) comprise obscure parts, which will bias the computation of the percentiles. For these images, the quantity $[(L^t_{80} - L^t_5) / F^t]$ may vary in time. Accordingly, one should use as much as possible the slots 23 or 24 for the calibration, or the neighbouring slots from 21 to 26. If these slots are not available, the calibration should not be performed for this day, resulting into a gap in the time-series.

As for the parameter CN^t_{dark}, we analysed the possibility of using night slots (6, 42 or 48) when the field of view is entirely or almost entirely in the obscurity. The results lead to calibrated values that are overestimated by a large amount compared to those obtained by Lefèvre *et al.*, Kriebel, Amman (1993) and Moulin *et al.* (1996). Accordingly, one should use as much as possible the slots 11 or 12 for the calibration, or the slots 35 or 36, whose images are symmetrical to those of the slots 11 and 12. If these slots are not available, the image of the slot 11 (or 12) of the day before can be used.

5.4.2 The sensor spectral response

The calibration law depends on the shape of the spectral sensitivity curve of the radiometer, S_λ. We adopt those used by Lefèvre *et al.* only for Meteosat-1 to -4 and those recommended by Govaerts (1999, see also the site *www.eumetsat.de*) for Meteosat-5, -6 and -7. This is a large departure from the initial method, which results into a relative change in calibrated

radiances of approximately 20 percent for these satellites. The total irradiances in the visible channel for the various Meteosat sensors, I_{0met} ($= \int_{0.3}^{1.1} I_{0\lambda} S_\lambda \, d\lambda$), are given in the table 5.2.

Meteosat-1	*Meteosat-2*	*Meteosat-3*	*Meteosat-4*	*Meteosat-5*	*Meteosat-6*	*Meteosat-7*
492,91	498,81	599,05	594,79	692,16	692,16	693,17

Table 5. 2. Total irradiance I_{0met} in the visible channel for the various Meteosat sensors, in W m^{-2}.

5.4.3 Application to the time-series of the B2 images

Taking into account the above remarks, the method of Lefèvre *et al.* is applied to the whole series of images in B2 format, spanning from 1985 to 1997. A series of calibration parameters is obtained: CN^t_{dark}, b^t and a^t. This series is discussed in the following in order to correct some drawbacks of the initial method and to establish the specifications of the operational scheme for calibration to be applied to the forthcoming years after 1997.

Time variations of the coefficients a^t and b^t are expected, which should be relating to the changes in properties of the sensor in time due to launch constraints and the hostile environment of the sensor: condensation of gases especially water vapour, deterioration in the optronic system, variation in the spectral filter characteristics, ... Some rapid changes correspond to changes in sensors or gain configuration or more rarely to operations of outgasing. The parameter CN^t_{dark} is mostly unchanged in the time-series. The two other parameters *a* and *b* exhibit unexpected variations, which are to be analysed and corrected.

In the following, the dates are expressed as the number of days since the 1 June 1983. This date is the initial one selected by Moulin *et al.* and adopting it eases the comparison between their work and ours. Table 5.3 gives the correspondence between the day numbers and the dates.

Date	*Day number*	*Date*	*Day number*	*Date*	*Day number*
01/06/1983	1	01/01/1989	2042	01/01/1994	3868
01/01/1985	581	01/01/1990	2407	01/01/1995	4233
01/01/1986	946	01/01/1991	2772	01/01/1996	4598
01/01/1987	1311	01/01/1992	3137	01/01/1997	4964
01/01/1988	1676	01/01/1993	3503	31/12/1997	5329

Table 5.3. Correspondence between the number of days since the 1 June 1983 and the dates.

5.4.4 Analysis of the coefficient b and correction

The time-series of the coefficient b^t is presented in the figure 5.2. The signal offers abrupt transitions, which are relating to changes in sensors or in gain configurations. Superimposed is a period of one year. This parameter b^t is actually the radiance measured when viewing darkness and should not vary from day to day, except for the changes due to the radiometers.

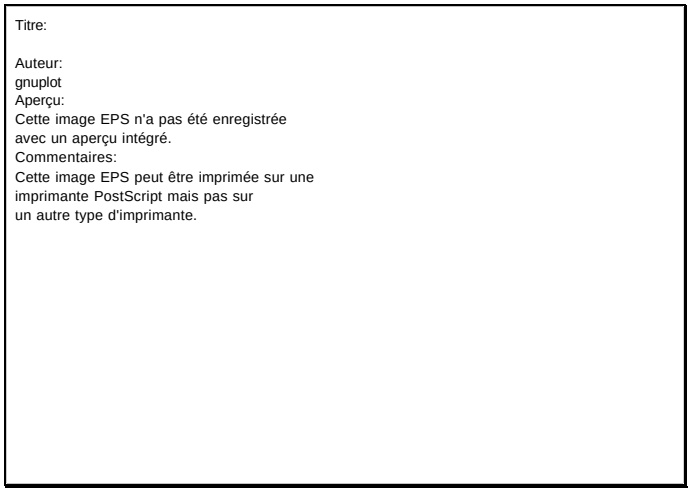

Figure 5.2. Time-series of the calibration coefficient b, in W m^{-2} sr^{-1}, computed by the method of Lefèvre et al. (2000), as a function of the number of days since 1 June 1983.

The period of one year corresponds to the period of the distance Sun-Earth. By carefully looking to the equations of Lefèvre *et al.*, one finds an error in Equation 5.4. The radiance of the dark part of the field of view does not depend upon the solar radiation since this part reflects no light. This radiance is constant in time and the eccentricity should not intervene in this Equation. The relationship should be:

$$L^{t0}_{dark} / I_{0met}(t_0) = L^{t}_{dark} / I_{0met}(t) \qquad (5.7)$$

and it comes

$$b^t = L^{t0}_{dark}\, I_{0met}(t) / I_{0met}(t_0) \qquad (5.8)$$

In the following, this corrected version of b^t is used.

5.4.5 Analysis of the coefficient a and correction

Figure 5.3 displays the time-series of the coefficient a^t. A large variability in time appears and several periods may be detected. These observations are illustrated by the Fourier transform of this time-series. The number of samples is 4543, the sampling time is one day and the cut-off frequency F_e is equal to 1 day^{-1}. Figure 5.4 displays the module of the Fourier transform for the interval [0, 0,01F_e] (*i.e.* [100, 4543] in day). The peak corresponding to the mean value was removed.

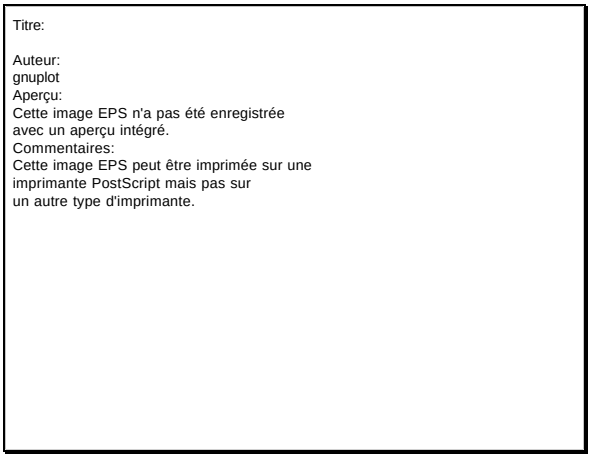

Figure 5.3. Time-series of the calibration coefficient a, in W m^{-2} sr^{-1} CN^{-1}, computed by the method of Lefèvre et al. (2000), as a function of the number of days

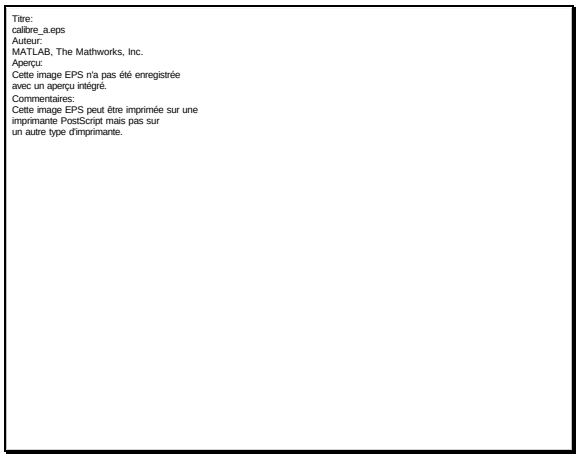

Figure 5.4. Module of the Fourier transform of the time-series of a. The signs underline the five spectral peaks in the interval [0, 0,01F_e]

Five peaks appear and are reported in the table 5.4. This confirms the visual analysis of the figure 5.3. At high frequencies (less than 100 days), the signal still presents noticeable energy, confirming the large variability of the estimates of the coefficient a^t.

Frequency ($days^{-1}$)	2.10^{-4}	9.10^{-4}	$1,2.10^{-3}$	$5,5.10^{-3}$	$6,1.10^{-3}$
Period (days)	4098	1170	819	182	164

Table 5.4. Position of the five peaks in the module of the Fourier transform

The low frequency peak (4098 days) is relating to the mean value. The changes of satellites and properties of radiometers likely induce the peaks: 1170 and 819 days. Our interest focuses on the peak at 182 days, which is well defined and presents a large amount of energy. This period corresponds to 6 months. By isolating this period in the signal, we discover that the maxima and minima correspond to respectively the solstices and equinoxes. The equations of the method of Lefèvre *et al.* do not take into account the position of the sun above a pixel. Because the method is based on the preservation of a quantity based on the radiances, and because the radiances reflected by a pixel are a function of the sun angles (zenith and azimuth), these angles should be incorporated in the equations of the method.

The preservation of the relative dynamics of the signal due to the preservation of the mixed presence of land, ocean, and clouds of different reflectivity along time, and expressed by the equation 5.5 is likely better fulfilled if bidimensional reflectances are used instead of radiances because the reflectance is independent of the position of the sun (at least at first order). The reflectance, $r^t(i,j)$ for the pixel (i, j), also called the apparent albedo in the Lambertian case, is given by:

$$r^t(i,j) = \frac{p\,L^t(i,j)}{I_0\,e(t)\,\sin g_S(t,i,j)} = \frac{p\,L^t(i,j)}{I_0\,e(t)\,\cos q_S(t,i,j)}$$

where g_S and q_S are respectively the sun elevation and the sun zenithal angle.

This does not affect the coefficient b^t, which is not a function of the sun radiation. Consequently, in principle, one should re-do the work of Lefèvre *et al.* and look for an invariant in reflectance such as:

$$(\rho^{t0}_{80} - \rho^{t0}_{5}) / F^{t0} = (\rho^{t}_{80} - \rho^{t}_{5}) / F^{t}$$

However, given the heuristic aspects of the approach, the percentiles may not be necessary 5 % and 80 %. Others may prove better. Considering the amount of efforts that may be needed to find a new invariant, we designed a simple correction. The radiances L^{t0}_{5}, L^{t0}_{80}, L^{t}_{5}, and L^{t}_{80} were divided by the cosine of the solar zenithal angle. Considering that the pixels contributing to the percentiles 5 % and 80 % are uniformly distributed in the field of view, a first-order correction may be performed by using the sun zenithal angle for the centre of the field of view, that is for a latitude φ and longitude λ equal to zero. The invariant is then:

$$(L^{t0}_{80} - L^{t0}_{5}) / F^{t0} \cos(\theta_S)_{t0,\ \varphi=0,\ \lambda=0} = (L^{t}_{80} - L^{t}_{5}) / F^{t} \cos(\theta_S)_{t,\ \varphi=0,\ \lambda=0} \qquad (5.9)$$

with

$$\cos\theta_S = \sin\varphi \sin\delta + \cos\varphi \cos\delta \cos\omega$$

where ω is the solar hour angle and δ is the declination for the day under concern.

Figure 5.5 displays the coefficient a^t after this correction. It may compare to the figure 5.3. The large variability is still there but the amplitude of the 6 months variations is smaller. The module of the Fourier transform is reported in the figure 5.6. In dotted line, is the module of the initial time-series and in full line is the module of the corrected time series. The difference for the peak 182 days is striking: the correction strongly diminishes the local energy. The diminution amounts to 7,2 dB; the remaining energy is approximately 0,44 times that before correction. This also holds for the peak at 164 days. This first-order correction is very efficient.

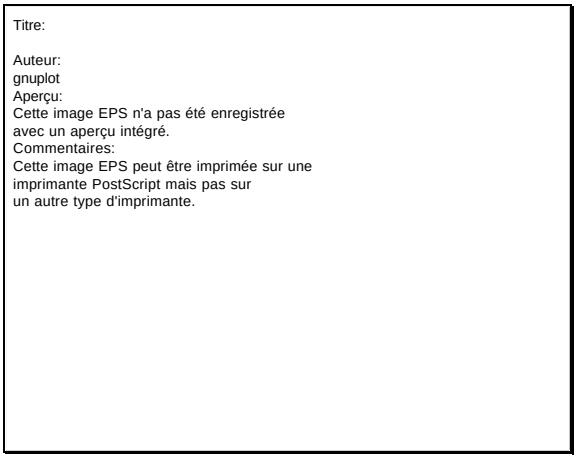

Figure 5.5. Time-series of the calibration coefficient a, once corrected for the sun angle

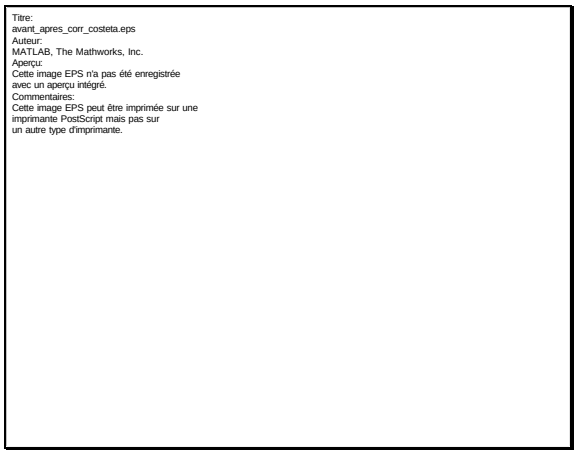

Figure 5.6. Module of the Fourier transform for the interval [0, 0,01F_e] before (dotted line) and after correction by the solar angle (full line)

5.4.6 Further analysis of the noise in the estimates of the coefficient a and filtering

As already mentioned, the energy at high frequencies is noticeable without peaks. This may be considered as a noise and consequently should be filtered out to produce a time series for operational use.

The standard deviation of a noise is not easy to determine. Two methods were employed. Following the work of Wald (1989) for other sensors, the variogram of the signal, also called the structure function, was analysed, especially for the nugget effect. A wavelet transform of the signal provides the highest frequencies of the signal, which are assumed here to be only noise (Blanc, 1999). Both methods give similar estimates of the standard deviation: 0,013 and 0,011 W m^{-2} sr^{-1} CN^{-1}.

The quantification step has also been assessed (Rigollier, 2000). Two cases were studied: before and after the 19 June 1989. Before this date, the quantification was made using six bits, while after, eight bits were used. The corresponding standard deviation is 0,006 before the 19 June 1989 and 0,003 W m^{-2} sr^{-1} CN^{-1} after. This standard deviation explains a large amount of the standard deviation of the noise (between 30 and 60 percent).

These various estimates of the noise permit to construct the appropriate filter to remove the noise. The cut-off frequency is 0,09 day^{-1}, that is a period of 11 days. Hence, any variations in time less than 11 days will not be taken into account. A filter was synthesised by the apodisation of Hemming; it comprises 33 coefficients *h(i)*, applying to the day *d-16* to the day *d+16* if *d* denotes the day under concern. The following relationships define the filtered signal a^{*t}:

$$\sum_{i=-16}^{i=+16} h(i) = 1$$

$$a^{*t} = \sum_{i=-16}^{i=+16} a^{t-i}\, h(i) \qquad (5.10)$$

Figure 5.7 displays the Fourier transform of the signal for all frequencies, and not only for frequencies less than 0,01 day^{-1}. Superimposed is the module of the Fourier transform of the filter. The shape of the filter is shown in the figure 5.8.

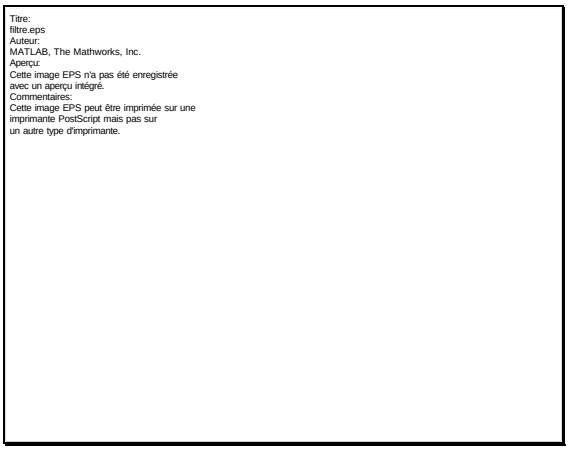

Figure 5.7. Fourier transform of the signal a^t and of the filter with a cut-off at 11 days

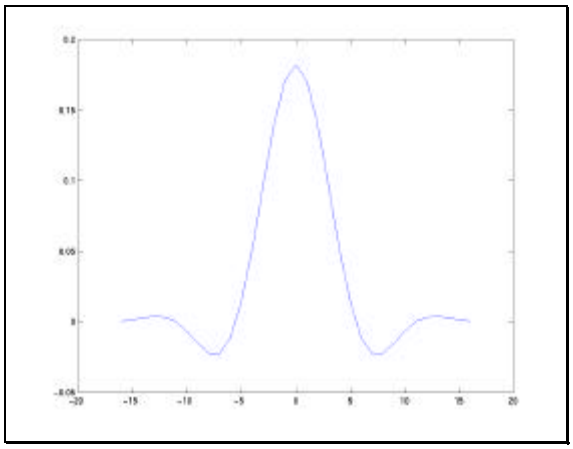

Figure 5.8. The filter curve. The 33 coefficients h(i) vary from i=-16 to i=+16

The standard deviation of the differences between the original and the filtered signals is equal to 0,014 W m^{-2} sr^{-1} CN^{-1}. This value is slightly larger than the standard deviations of the noise previously assessed.

To definitely assessed the influence of the filtering, the figure 5.9 exhibits the radiance that is computed from the numerical count 100 between the 1st January 1985 and 31 December 1997, before the filtering of the coefficient *a* and after. The difference in signals is almost unbiased. The bias is equal to -0,010 W m^{-2} sr^{-1}, that is 0,015 percent of the mean value. The standard deviation is equal to 9,69 W m^{-2} sr^{-1} for the filtered time series to compare to 9,72 before filtering. The filtering reduces some of the variations in high frequencies, which leads to a slight decrease of the standard deviation.

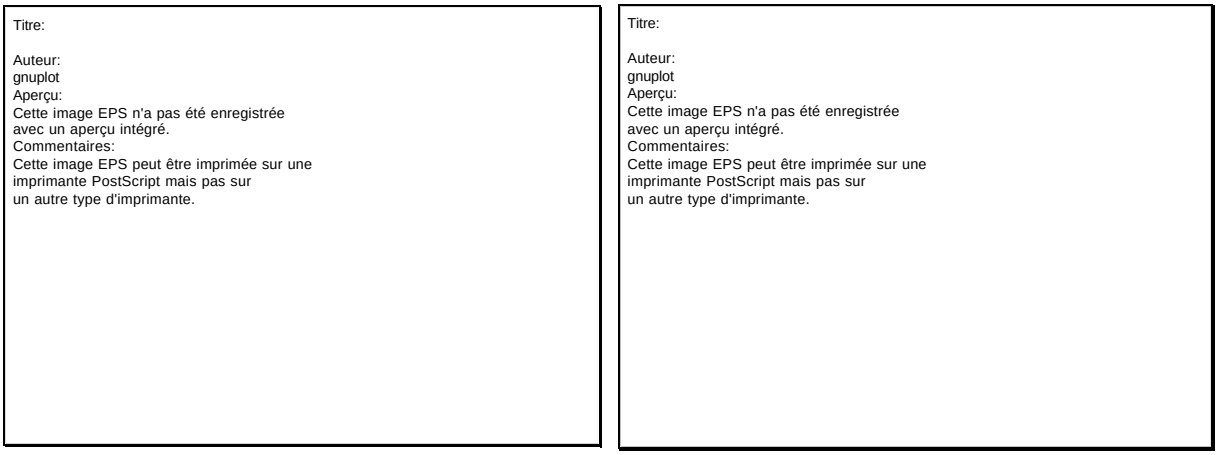

Figure 5.9. Radiance computed for the digital count 100 between 1st January 1985 and 31 December 1997, before filtering of the coefficient a (left) and after (right)

5.5 Operational implementation of the modified method of Lefèvre *et al.*

To summarise, the method of Lefèvre *et al.* was corrected for the coefficients a and b and a filter was designed to remove high frequencies. The reference day was selected as the 1st January 1985 (t_0). The calibration law for this reference date is that of Moulin *et al.* (1996) The corrected equations are:

$$L^t = a^{*t} (CN^t - CN^t_{dark}) + b^t \qquad (5.11)$$

$$b^t = L^{t0}_{dark} \, I_{0met}(t) / I_{0met}(t_0)$$

$$a^{*t} = \sum_{i=-16}^{i=+16} a^{t-i} \, h(i)$$

$$a^t = \frac{L^{t0}_{80} - L^{t0}_{5}}{CN^t_{80} - CN^t_{5}} \, \frac{F^t \cos(\theta_s)_{t \; F=0 \; l=0}}{F^{t0} \cos(\theta_s)_{t0 \; F=0 \; l=0}}$$

and the values for the reference date are:

$$L^{t0}_{dark} = 0{,}97 \, (CN^{t0}_{dark} - 1{,}87)$$

$$L^{t0}_{80} - L^{t0}_{5} = 0{,}97 \, (CN^{t0}_{80} - CN^{t0}_{5})$$

These equations are applied to the series of images spanning from 1985 to 1997. Several images are missing and 4543 days (*i.e.* 9086 images) are processed. We recall that each image of the time series was visually scrutinised for quality check; the rejection of some images of insufficient quality is the main cause of gaps in the time series. A series of calibration coefficients is obtained: CN^t_{dark}, b^t and a^t. This series should be processed in order to take care of the gaps and of the abrupt changes in radiometers or gain configuration. Once the series is completed with values for the three coefficients per day, then the filtering is applied to obtain the series of the coefficient a^{*t}. The final result is a series of daily sets of three coefficients that can be used to calibrate any image in this given period. This operational scheme for calibration will further be applied to the images of the years after 1997.

The visual analysis of the series of the parameters CN^t_{dark}, b^t and a^t drawn as a function of the day reveals an efficient means to evidence anomalies in quality that escaped the first screening. These days are removed from the time-series.

The gaps are filled by the interpolation of the three coefficients, using the known values for the days before and after the gap. The number of days used for interpolation is of little importance, given the filter to be applied later, except if the gap is larger than 11 days.

Changes in radiometers usually occur within the same day around 0800 UT (Table 5.1). Accordingly, one cannot use the image of the early slot 11 (0500 - 0530 UT) and the mid-day image to compute the calibration coefficients since they were not acquired by the same sensor. In principle, two sets of coefficients should be computed for such days: one before the change and one after. However, for the sake of the simplicity in the management of the calibration database and in the presentation of the calibration coefficients to the customer, we decided to compute only one set per day. This set corresponds to the mid-day image. The night slot is taken at the closest to this mid-day image: either the slot 35 (or neighbours) of the same day, or the slot 11 (or neighbours) of the day after.

Then the coefficient a^t is filtered to produce the series of a^{*t}. To cope with the changes in radiometers, the filter is applied period after period, the radiometer and its gain configuration being constant for a given period. The mirror technique is used for the limits of the time interval.

Figure 5.10 displays the time series of the coefficients a^t and a^{*t}. One may note for the day 1400 approximately an abrupt change in a^t and a^{*t}, which denotes a change in gain configuration for the radiometer of Meteosat-2. Others are also visible for other satellites (e.g., Meteosat-3 and -4).

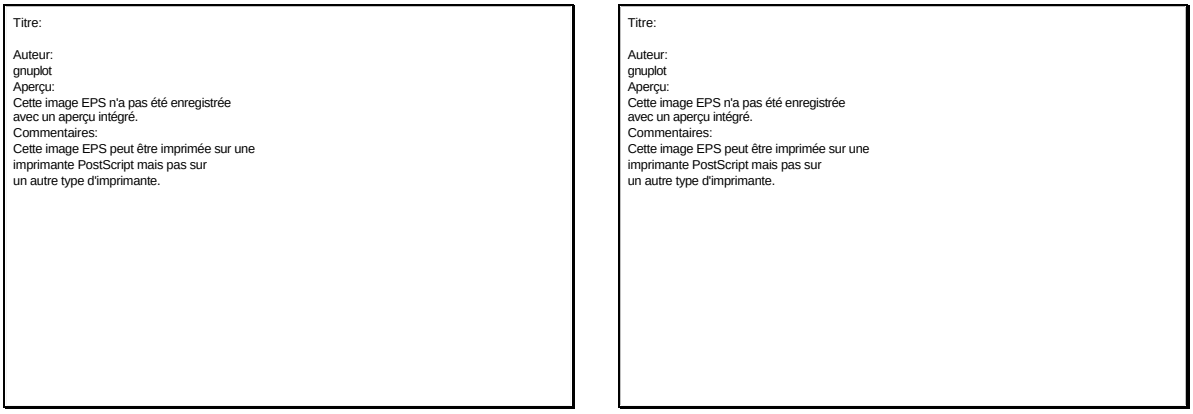

Figure 5.10. Time series of the coefficients a^t (left) and a^{*t} (right), as a function of the number of days

5.6 Comparison with other estimates of the calibration coefficients

The results of this operational implementation were compared to published estimates of the calibration law. Three concurrent laws were identified. Moulin *et al.* (1996) and Moulin, Schneider (1999) published analytical formulae for assessing daily sets of calibration coefficients. In the framework of the project ISCCP (International Satellite Cloud Climatology Project), Rossow *et al.* (1992), Desormeaux *et al.* (1993), Brest *et al.* (1997), and Rossow *et al.* (1995) published monthly sets of calibration coefficients (*i.e.* one set per month). Finally, Eumetsat supplies yearly sets of calibration coefficients in its web site (Govaerts *et al.* 1998).

For each case, the comparison is performed on the time series of radiances that are computed by the various methods using an initial numerical count *CN=100*. The monthly or yearly values are duplicated to lead to daily values. In these cases, the correlation coefficient does not have any signification.

5.6.1 Comparison with Moulin et al. (1996) and Moulin and Schneider (1999)

That of Moulin, Schneider (1999) completes the initial study of Moulin *et al.* (1996), providing calibration laws from the 1 June 1983 (Meteosat-2) to the 14 February 1997 (Meteosat-5). However, Moulin, Schneider make use of the old estimates of the spectral sensitivity curves for Meteosat-5, -6 and -7, and not those recommended by Govaerts (1999).

This leads to an under-estimation of their retrieved radiances by approximately 20 percent. Accordingly, the comparison is performed for the sole satellites Meteosat-2 to -4.

Table 5.5 reports some statistics of the comparison. The time series spans from the 1 January 1985 to the 4 February 1994 and comprises 3126 samples. Both methods give similar results, as already underlined by Lefèvre *et al*. The bias is negligible and the root mean square error (RMSE) is low, less than the errors reported by Moulin *et al*. (13 percent in relative value). Figure 5.11 exhibits the time-series of the radiances assessed by both methods as a function of the number of days.

	Method of Moulin et al.	*Modified method of Lefèvre et al.*	*Difference (Lefèvre - Moulin)*
Mean	62,20	62,47	0,273 (0,44 %)
RMSE		2,46 (3,95 %)	
Correlation coefficient		0,95	

Table 5.5. Statistical results of the comparison of radiances (in W m^{-2} sr^{-1}) assessed by the methods of Moulin et al. and Lefèvre et al. for a numerical count of 100.

The calibration laws of Moulin *et al.* are made of linear relationships of the number of days. Therefore, they cannot reproduce the high frequencies variations. Nevertheless, the correlation coefficient is large. There is a very good agreement between both methods, except for the rapid fluctuations (fig. 5.11). If linear regression were to be made on our estimates, the results would be very similar to those of Moulin *et al.*

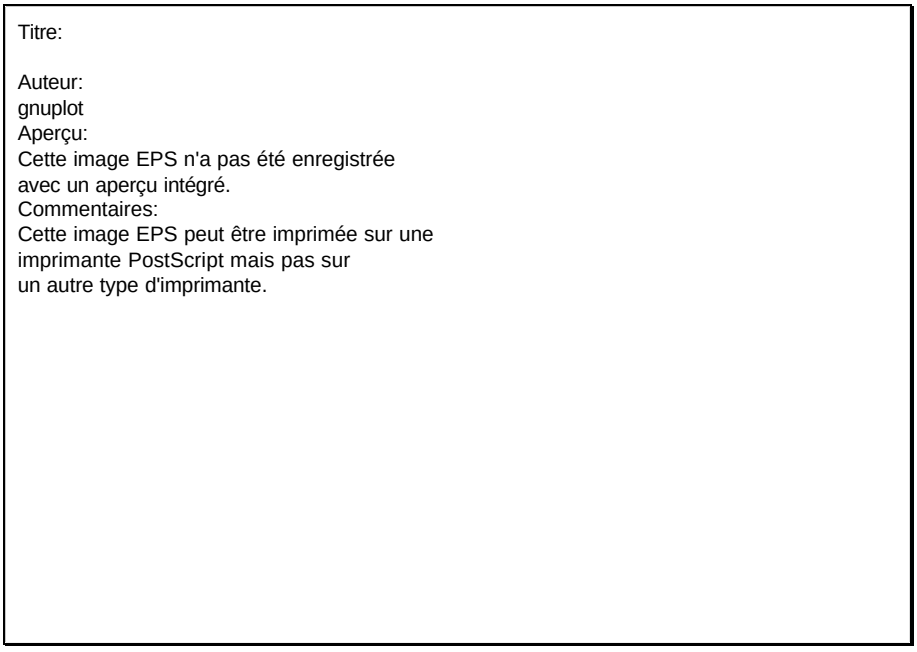

Figure 5.11. Comparison of radiances (in W m^{-2} sr^{-1}) assessed by the methods of Moulin et al. and Lefèvre et al. for a numerical count of 100, as a function of the number of days. The overlapping of the symbol à for the method of Moulin et al. results into a very thick line

5.6.2 Comparison with Rossow et al. (1992), Desormeaux et al. (1993), Brest et al. (1997) and Rossow et al. (1995)

Rossow *et al*. (1992), Desormeaux *et al*. (1993), Brest *et al.* (1997) and Rossow *et al*. (1995) describes the method developed for the project ISCCP (International Satellite Cloud Climatology Project). The method ISCCP is based upon the comparison of reflectances measured by various sensors, including the Meteosat series, and by the NOAA AVHRR-9 (AVHRR-7 in the early publications). For the same reasons as above, the comparison is limited to the series Meteosat-2 to -4, that is 1942 samples.

Table 5.6 reports some statistics of the comparison and the figure 5.12 exhibits the time-series of the radiances assessed by both methods as a function of the number of days. The method ISCCP provides monthly sets of calibration coefficients; the estimated radiances are greater than ours until the day 2000, then similar to ours for the initial period of Meteosat-3 and then less than ours for the remaining days of the comparison. The relative bias amounts to 6 percent and the relative RMSE to 16 percent. The method ISCCP agrees with ours, even if the results are less good than with the other methods. Indeed, it is difficult to precisely conclude this comparison; the method ISCCP is rather complex and contains several heuristic aspects. It may be possible that we made some errors. We were unable to find other sources of information confirming the results of the method ISCCP.

	Method of ISCCP	*Modified method of Lefèvre et al.*	*Difference (Lefèvre - ISCCP)*
Mean	62,98	58,97	-4,01 (-6,37 %)
RMSE		9,77 (15,51 %)	

Table 5.6. As for Table 5.5, but for the method ISCCP

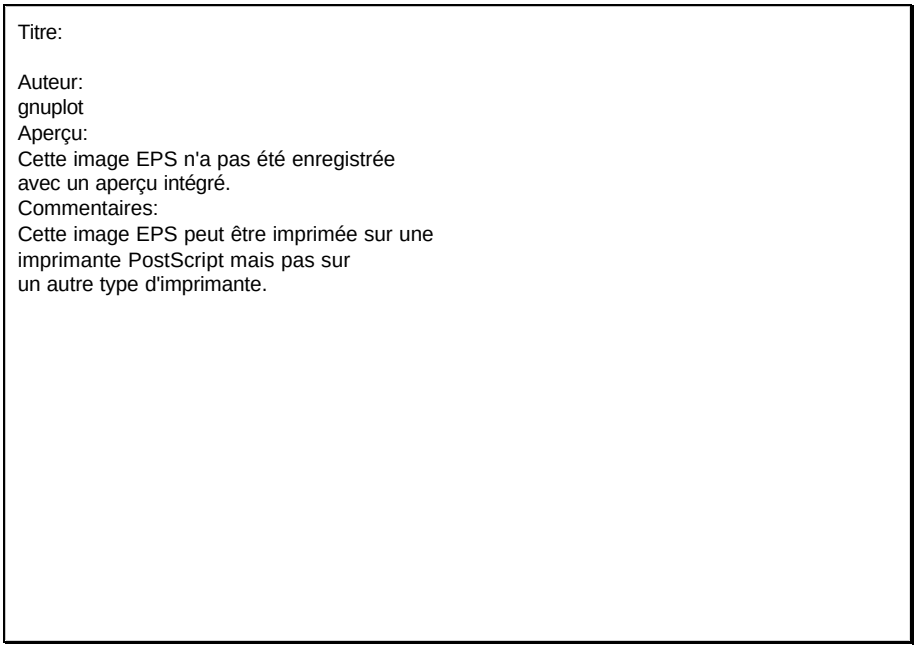

Figure 5.12. As for Figure 5.11, but for the method ISCCP

5.6.3 Comparison with Govaerts et al. (1998)

The method of Govaerts *et al.* (1998) is based upon the simulation of the radiances at the top of the atmosphere over specific targets such as deserts and is used to monitor the quality and trend of the calibration. The calibration coefficients are computed for each year and are available on the web site of Eumetsat (*www.eumetsat.de*).

The comparison of the radiances is performed for the years 1995 to 1997 (1089 samples). Some statistics of the comparison are reported in the table 5.7 and the figure 5.13 exhibits the time-series of the radiances assessed by both methods as a function of the number of days. The yearly values cannot reproduce the observed variations and the changes of radiometers that occur in this period (Meteosat-5, then Meteosat-6, again Meteosat-5 and Meteosat-6). The radiances produced by the method of Govaerts *et al.* are greater than ours are. Nevertheless, the bias is small (5 percent in relative value) as well as the RMSE (6 percent in relative value). We may conclude that as a whole both methods agree.

	Method of Govaerts et al.	*Modified method of Lefèvre et al.*	*Difference (Lefèvre - Govaerts)*
Mean	82,05	77,70	-4,35 (-5,31 %)
RMSE		5,24 (6,4 %)	

Table 5.7. As for Table 5.5, but for the method of Govaerts et al. (1998)

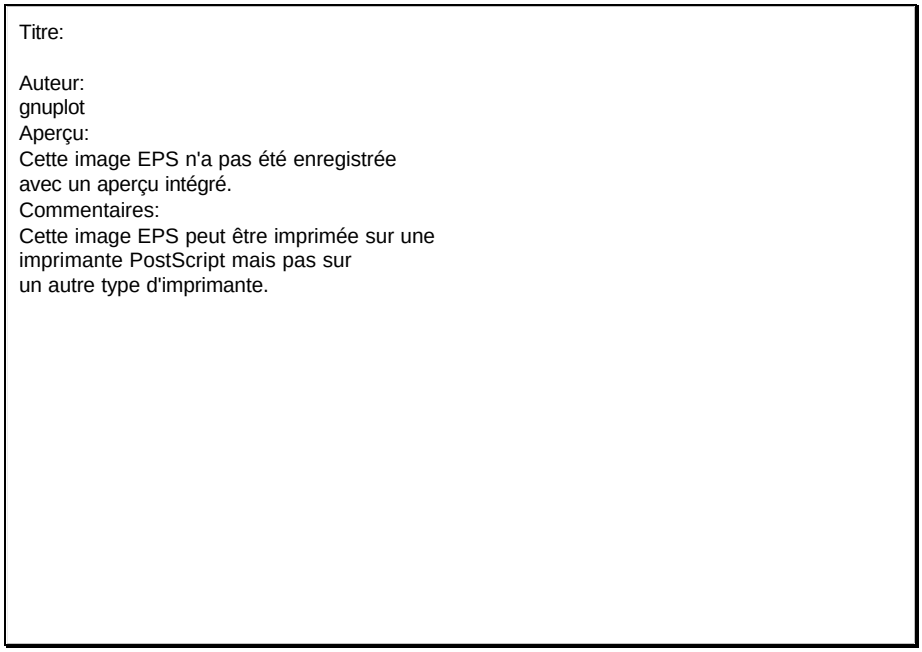

Figure 5.13. As for Figure 5.11, but for the method of Govaerts et al. (1998)

5.6.4 The variability of the signal

The previous figures clearly show rapid fluctuations of the radiance for the same numerical count. The calibration coefficients are computed every day, independently from the others. The filtering for limited periods of approximately 11 days creates a relationship. This may partly explain the observed fluctuations. However, we cannot exclude the possibility that some of the fluctuations originate from the radiometer itself.

Such a variability of the calibration of the visible channels is poorly documented in the literature. The calibration of the sensor SeaWiFS is the subject of many studies. Eplee *et al.* (2000) and Barnes *et al.* (200a) report short term variability in the observations of the lunar measurements for the calibration of this system. Observations are made approximately once per month; the changes in calibration values are similar to those observed in e.g., Figure 5.10. These changes are caused by the annual cycle for the temperature of the SeaWiFS focal planes, which are warmest near the winter solstice and colder near the summer solstice. The authors also write that changes may occur by decreases in the quantum efficiencies of the photodiodes from exposure to infrared radiation in orbit. Eplee, McClain (2000) used well-calibrated ground instruments for the comparison with SeaWiFS observations and presents changes of the calibration factors with time during the 900 first days of the instrument. High-frequencies variations may be observed (approx. 15 days), which are similar to those we observed and are not explained. Barnes *et al.* (200b) observe transitions in the instrument-diffuser sensitivity during 8 days for this radiometer that are not explained either. The radiometer CZCS experienced abrupt changes in calibration that were mostly due to outgasing. Evans, Gordon (1994) report a time scale of two weeks for short-term variations. This period is similar to our observations. Most of the publications focus of the assessment of

trends in calibration assuming a linear, polynomial, or exponential function of a number of days since launch. The estimated coefficients are usually scattered around this function, but there is no attention paid to the possible signification of this scattering on short, medium and long terms.

5.7 Conclusion

An operational method has been developed, tested and validated for the calibration of the visible channel of the series of satellites of the Meteosat Operational Programme. It performs on an automatic basis and is well suited for the processing of large volume of data.

The development took place within the development of the method Heliosat-II. We succeeded in making an independent calibration process, which can be used for other purposes. As already stated by Lefèvre *et al.* (2000), we think that it should be also applicable to other geostationary satellites having spectral bands similar to Meteosat, such as GOMS, GMS, Insat, and the first GOES series, but no check has been performed so far. The method can also be applied to full resolution images, since the original measurements are preserved through the construction of the B2 images. However, since the calibration is based upon the preservation of statistical quantities (in radiances), it is likely that it can only be performed onto an entire field of view of the sensor, and not onto a smaller portion of it. The mixed presence of land, ocean, and clouds of different reflectivity over approximately one third of the Earth, whatever the day and time of the year, is the responsible for the preservation of the statistical quantities, while this may not be the case for less extended areas.

Daily sets of calibration coefficients are obtained by this method, compared to the monthly or yearly sets of some methods or to the approximated analytical laws of others. The present work resulted into a time series of daily sets for the years 1985 to 1997, which constitutes a unique database. This database will be necessary for the execution of the method Heliosat-II. Beyond this, efforts were made to disseminate this database to the public. The developed service is unique in the world to our knowledge.

A database was created using the language MySQL. Several fields were defined:

- the year,
- the julian day within the year,
- the index for change of sensor during that day and slot if relevant,
- the index of interpolation (were these values interpolated?),
- the incoming extraterrestrial solar irradiance F^t for that day,
- and the three coefficients: CN^t_{dark}, b^t and a^t.

Then a script was written in PHP, which links this database to the standard browser of a customer through the web site *www-helioserve.cma.fr*. This site comprises also a history of the Meteosat sensors. Request forms and output forms were defined, which permit to the customer to access the database. Figures 5.14 and 5.15 illustrate the two possible cases.

In the first case, the customer queries the calibration coefficients for a given day. The answer is comprised of these coefficients, with explanations, the formula to apply and a look-up table

giving the corresponding radiance for each of the 256 possible numerical (digital) counts present in a Meteosat image.

In the second case, the customer queries the calibration coefficients for a given period. The answer is comprised of these coefficients for each day within the period, with explanations, the formula to apply and the mean and standard deviation of each coefficient for the period.

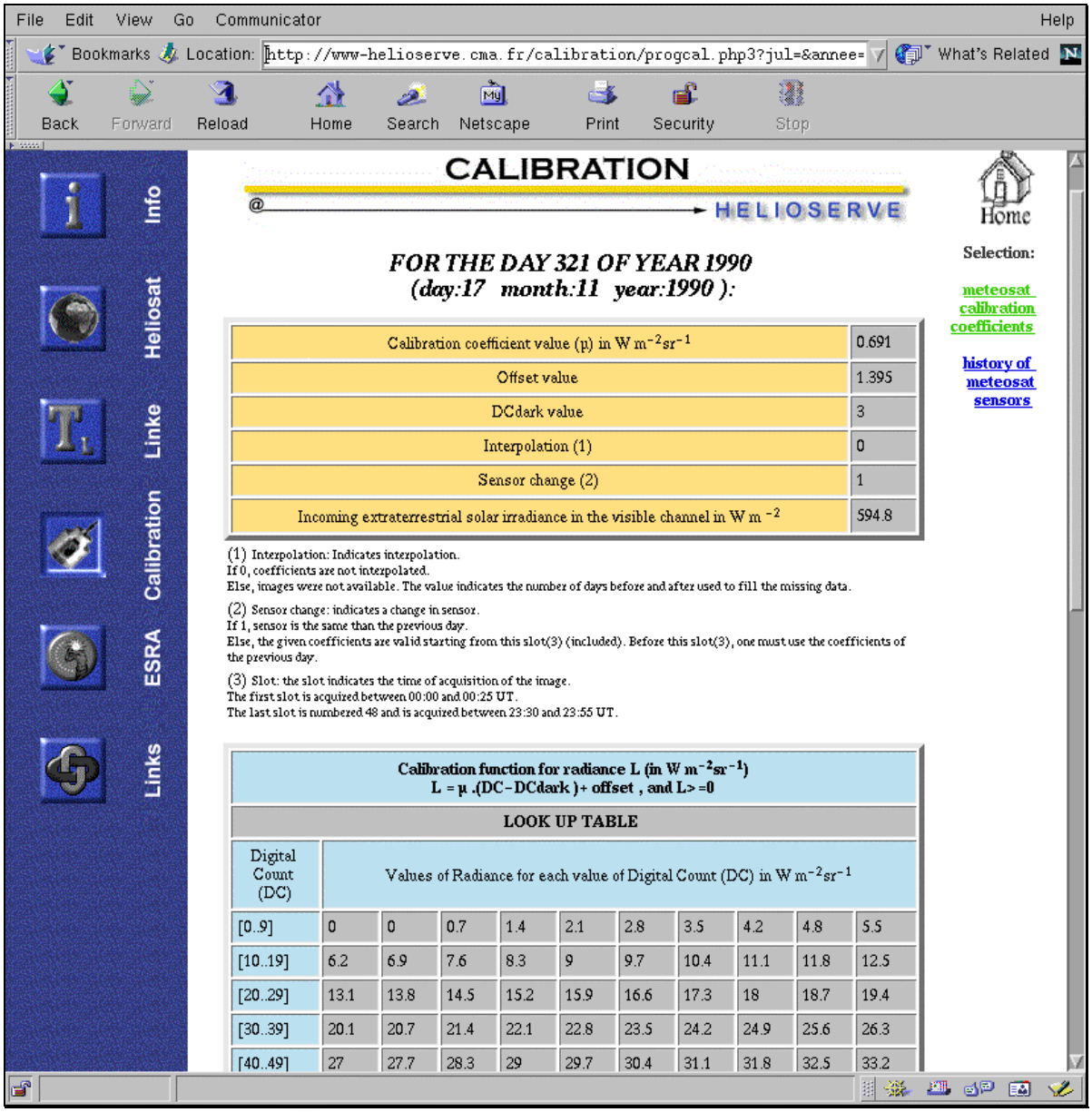

Figure 5.14. HTML page showing the answer to a query for a given day

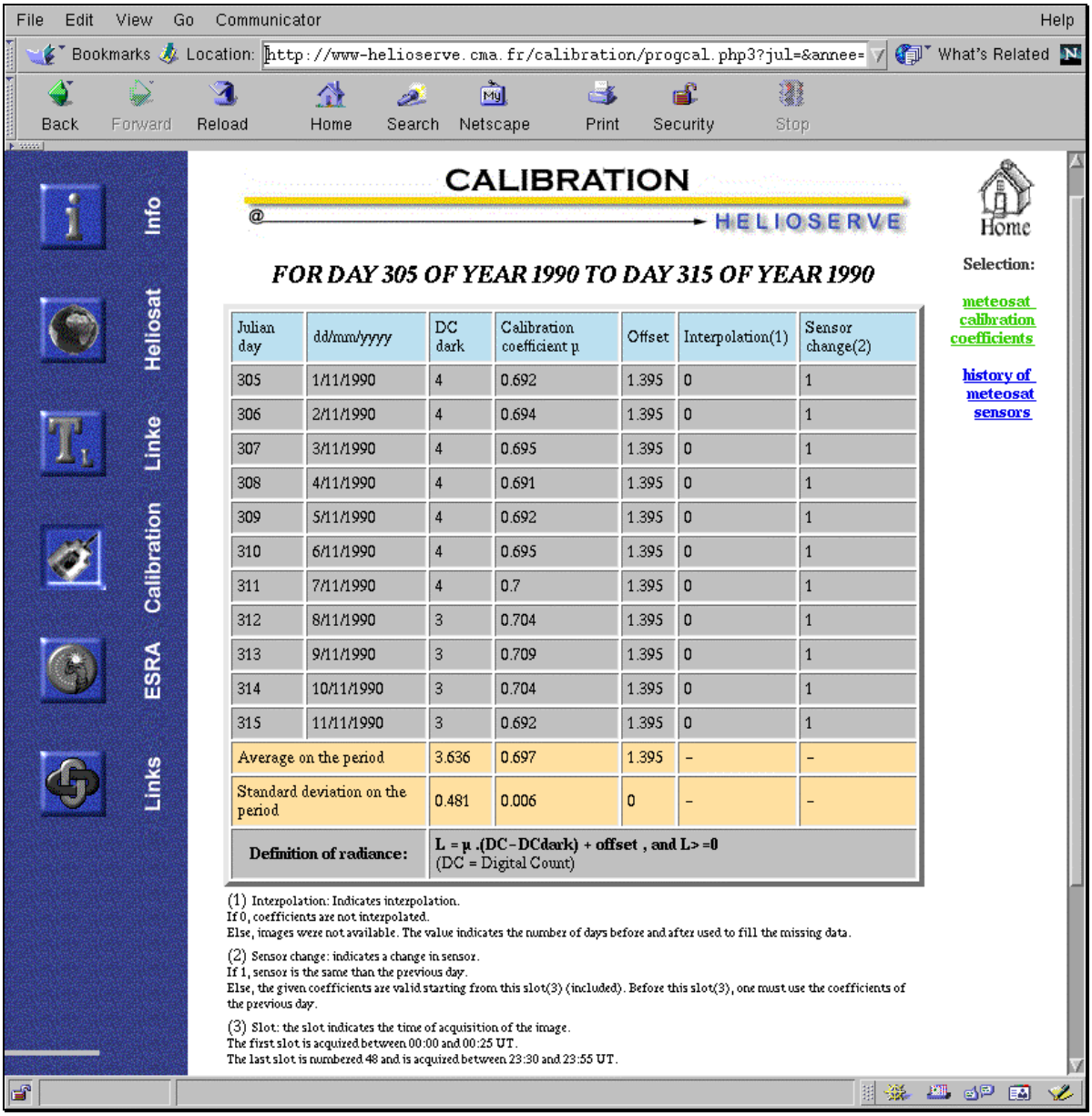

FOR DAY 305 OF YEAR 1990 TO DAY 315 OF YEAR 1990

Julian day	dd/mm/yyyy	DC dark	Calibration coefficient μ	Offset	Interpolation(1)	Sensor change(2)
305	1/11/1990	4	0.692	1.395	0	1
306	2/11/1990	4	0.694	1.395	0	1
307	3/11/1990	4	0.695	1.395	0	1
308	4/11/1990	4	0.691	1.395	0	1
309	5/11/1990	4	0.692	1.395	0	1
310	6/11/1990	4	0.695	1.395	0	1
311	7/11/1990	4	0.7	1.395	0	1
312	8/11/1990	3	0.704	1.395	0	1
313	9/11/1990	3	0.709	1.395	0	1
314	10/11/1990	3	0.704	1.395	0	1
315	11/11/1990	3	0.692	1.395	0	1
Average on the period		3.636	0.697	1.395	-	-
Standard deviation on the period		0.481	0.006	0	-	-
Definition of radiance:		**L = μ .(DC−DCdark) + offset , and L> =0** (DC = Digital Count)				

(1) Interpolation: Indicates interpolation.
If 0, coefficients are not interpolated.
Else, images were not available. The value indicates the number of days before and after used to fill the missing data.

(2) Sensor change: indicates a change in sensor.
If 1, sensor is the same than the previous day.
Else, the given coefficients are valid starting from this slot(3) (included). Before this slot(3), one must use the coefficients of the previous day.

(3) Slot: the slot indicates the time of acquisition of the image.
The first slot is acquired between 00:00 and 00:25 UT.
The last slot is numbered 48 and is acquired between 23:30 and 23:55 UT.

Figure 5.15. HTML page showing the answer to a query for a given period

6 MODELLING THE CLEAR-SKY RADIATION

Iehlé *et al.* (1997) and Rigollier (2000) showed the importance of the model used for modelling the clear-sky irradiation. The better the accuracy of the model, the better the accuracy of the estimate performed by the method Heliosat. Using different models, these authors found discrepancies larger than 200 Wh m^{-2} between the retrieved values of hourly global irradiation. The clearer the skies, the larger the discrepancies.

The input parameters of the clear-sky model to be used in the Heliosat II method should be known for every pixel of the Meteosat image and for each acquisition time. Many models exist but only a few meet such a constraint. This was underlined by Moussu *et al.* (1989) and was one of the reasons to select the model of Perrin de Brichambaut and Vauge (PdBV). However such models are too simple and do not offer enough accuracy permitting to increase the accuracy of the retrieved irradiation. Iehlé *et al.* (1997) and Fontoynont *et al.* (1997) found that replacing the clear-sky model PdBV by others using the Linke turbidity factor $T_L(AM2)$ (air mass of 2) leads to better results. $T_L(AM2)$ is a simple parameter to use, which characterises the optical attenuation of the clear atmosphere. It is known for a limited number of sites but global models exist that provide approximate values for any location in the world, such as that of Dogniaux and Lemoine (1983), Molineaux *et al.* (1995) or Perrin de Brichambaut and Vauge (1982).

In the framework of the project SoDa, Rigollier *et al.* (2000) study the clear sky models of the 4th European Solar Radiation Atlas (ESRA 1999) with respect to the Heliosat method, and compared it to several other models and to ground measurements. This published study was completed for additional measurements. and by the comparison between the ESRA models and that of Kasten (1990), used in the previous editions of the European Solar Radiation Atlas (ESRA, 1984) and also used by the partner Meteotest in its commercial product MeteoNorm (2000). The ESRA models have been compared to several other clear-sky models, included those used by the partners ENTPE and EHF in their advanced versions of Heliosat I. Well quality-controlled measurements performed by reliable meteorological stations were used for that purpose. They spanned over several years and comprised measurements of the global, direct and diffuse hourly irradiation. These ESRA models have proved to be the most accurate as a whole, though other models lead to similar results. The authors investigated the variations of these ESRA models with various parameters, namely the sun elevation and the Linke turbidity factor. They concluded that these models could be used in the framework of the Heliosat method.

The ESRA proposes two sets of models, each providing the global value G and the beam B and the diffuse D components. One is best suited for the assessment of the irradiance. The other should be preferred for the computation of hourly irradiation and daily sum of irradiation. Figure 6.1 displays the global irradiance simulated by the ESRA model for irradiance and the MeteoNorm / Kasten model for several values of the Linke turbidity factor. For large values of $T_L(AM2)$ the models act very similarly. For lower $T_L(AM2)$ (2 or 3, very clear skies), the estimate given by MeteoNorm is smaller than that of the ESRA (difference of 100 W.m^{-2} at zenith for $T_L(AM2) = 2$, that is 10 %). This implies an under-estimation of the radiation for clear-skies. Iehlé *et al.* (1997) confirmed these findings; they found a higher bias

with the Kasten model than with the ESRA model when including these models in modified versions of the Heliosat I method.

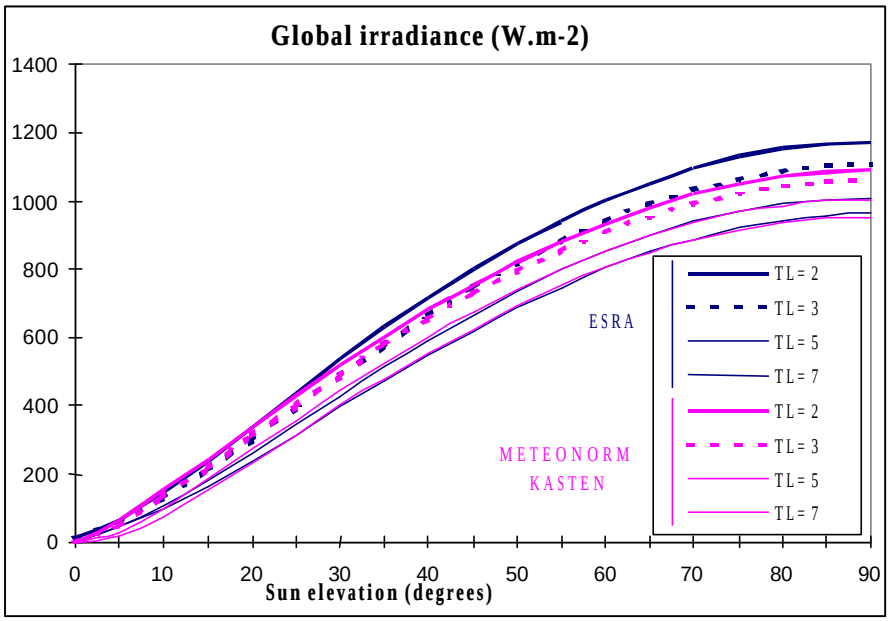

Figure 6.1. Comparison between the global irradiance simulated by the ESRA model for irradiance and the MeteoNorm / Kasten model for several values of the Linke turbidity factor.

These studies strongly encourage the introduction of the ESRA models in the Heliosat-II method. The accuracies of these models are among the best, and their robustness (*i.e.*, the constancy of their performances with respect to different conditions) are a clear advantage with the aim of producing a robust method. The accuracy (RMSE) in the assessment of the diffuse hourly irradiation ranges from 11 Wh m^{-2} to 35 Wh m^{-2} for diffuse irradiations up to 250 Wh m^{-2}.

Compared to the other models used up to now in the Heliosat method, the accuracy in the ESRA model is mostly gained by the introduction of the Linke turbidity factor. From an operational point of view, the use of the ESRA model implies the knowledge at each pixel of the image, of the Linke turbidity factor and of the ground elevation.

Digital maps of ground elevation are currently available for the whole Earth with a spatial resolution suitable for the processing of images from the meteorological satellites (e.g., that of the U.S. Geological Survey: *http://edcdaac.usgs.gov/gtopo30/gtopo30.html*). Accuracy elevation may be questioned in several parts of such maps. However the impact of this accuracy on the outputs of the ESRA model is less than the impact of an error on $T_L(AM2)$. This factor is not known everywhere and an effort should be devoted to its assessment at each pixel of the image, at least on a climatological basis, season by season.

The ESRA models have been coded in language C and can be run in the WWW site Helioserve: *www-helioserve.cma.fr*. In this site, user can already simulate the clear-sky irradiation, given the geographical site, the elevation and the Linke turbidity factor.

6.1 The horizontal global irradiance under cloudless skies

6.1.1 The beam component

In this model, the global horizontal irradiance for clear sky, G_c, is split into two parts: the direct component, B_c, and the diffuse component, D_c. Each component is determined separately. The unit for irradiance is W m^{-2}. The direct irradiance on a horizontal surface (or beam horizontal irradiance) for clear sky, B_c, is given by:

$$B_c = I_0 \, \varepsilon \sin \gamma_S \; \exp(-0{,}8662 \; T_L(AM2) \; m \; \delta_R(m)) \qquad (6.1)$$

The quantity:

$$\exp(-0{,}8662 \; T_L(AM2) \; m \; \delta_R(m)) \qquad (6.2)$$

represents the beam transmittance of the beam radiation under cloudless skies. The relative optical air mass m expresses the ratio of the optical path length of the solar beam through the atmosphere to the optical path through a standard atmosphere at sea level with the sun at the zenith. As the solar altitude decreases, the relative optical path length increases. The relative optical path length also decreases with increasing site height above the sea level, z. A correction procedure is applied, obtained as the ratio of mean atmospheric pressure, p, at the site elevation, to mean atmospheric pressure at sea level, p_0. This correction is particularly important in mountainous areas. The relative optical air mass has no unit; it is given by Kasten, Young (1989), where γ_s^{true} is in degrees:

$$m(\gamma_s^{true}) = \frac{p/p_0}{\sin\gamma_s^{true} + 0.50572 \; (\gamma_s^{true} + 6.07995)^{-1.6364}} \qquad (6.3)$$

with the station height correction given by:

$$p/p_0 = \exp(-z/z_h) \qquad (6.4)$$

where z is the site elevation and z_h is the scale height of the Rayleigh atmosphere near the Earth surface, equal to 8434,5 meters.

The solar altitude angle, γ_s^{true}, is corrected for refraction:

$$\gamma_s^{true} = \gamma_s + \Delta\gamma_{refr} \qquad (6.5)$$

$$\Delta\gamma_{refr} = 0{,}061359\,(180/\pi)\,\frac{0{,}1594 + 1{,}1230\,(\pi/180)\gamma_S + 0{,}065656\,(\pi/180)^2\gamma_S^{\,2}}{1 + 28{,}9344\,(\pi/180)\gamma_S + 277{,}3971\,(\pi/180)^2\gamma_S^{\,2}}$$

The Rayleigh optical thickness, δ_R, is the optical thickness of a pure Rayleigh scattering atmosphere, per unit of air mass, along a specified path length. As the solar radiation is not monochromatic, the Rayleigh optical thickness depends on the precise optical path and hence on relative optical air mass, m. The parameterisation used is the following (Kasten, 1996):

if $m \leq 20$ ($\gamma_S \geq 1{,}9°$), $1 / \delta_R(m) = 6{,}6296 + 1{,}7513\, m - 0{,}1202\, m^2 + 0{,}0065\, m^3 - 0{,}00013\, m^4$

if $m > 20$ ($\gamma_S < 1{,}9°$), $1 / \delta_R(m) = 10{,}4 + 0{,}718\, m$

The discrepancy between both formula at $m=20$ is equal to $1{,}6.10^{-2}$, which is negligible (less than 0,1 per cent of $1/\delta_R(m)$).

All the variation of the beam transmittance with air mass is included in the product $m\,\delta_R(m)$. Figure 6.2 displays the beam transmittance and irradiance for $p=p_0$ (sea level), and for different values of turbidity factor ($T_L(AM2)$ = 2, 3, 5, 7), as a function of solar elevation γ_S.

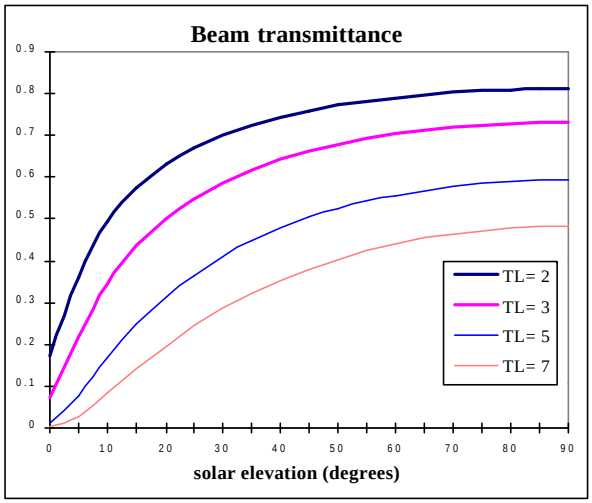

Fig. 6.2a. *The beam transmittance for clear sky*

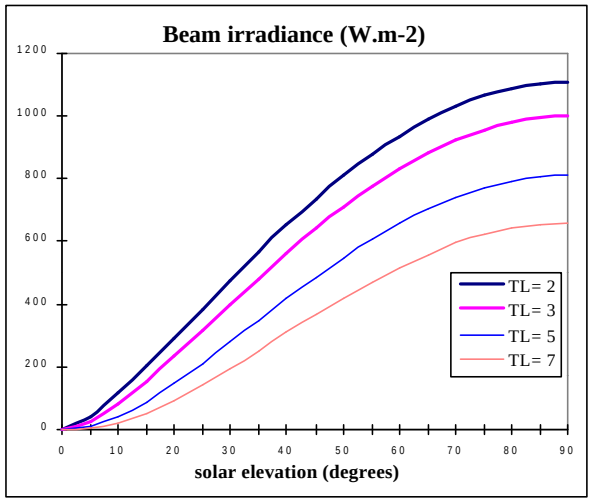

Fig. 6.2b. *The beam horizontal irradiance for clear sky, B_c*

6.1.2 The diffuse component

The diffuse irradiance falling on a horizontal surface for clear sky (or diffuse horizontal irradiance), D_c, also depends on the Linke turbidity factor, $T_L(AM2)$, at any solar elevation. In fact, the proportion of the scattered energy in the atmosphere increases as the turbidity increases, and as the beam irradiance falls, the diffuse irradiance normally rises. At very low solar altitudes and high turbidity, however, the diffuse irradiance may fall with turbidity increase due to high overall radiative energy loss in the atmosphere associated with long path length. Thus, the diffuse horizontal irradiance, D_c, is determined by:

$$D_c = I_0\, \varepsilon\, T_{rd}\left(T_L\left(AM2\right)\right) F_d\left(\gamma_s, T_L(AM2)\right) \qquad (6.6)$$

In this equation, the diffuse radiation is expressed as the product of the diffuse transmission function at zenith (i.e. sun elevation is 90°), T_{rd}, and a diffuse angular function, F_d.

$$T_{rd}(T_L(AM2)) = -1{,}5843\ 10^{-2} + 3{,}0543\ 10^{-2}\ T_L(AM2) + 3{,}797\ 10^{-4}\ [T_L(AM2)]^2 \qquad (6.7)$$

For very clear sky, the diffuse transmission function is very low: there is almost no diffusion, but by the air molecules. As the turbidity increases, the diffuse transmittance increases while the direct transmittance decreases. Typically, T_{rd} ranges from 0,05 for very clear sky ($T_L(AM2)=2$) to 0.,2 for very turbid atmosphere ($T_L(AM2)=7$). Figure 6.3 displays T_{rd} as a function of $T_L(AM2)$. The diffuse angular function, F_d, depends on the solar elevation angle and is fitted with the help of second order sine polynomial functions:

$$F_d(\gamma_S, T_L(AM2)) = A_0 + A_1 \sin(\gamma_S) + A_2\, [\sin(\gamma_S)]^2 \qquad (6.8)$$

The coefficients A_0, A_1, and A_2, only depend on the Linke turbidity factor. They are unitless and are given by:

$$A_0 = 2{,}64631\ 10^{-1} - 6{,}1581\ 10^{-2}\ T_L(AM2) + 3{,}1408\ 10^{-3}\ [T_L(AM2)]^2$$

$$A_1 = 2{,}0402 + 1{,}89451\ 10^{-2}\ T_L(AM2) - 1{,}1161\ 10^{-2}\ [T_L(AM2)]^2$$

$$A_2 = -1{,}3025 + 3{,}9231\ 10^{-2}\ T_L(AM2) + 8{,}5079\ 10^{-3}\ [T_L(AM2)]^2$$

with a condition on A_0:

$$\text{if } (A_0\ T_{rd}) < 2\ 10^{-3} \text{ then } A_0 = 2\ 10^{-3} / T_{rd} \qquad (6.10)$$

This condition is required because A_0 yields negative values for $T_L(AM2)>6$. It was therefore decided to impose this limiting condition to achieve acceptable values at sunrise and sunset.

The diffuse function is represented in Figure 6.4. One can note that F_d is not exactly equal to 1 for $g_S = 90°$. Equations suggest that this should be the case, whatever the turbidity. The model can be improved on that point.

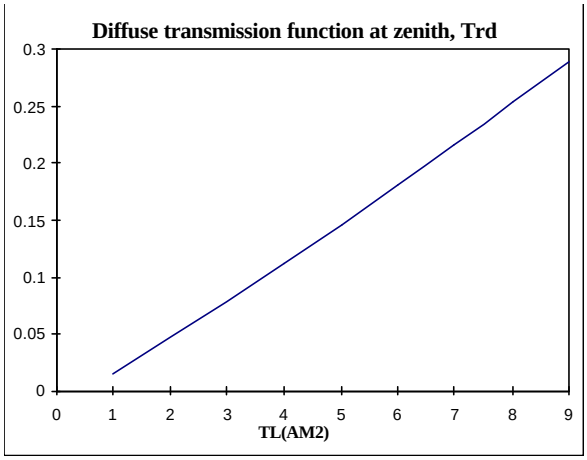

Fig. 6.3 *The diffuse transmission function at zenith, T_{rd}, as a function of the Linke turbidity factor.*

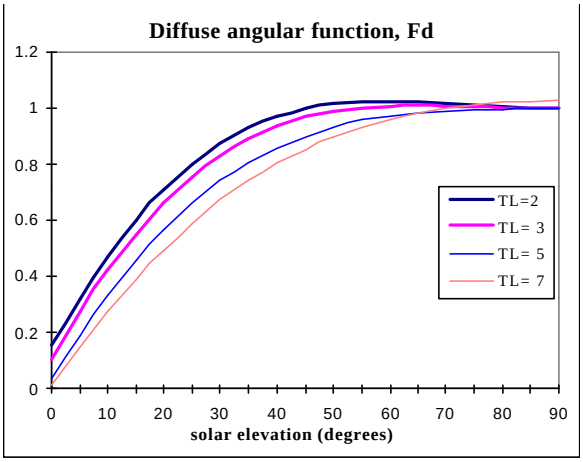

Fig. 6.4 *The diffuse solar zenith function, F_d*

Once F_d computed, the diffuse horizontal irradiance, D_c can be determined. It is displayed in Figure 6.5 for several Linke turbidity factors, as a function of the solar elevation. D_c clearly increases as the turbidity increases, due to the increase in scattering by the aerosols. As already mentioned, it may be the opposite at very low solar altitudes and high turbidity.

The direct and diffuse irradiances under cloudless sky conditions are summed to yield the global clear sky horizontal irradiance, which is represented in Figure 6.6. The global irradiance decreases as the turbidity increases and as the solar elevation decreases. It is not equal to 0 at sunset or sunrise because of the diffuse component, which is still noticeable while the sun is below the horizon.

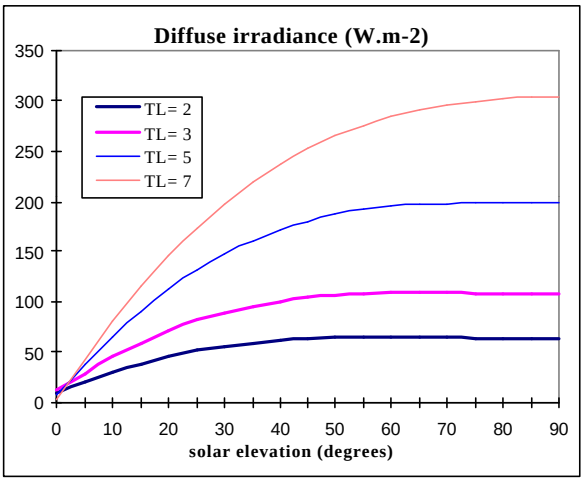

Figure 6.5. *The diffuse horizontal irradiance for clear sky, D_c*

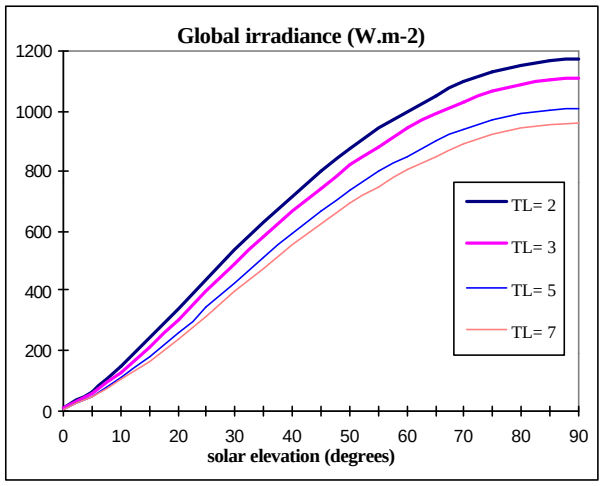

Fig. 6.6 *The global horizontal irradiance for clear sky, G_c*

6.2 The horizontal global irradiation under cloudless skies

6.2.1 The beam component

Once m, $T_L(AM2)$, and $\delta_R(m)$ are known, the beam horizontal irradiation for clear sky can be evaluated for any part of the day by numerical integration of the irradiance B_c using suitable time steps. The site, however, may be partially obstructed and/or the beam may not shine on a certain surface of interest for part of the time period inspected. Using a range of techniques, like shading masks on solar charts, it is possible to identify the periods of day during which the beam will actually reach the surface. The numerical integration can be adjusted for this, but the task becomes easier if the solutions can be assessed analytically rather than numerically. Thus the beam irradiance B_c has been reformulated and constructed by data fitting techniques to provide a $T_L(AM2)$-dependent output that can be handled with ease analytically. Rigollier *et al.* (2000) show that both formulations are equivalent. The differences are small, they do not exceed 18 W m^{-2}. The new form is:

$$B_c = I_0 \, \varepsilon \, T_{rb}(T_L(AM2)) \, F_b(\gamma_S, T_L(AM2)) \qquad (6.11)$$

where $T_{rb}(T_L(AM2))$ is a transmission function for beam radiation at zenith and F_b is a beam angular function. B_c is set to 0 if the equation leads to a negative value. The computation of T_{rb} is made for $\gamma_s = \pi/2$. In this case, $m = p/p_0$. Thus, T_{rb} is only dependent on $T_L(AM2)$ and on p/p_0, which is determinated by the site elevation:

$$T_{rb}(T_L(AM2)) = \exp[-0{,}8662 \, T_L(AM2) \, (p/p_0) \, \delta_R(p/p_0)] \qquad (6.12)$$

$F_b(\gamma_S, T_L(AM2))$ has the form of a second order polynomial, with coefficients solely dependent on $T_L(AM2)$:

$$F_b(\gamma_S, T_L(AM2)) = C_0 + C_1 \sin(\gamma_S) + C_2 \sin^2(\gamma_S) \qquad (6.13)$$

These equations correspond to a re-writing of the beam irradiance, using the form used for the diffuse irradiance. Setting $F_b(g_S, T_L(AM2))$ to 0 or very close to 0 may produce negative values at high turbidities. This situation arises only at very low altitudes and results of the imperfect fit by the polynomials. To increase the accuracy of the fits at very low solar elevation, the values of the coefficients C_0, C_1 and C_2 were computed for three ranges of the solar altitude angle at noon, g_s^{noon}: below 15°, between 15° and 30°, and over 30°. Thus, the polynomials take the form:

$$\begin{cases} C_0 = L_{00} + L_{01}T_L(AM2)(p/p_0) + L_{02}\left[T_L(AM2)(p/p_0)\right]^2 \\ C_1 = L_{10} + L_{11}T_L(AM2)(p/p_0) + L_{12}\left[T_L(AM2)(p/p_0)\right]^2 \\ C_2 = L_{20} + L_{21}T_L(AM2)(p/p_0) + L_{22}\left[T_L(AM2)(p/p_0)\right]^2 + L_{23}\left[T_L(AM2)(p/p_0)\right]^3 \end{cases} \quad (6.14)$$

with the L_{ij} coefficients listed in Table 6.1 for the three considered ranges. These coefficients, as well as the coefficients C_i, B_i, and D_i (see further) are unitless.

C_0	L_{00}	L_{01}	L_{02}
$g_s^{noon} > 30^0$	-1,7349.10^{-2}	-5,8985.10^{-3}	6,8868.10^{-4}
$15^0 < g_s^{noon} \leq 30^0$	-8,2193.10^{-3}	4,5643.10^{-4}	6,7916.10^{-5}
$g_s^{noon} \leq 15^0$	-1,1656.10^{-3}	1,8408.10^{-4}	-4,8754.10^{-7}

C_1	L_{10}	L_{11}	L_{12}
$g_s^{noon} > 30^0$	1,0258	-1,2196.10^{-1}	1,9229.10^{-3}
$15^0 < g_s^{noon} \leq 30^0$	8,9233.10^{-1}	-1,9991.10^{-1}	9,9741.10^{-3}
$g_s^{noon} \leq 15^0$	7,4095.10^{-1}	-2,2427.10^{-1}	1,5314.10^{-2}

C_2	L_{20}	L_{21}	L_{22}	L_{23}
$g_s^{noon} > 30^0$	-7,2178.10^{-3}	1,3086.10^{-1}	-2,8405.10^{-3}	0
$15^0 < g_s^{noon} \leq 30^0$	2,5428.10^{-1}	2,6140.10^{-1}	-1,7020.10^{-2}	0
$g_s^{noon} \leq 15^0$	3,4959.10^{-1}	7,2313.10^{-1}	-1,2305.10^{-1}	5,9194.10^{-3}

Table 1 *Coefficients L_{ij} for the computation of the C_i coefficients.*

Finally, the analytical integral of the beam irradiation for a period ranging from solar hour angles w_1 to w_2, takes the form:

$$B_c(w_1, w_2) = I_0 \, e \, T_{rb}(T_L(AM2)) \int_{w_1}^{w_2} F_b(g_S, T_L(AM2)) \left(\frac{Dl}{2p}\right) dw \quad (6.15)$$

where Dl is the length of the day and w_1 to w_2 are related to two instants t_1 and t_2. The unit of $B_c(w_1, w_2)$ is Wh m^{-2} if Dl is expressed in hours, or J m^{-2} if Dl is in seconds. In this equation,

$$F_b(g_S, T_L(AM2)) = C_0 + C_1 \sin(g_S) + C_2 \sin^2(g_S) \quad (6.16)$$

and can be re-written

$$F_b(w, F, d, T_L(AM2)) = B_0 + B_1 \cos w + B_2 \cos(2w) \qquad (6.17)$$

since

$$\sin g_S = \sin F \sin d + \cos F \cos d \cos w \qquad (6.18)$$

It comes

$$B_c(w_1, w_2) = I_0 \, e \left(\frac{Dl}{2p}\right) T_{rb}(T_L(AM2)) \left[B_0 w + B_1 \sin(w) + B_2 \sin(2w)\right]_{w_1}^{w_2} \qquad (6.19)$$

with the coefficients B_0, B_1 and B_2 given by:

$$\begin{cases} B_0 = C_0 + C_1 \sin(F)\sin(d) + C_2 \left[\sin(F)\right]^2 \left[\sin(d)\right]^2 + 0.5\, C_2 \left[\cos(F)\right]^2 \left[\cos(d)\right]^2 \\ B_1 = C_1 \cos(F)\cos(d) + 2C_2 \sin(F)\sin(d)\cos(F)\cos(d) \\ B_2 = 0.25\, C_2 \left[\cos(F)\right]^2 \left[\cos(d)\right]^2 \end{cases} \qquad (6.20)$$

where F is the latitude of the site and d is the declination. The B_i coefficients only depend on F and d. The transmission function T_{rb}, and the C_i coefficients only depend on $T_L(AM2)$. Thus, all these factors can be computed only once for each day. The daily integral is achieved by setting w_1 equal to the sunrise hour angle, w_{SR}, and w_2 to the sunset hour angle, w_{SR} *i.e.*:

$$B_{cd} = B_c(w_{SR}, w_{SS}) \qquad (6.21)$$

The daily beam irradiation at different latitudes (30° and 60°), B_{cd}, is displayed in Figure 6.7 for various turbidities, as a function of the julian day. The daily irradiation decreases as the turbidity increases. The distribution over the year of the daily irradiation is more peaked as the latitude increases, and as the turbidity decreases.

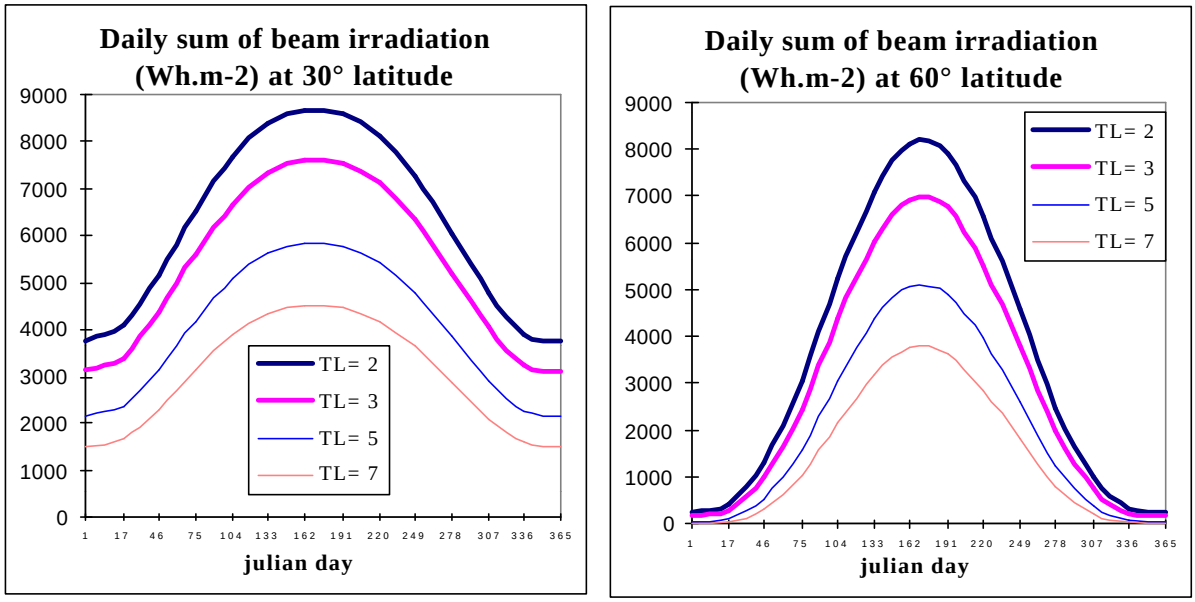

Fig. 6.7 *The daily beam horizontal irradiation for clear sky, B_{cd} computed at 30° and 60° latitude.*

6.2.2 The diffuse component

The diffuse horizontal irradiation, $D_c(w_1, w_2)$, is computed by the analytical integration of the diffuse irradiance over any period defined by w_1 and w_2, and is equal to:

$$D_c(w_1,w_2) = I_0\, e\left(\frac{Dl}{2p}\right) T_{rd}\left(T_L(AM2)\right)\left[D_0 w + D_1 \sin(w) + D_2 \sin(2w)\right]_{w_1}^{w_2} \qquad (6.22)$$

with the coefficients D_0, D_1 and D_2 given by:

$$\begin{cases} D_0 = A_0 + A_1 \sin(F)\sin(d) + A_2\left[\sin(F)\right]^2\left[\sin(d)\right]^2 + 0.5\, A_2\left[\cos(F)\right]^2\left[\cos(d)\right]^2 \\ D_1 = A_1 \cos(F)\cos(d) + 2A_2 \sin(F)\sin(d)\cos(F)\cos(d) \\ D_2 = 0.25\, A_2\left[\cos(F)\right]^2\left[\cos(d)\right]^2 \end{cases} \qquad (6.23)$$

where the A_i coefficients have been given previously. The daily integral is achieved by setting w_1 equal to the sunrise hour angle, w_{SR}, and w_2 to the sunset hour angle, w_{SS}, *i.e.*

$$D_{cd} = D_c(w_{SR}, w_{SS}) \qquad (6.24)$$

The daily diffuse irradiation at different latitudes (30° and 60°), D_{cd}, is displayed in Figure 6.8 for various turbidities, as a function of the julian day. The daily irradiation increases as the turbidity increases. The distribution over the year of the daily irradiation is more peaked as the latitude increases, and as the turbidity increases.

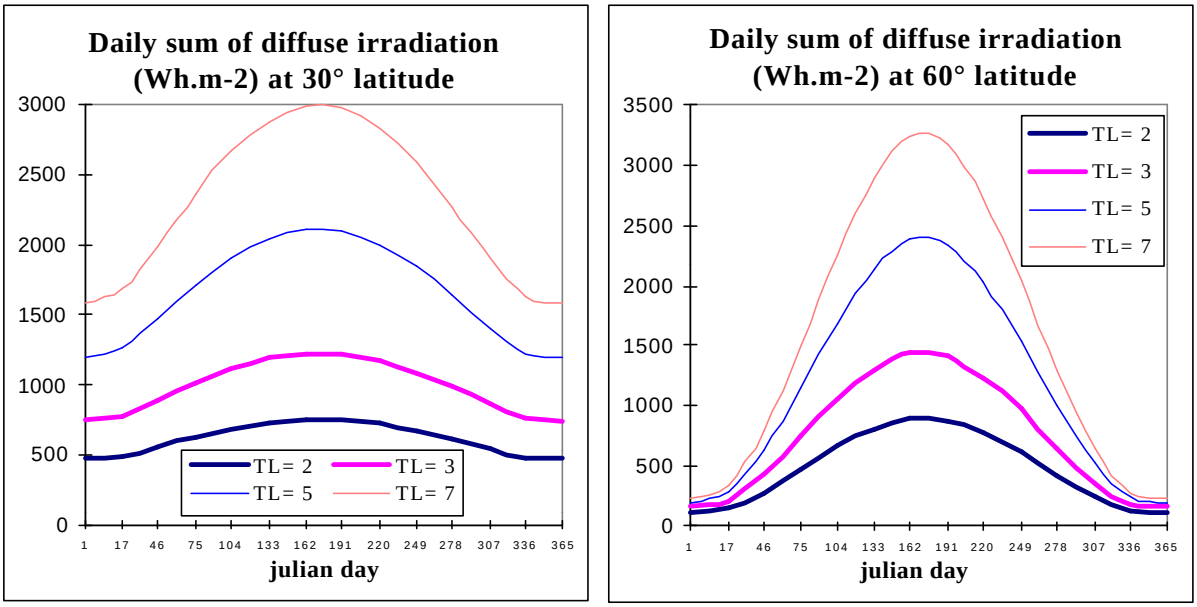

Fig. 6.8 *The daily diffuse horizontal irradiation for clear sky, D_{cd} computed at 30° and 60° latitude.*

6.2.3 The global irradiation

The global irradiation under clear sky is obtained as the sum of the beam and diffuse horizontal irradiations under clear sky between two instants t_1 and t_2.

$$G_c(w_1, w_2) = B_c(w_1, w_2) + D_c(w_1, w_2) \qquad (6.25)$$

The parameters w_1 and w_2 are respectively set to w_{SR} and w_{SS} for the computation of the daily global irradiation:

$$G_c(w_{SR}, w_{SS}) = B_c(w_{SR}, w_{SS}) + D_c(w_{SR}, w_{SS}) \;\hat{U}\; G_{cd} = B_{cd} + D_{cd} \qquad (6.26)$$

The daily global irradiation at different latitudes (30° and 60°), G_{cd}, is displayed in Figure 6.9 for various turbidities, as a function of the julian day. The daily irradiation decreases as the turbidity increases. The distribution over the year of the daily irradiation is more peaked as the latitude increases, and as the turbidity decreases.

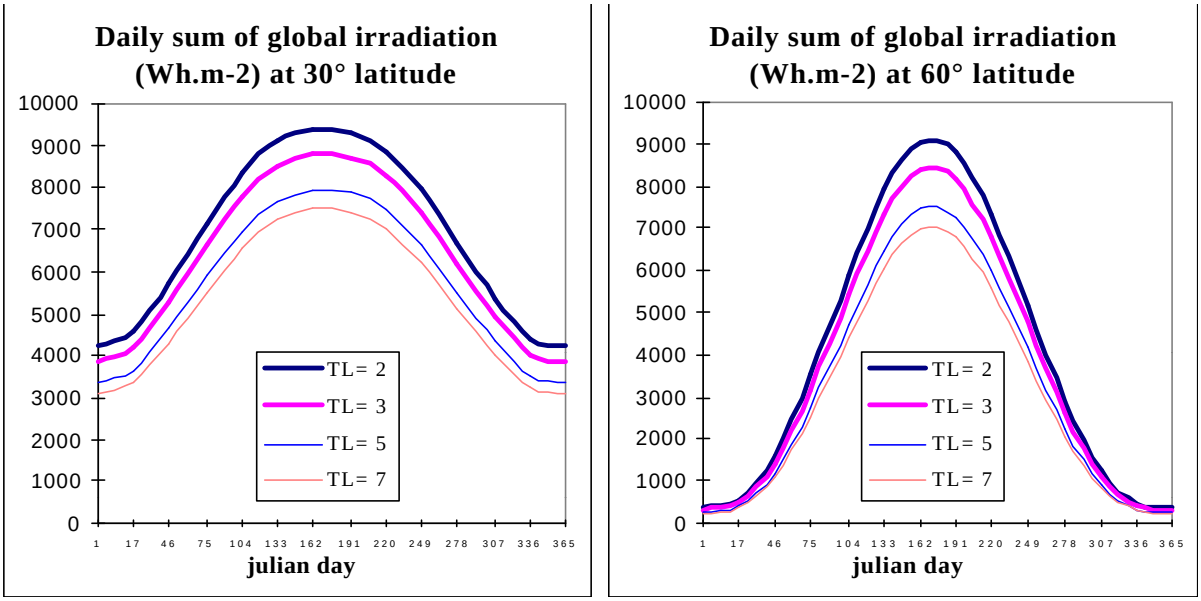

Fig. 6.9 *The daily sum of global horizontal irradiation for clear sky, G_{cd} computed at 30° and 60° latitude.*

7 THE CLOUD INDEX

A key parameter in the principles of the methods Heliosat-I and -II, is the cloud index *n*, resulting from a comparison of what is observed by the sensor to what should be observed over that pixel if the sky were clear, which is related to the "clearness" of the atmosphere. In principle, it can be written as:

$$n^t(i,j) = [\rho^t(i,j) - \rho^t_g(i,j)] / [\rho^t_{cloud} - \rho^t_g(i,j))] \qquad (7.1)$$

where

- $\rho^t(i,j)$ is the reflectance, or apparent albedo, observed by the spaceborne sensor for the time t and the pixel (i,j): $\rho^t(i,j) = \frac{\pi L^t(i,j)}{I_{0met}\, \varepsilon(t) \cos\theta_S(t,i,j)}$, where $L^t(i,j)$ is the observed radiance,
- $\rho^t_{cloud}(i,j)$ is the apparent albedo over the brightest clouds,
- and $\rho^t_g(i,j)$ is the apparent albedo over the ground under clear skies.

The computation of n^t is pending to the determination of the reflectances or apparent albedoes ρ^t_g and ρ^t_{cloud}. In turn, these reflectances are computed from the analysis of a time-series of the reflectance observed by the sensor ρ^t.

The reflectance observed by the sensor ρ^t under clear skies is a function of the reflectance of the ground, ρ^t_g, the sun zenithal angle, θ_S, the viewing angle,θ_v, and the difference, γ, of the sun and satellite azimuthal angles. At the first order, given the large size of the pixel, the multiple reflection and scattering effects are negligible. Assuming a Lambertian ground, the reflectance observed by the sensor is (Tanré *et al.* 1990):

$$\rho^t(i,j) = \rho^t_{atm}(\theta_S, \theta_v, \gamma) + \rho^t_g(i,j)\, T^t(\theta_S)\, T^t(\theta_v) \qquad (7.2)$$

where $\rho^t_{atm}(\theta_S, \theta_v, \gamma)$ is the intrinsic reflectance of the atmosphere, caused by the scattering of the incident and upward radiation towards the sensor. The parameters $T^t(\theta_S)$ and $T^t(\theta_v)$ are the global transmittances of the atmosphere for the incident and upward radiation. The global transmittance is the sum of the direct (or beam) and diffuse transmittance. The principle of reciprocity implies that the same formulation applies to both transmittances.

Numerous works show that the ground is not exactly of Lambertian nature. Vermote *et al.* (1994) propose several bi-directional models to consider these effects in the simulation of $\rho^t(i,j)$. From an operational point of view, the method Heliosat-II cannot consider these effects by lack of information. In particular, it would imply the knowledge of the landuse for each pixel of the field of view of the satellite Meteosat and of the associated model.

The influence of the sun zenithal angle θ_S is important as is that of the Linke turbidity factor, which affects the transmittance. The air mass increases with θ_S, causing an increase of the intrinsic reflectance of the atmosphere ρ^t_{atm}. The transmittance decreases as the turbidity increases, or similarly as the visibility decreases. Simulations of the radiative transfer in the atmosphere for the Meteosat case were performed by the Modtran model (Kneizys *et al.*, 1996). The inputs were the standard atmosphere US 1976 with maritime aerosols and three

values of visibility: 5, 23 and 50 km. The date of 11 May was selected. Four ground albedoes were used: 0,003, 0,05, 0,2 and 0,3; the ground is Lambertian. Nine sites of diverse latitudes: 40, 50 and 60° N, and diverse longitudes: 0, 10 and 20° E, were simulated in the field of view of the Meteosat sensor, every three hours in Universal Time, starting at 0900 UT. The figure 7.1 displays the simulated reflectance ρ at sensor level, or apparent albedo, as a function of the sun zenithal angle θ_S for various visibilities and albedoes and for the nine sites. As θ_S increases, the reflectance ρ increases. This is due to the increase of the intrinsic reflectance of the atmosphere, ρ_{atm}, and the effect is more pronounced for the objects of low albedo and for low visibility. The visibility influences the apparent albedo, which increases as the visibility decreases.

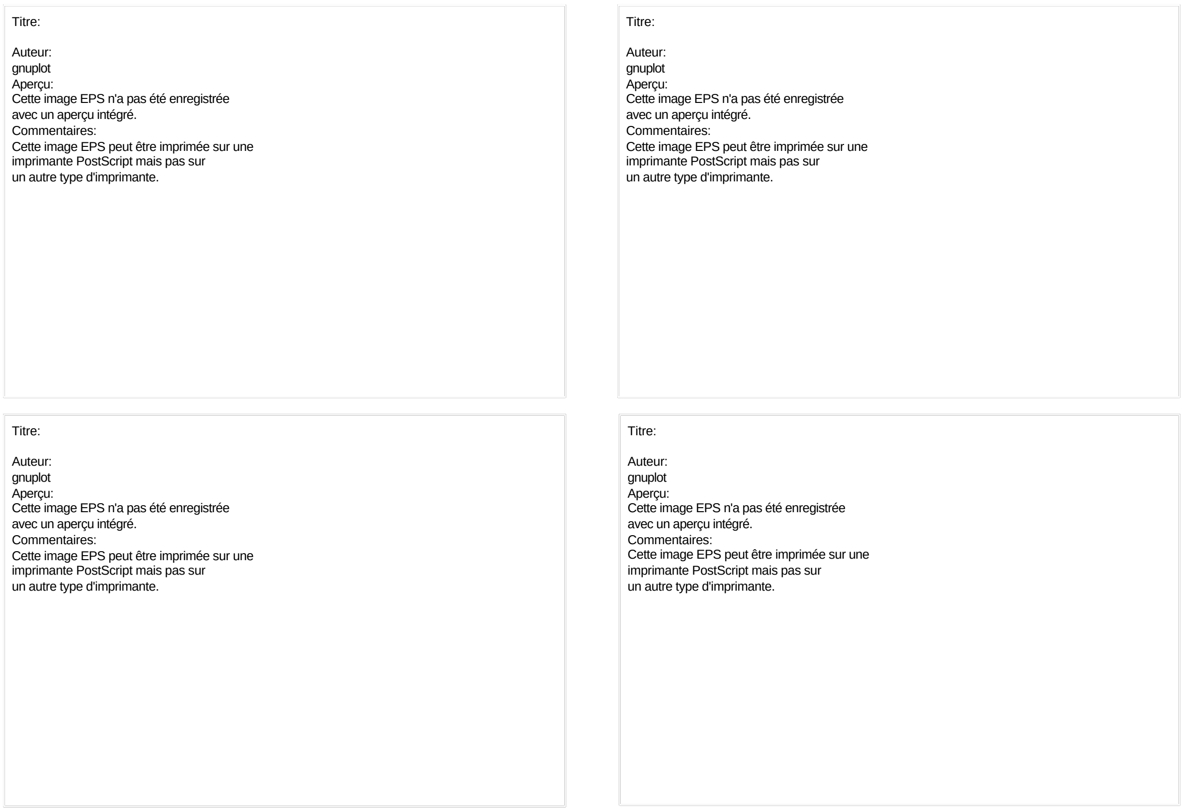

Figure 7.1. Simulation of the apparent albedo as a function of the sun zenithal angle θ_S for various visibilities (50, 23 and 5 km) and various albedoes: 0,003 (upper left), 0,05 (upper right), 0,2 (lower left) and 0,3 (lower right)

The difference, ψ, of the sun and satellite azimuthal angles impacts on the reflectance observed by the sensor, though it is less important than the sun zenithal angle. Figure 7.2 exhibits the reflectance observed by the sensor as a function of ψ, for various visibilities, ground albedoes and latitudes.

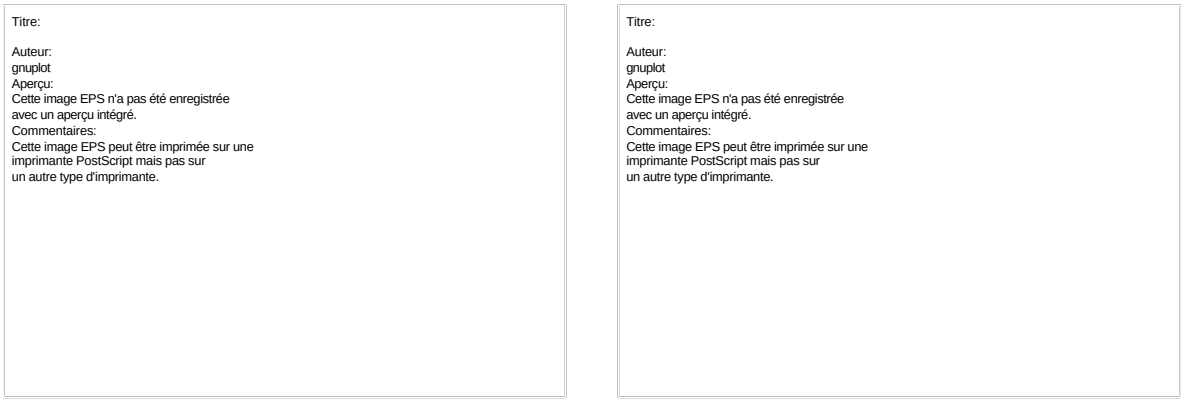

Figure 7.2. *Simulation of the apparent albedo as a function of* ψ *for various visibilities: 50 (left) and 5 km (right) and various albedoes: 0,003, 0,05, 0,2 and 0,3*

7.1 The determination of the apparent ground albedo in the method Heliosat-I

The method Heliosat-I does not comprise the absolute calibration of the outputs of the sensor. It is thus impossible to compute reflectances but the outputs were normalised in order to obtain a quantity proportional or similar to an albedo. The normalisation procedure varies according to the versions of the method Heliosat-I. Cano *et al*. (1986) and Diabaté *et al*. (1988) normalise the numerical counts of the sensor as:

$$CN^{*t}(i,j) = (CN^{t}(i,j) - CN0^{t}) / [I_0\, \varepsilon(t)\, (\cos \theta_S(i,j))\, (\cos \theta_S(i,j))^{0,15}] \qquad (7.3)$$

where $CN^{*t}(i,j)$ is the normalised count, $CN^{t}(i,j)$ is the numerical count observed by the sensor at time t for this pixel (i, j), $CN0^{t}$ being what can be called the sensor zero, and $(\cos \theta_S)^{0,15}$ is the clear sky transmittance (model of Perrin de Brichambaut, Vauge 1982).

Moussu *et al*. (1989) take into account the transmittance of the upwards radiation ($(\cos \theta_v)^{0,15}$) and the non-Lambertian nature of the ground ($\cos \theta_v$) and write:

$$CN^{*t}(i,j) = (CN^{t}(i,j) - CN0^{t}) / [I_0\, \varepsilon(t)\, (\cos \theta_S)^{1,15}\, (\cos \theta_v)^{1,15}] \qquad (7.4)$$

Taking into account that the relative factor of anisotropy of the clouds is not larger than 10 percent (Taylor, Stowe 1984), Bauer (1996) demonstrates that the correction in $\cos \theta_v$ is exaggerated. The very bright clouds of the intertropical convergence zone appear less bright than the low clouds far from the nadir. Similar conclusions were found by Obrecht (1990) when analysing the reflectances of the ocean.

Beyer *et al*. (1996) use the original procedure of Cano *et al*. (1986) and Diabaté *et al*. (1988) but correct the sensor zero to include the intrinsic contribution of the atmosphere to the signal observed by the sensor.

$$CN^{*t}(i,j) = (CN^{t}(i,j) - CN0'^{t}) / [I_0\, \varepsilon(t)\, (\cos \theta_S(i,j))^{1,15}] \qquad (7.5)$$

with $CN0' = CN0 + 4{,}5\, [1 + \cos^2 \psi\,]\, (\cos \theta_S)^{0,15} / (\cos \theta_V)^{0,8}$. The numerical coefficients were empirically defined using some Meteosat images of the Western Europe of August 1993. Hammer *et al*. (1997a, b) develop a similar relationship based on the observations of the

Northern Atlantic. The heuristic aspect remains. Other relationships were proposed by other authors to correct for the influence of the sun zenithal angle (Zelenka *et al.* 1999; Ineichen, Perez 2000). Rigollier (2000) analyses these relationships and conclude that they do not reproduce the expected behaviour displayed in the figures 7.1 and 7.2. She proposes a similar approach, including explicit formulations of the transmittance, but failed to obtain results that are more satisfactory.

7.2 Modelling the path reflectance and the atmospheric transmittance

Rigollier (2000) benefits from the capabilities of calibrating the sensor outputs and proposes another approach based upon the modelling of the intrinsic reflectance of the atmosphere, also called the path reflectance, and the atmospheric transmittance. The starting equation is the equation 7.2, recalled hereafter:

$$r^t(i,j) = r^t_{atm}(q_S, q_V, y) + r^t_g(i,j)\, T^t(q_S)\, T^t(q_V) \qquad (7.2)$$

Each term, r^t_{atm} and $T^t(q_S)$ or $T^t(q_V)$ will be modelled, resulting into the explicit formulation of r^t as a function of q_S, q_V, y and r^t_g. Inversely, this will permit to compute r^t_g and r^t_{cloud}.

Assuming that the scattering by the atmosphere is isotropic, it is conceivable that the path radiance L_{atm} reaching the sensor is proportional to the path radiance reaching the ground. This path radiance can be expressed using the expression of the diffuse irradiance under clear sky at ground level, D_c:

$$L_{atm} = (D_c / p)\, (I_{0met} / I_0)\, (<\cos q_V> / \cos q_V)^{0,8} \qquad (7.6)$$

The factor p permits to convert an irradiance D into a radiance. The ratio (I_{0met} / I_0) normalises the extraterrestrial irradiance to the Meteosat sensor case. Following Beyer *et al.* (1996), the ratio $(<\cos q_V> / \cos q_V)^{0,8}$ empirically corrects for the viewing angle without bias ($<\cos q_V>=0,5$).

This relationship was applied to the nine sites simulated using the model Modtran and in the case of an null albedo, for which the path radiance is the only contributor to the observed radiance. Figure 7.3 exhibits the path radiances simulated by the model Modtran (vertical axis) versus the path radiances estimated by the equation (7.6). The agreement between both formulations is satisfactory taking into account the limitations of the models. In particular, the Linke turbidity factor, an input to the equation (7.6), was set in order to approximately fit the visibility, an input to the model Modtran.

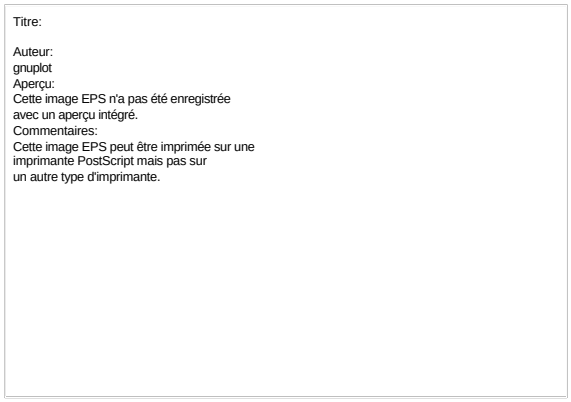

Figure 7.3. Path radiances simulated by the model Modtran (vertical axis) versus the path radiances estimated by the equation (7.6) (horizontal axis) for nine sites and two visibilities: 23 and 50 km

The ESRA model simulating the irradiance under clear skies provides an expression for the beam transmittance, $Tr_B(\theta_S)$, and the diffuse transmittance, $Tr_D(\theta_S)$:

$$Tr_B(\theta) = exp(-0{,}8662\ T_L(AM2)\ m\ \delta_r(m)) \qquad (7.7)$$

$$Tr_D(\theta) = T_{rd}(T_L(AM2))\ F_d(\theta_S, T_L(AM2))$$

where $T_{rd}(T_L(AM2))$ is the transmittance at zenith and $F_d(\theta_S, T_L(AM2))$ the angular correction.

According to the principle of reciprocity, the formulations of the downward and upward transmittances are identical:

$$T(\theta_S) = Tr_B(\theta_S) + Tr_D(\theta_S) \qquad (7.8)$$

$$T(\theta_v) = Tr_B(\theta_v) + Tr_D(\theta_v)$$

To validate our approach, we apply these formulae to the reflectances ρ^t simulated by the model Modtran for various ground albedoes and try to retrieve these ground reflectances ρ^t_g. We use the equations (7.2), (7.6) to (7.8) and:

$$\rho_g = [\ \rho\ -\ \rho_{atm}(\theta_S,\theta_v,\psi)\ ]\ /\ T(\theta_S)\ T(\theta_v) \qquad (7.9)$$

$$\rho_{atm}(\theta_S,\theta_v,\psi) = \pi\, L_{atm}\ /\ (I_{0met}\ \varepsilon \cos\theta_S)$$

Figure 7.4 displays the retrieved ground reflectances as a function of the sun zenithal angle for various cases. The results should be a constant value. This is almost achieved for the low albedo of 0,05 (the typical case of the ocean), whatever the visibility and the angle θ_S. As the ground albedo increases, discrepancies appear, especially for low visibility (large turbidity) and large zenithal angles. The case of the three sites located at 60° N for a visibility of 5 km and for a ground albedo of 0,33 demonstrates the limits of this approach. This case is exaggerated and we may conclude that the approach is satisfactory, provided it is restricted to zenithal angles less than 78°, as was the case with the method Heliosat-I (Diabaté 1989; Bauer 1996). It follows that the method Heliosat-II will be unable in principle to accurately estimate the irradiation north of the latitude 65° N, and south of the latitude 65° S.

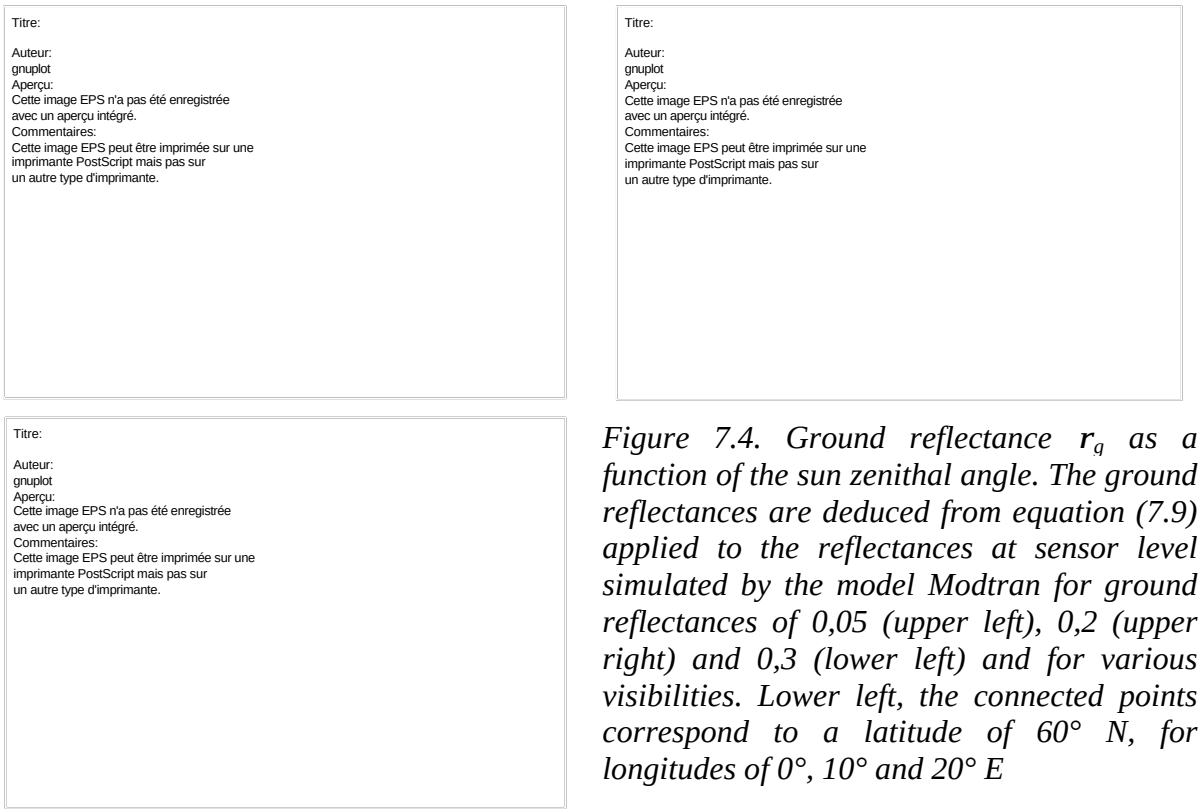

Figure 7.4. Ground reflectance ρ_g as a function of the sun zenithal angle. The ground reflectances are deduced from equation (7.9) applied to the reflectances at sensor level simulated by the model Modtran for ground reflectances of 0,05 (upper left), 0,2 (upper right) and 0,3 (lower left) and for various visibilities. Lower left, the connected points correspond to a latitude of 60° N, for longitudes of 0°, 10° and 20° E

Rigollier (2000) tested an additional correction in the form of $(1 + \cos^2 \gamma)$, which reminds of the Rayleigh law. She saw no improvement as the present approach seems to take into account most of the influence of the sun -satellite geometry upon the ground albedo.

7.3 The apparent ground albedo ρ_g

The apparent ground albedo $\rho_g(i,j)$ may then be defined from a time-series of Meteosat observations as follows. First, sensor outputs are converted into radiances $L^t(i,j)$. The analysis of several years of images from Meteosat shows that it happens that some pixels exhibit very low radiances, similar to those observed during the night, while the sun is well above the horizon. A constraint is imposed on radiances to avoid such cases; they should be greater than 3 percent of the maximal radiance that can be observed by the sensor:

$$L^t(i,j) \geq 0{,}03\, I_{0met}(t)/\pi + b(t) \qquad (7.10)$$

where $b(t)$ is the calibration coefficient, and more exactly the radiance measured when viewing darkness.

Then the radiances are converted into reflectances $\rho^t(i,j)$:

$$\rho^t(i,j) = \frac{\pi L^t(i,j)}{I_{0met}\, \varepsilon(t) \cos \theta_S(t,i,j)} \qquad (7.11)$$

Then, we compute, assuming that the Linke turbidity factor as well as the site elevation are known:

$$L^t_{atm}(i,j) = (D^t_c(i,j) / p) (I_{0met}(t) / I_0) (1 / 2 \cos \theta_V)^{0,8} \quad (7.12)$$

and

$$\rho^t_{atm}(\theta_S,\theta_v,\gamma) = p\, L^t_{atm}(i,j) / (I_{0met}(t)\, \varepsilon(t) \cos \theta_S) \quad (7.13)$$

Finally, we get a quantity $\rho^{*t}(i,j)$ that is a ground albedo if the sky were clear at the instant t.

$$\rho^{*t}(i,j) = [\, \rho^t(i,j) - \rho_{atm}(\theta_S,\theta_v,\gamma)] / T(\theta_S)\, T(\theta_v) \quad (7.14)$$

The ground albedo is computed $\rho_g(i,j)$ by taking the minimum value of the time-series of $\rho^{*t}(i,j)$ limited to the angles θ_S less than 70°. The period of the time-series should be the shortest as possible in order to take into account the rapid variations of the ground albedo, if any.

Compared to the method Heliosat-I, wherein it is preferable to have one estimate of the ground albedo per slot, the accurate correction of the effects of the sun and satellite angles permits to merge all the slots into the time-series. Thus, the period may be shortened. In an operational mode, especially when real time is at stake, a moving period is adopted.

Another advantage of this approach is that the retrieved ground albedo is actually a ground albedo and not an approximate quantity. This permits on the one hand to perform checking and monitoring of the method, even on an operational basis. On the second hand, it helps in solving the problem of the constant cloud cover over a pixel or a group of pixel. In that case, the minimal value will correspond to a cloudy instant. Using external knowledge of the expected albedo together with image processing techniques applied to the time-series of the checked ground albedoes, one may detect such cases and compute the likely value.

7.4 The apparent cloud albedo ρ_{cloud}

The apparent albedo of the clouds ρ_{cloud} has been defined by Cano (1982) as the typical value for the brightest clouds. The histogram of cloud albedoes is flat and it is very difficult to characterise this parameter ρ_{cloud} by a statistical quantity, such as a mode or a percentile. Costanzo (1994) or Hammer *et al.* (1997a, b) compute the mean value of the brightest albedoes observed in a time-series of images. The results may depend upon the length of the time-series and of the selected threshold. It should be added that some sites exhibit clear skies during several months (e.g. the Mediterranean basin), making it difficult to find very bright clouds. Of course, the adopted cloud albedo depends upon the adopted normalisation of the outputs of the sensor.

Given the fact that we are dealing with actual values of albedo, we may adopt an actual albedo of the brightest clouds. Rigollier (2000) refers to the maximum value given by Grüter *et al.* (1986), that is 0,9. According to the experience of L. Wald, who set up several implementations of the Heliosat-I method for various cases, to the works of Möser, Raschke (1983), Grüter *et al.* (1986), Moussu *et al.* (1989), Stuhlmann *et al.* (1990), Raschke *et al.* (1991) and Wald (1998), this parameter is not a maximum value and should not be taken too high. An effective albedo of 0,8 is selected for the cloud albedo.

However, the parameter ρ_{cloud} is to be compared to the quantities $\rho^{*t}(i,j)$ that derive from the observed radiances (equation 7.14) to compute the cloud index n. For $\rho^{*t}(i,j) = \rho^t_{cloud}(i,j)$, the

cloud index *n* should be equal to unity. It follows that the same equation (7.14) should apply to the effective cloud albedo, leading to the apparent cloud albedo $\rho^t_{cloud}(i,j)$:

$$\rho^t_{cloud}(i,j) = [\,0{,}8 - \rho_{atm}(\theta_s,\theta_v,\gamma)] \,/\, T(\theta_s)\,T(\theta_v) \qquad (7.15)$$

$\rho^t_{cloud}(i,j)$ is not an actual albedo of cloud. The brightest clouds are at high latitude, well above the aerosols layer. At altitudes greater than 6 km, the intrinsic radiance of the atmosphere is small and the transmittance is close to unity. The quantity $\rho^t_{cloud}(i,j)$ is larger than the effective cloud albedo but is comparable to the quantities $\rho^{*t}(i,j)$. Making it depending upon the sun and satellite angles permits to correct for the drawbacks observed by Bauer (1996) with the method Heliosat-I, wherein the quantity $\rho^t_{cloud}(i,j)$ is a constant.

7.5 Conclusion

We propose an approach to assess in an accurate way the quantities ρ_g and ρ^t_{cloud}. This approach is based upon explicit formulations of the radiance and the transmittance. These formulations makes use of the modelling of the clear sky radiation, thus offering a strong consistency. This explicit approach offers several advantages. It removes many empirical parameters, compared to the versions of the method Heliosat-I. It makes use of recognised expressions of the radiance and the transmittance. It permits to use known values of the albedo of specific objects, or to estimate such albedoes.

The expected gain in accuracy may be dampened by the use of the Linke turbidity factor. The latter may be an additional source of error compared to the method Heliosat-I. The maximum errors on the assessment of ρ_g due to the Linke turbidity factor are approximately 15 percent and are negligible for ρ^t_{cloud}. These maxima are observed for large Linke turbidity factor. The actual errors are smaller since ρ_g is assessed from the minima of ρ^t, hence for small Linke turbidity factor. Similarly to the method Heliosat-I, the approach does not behave satisfactorily for sun zenithal angles larger than 75 - 78°. Though applicable, it produces larger errors.

From an operational point of view, these parameterisations of ρ_g and ρ^t_{cloud} request the knowledge of the Linke turbidity factor and the elevation for each pixel of the Meteosat image to be processed. This constraint is not an additional one, since these informations are also requested by the model of the clear sky irradiation. The good point is that this study demonstrates that the Linke turbidity factor is sufficient to describe the optical state of the clear atmosphere in the broadband of the satellites Meteosat.

The gain in implementation is here evident. The use of known formulations of the radiance and transmittance and the use of actual albedoes permit to remove the empirical parameters of the method Heliosat-I that are site-dependent. The approach is valid everywhere in the world and depend only on the availability of the external knowledge. The gain in operation is also important. Only one map of the ground albedo will be necessary, instead of having one map per slot as presently in the most advanced versions of the method Heliosat-I.

The whole approach is applied to two pixels of the Meteosat field of view for illustration. One of the pixel is located over the city of Weihenstephan, in a vegetated area in the Southern Germany (48,40 N; 11,70 E) and the other is over the Indian ocean (- 35,36 S; 40,50 E).

Figure 7.5 displays the reflectances $r^t(i,j)$ observed by the sensor as a function of the sun zenithal angle in summer 1990. From these reflectances, the ground albedo r_g is computed: 0,105 for Weihenstephan and 0,02 for the ocean pixel. These values are well in concordance with the present knowledge. It may be observed for the ocean pixel that the reflectance is not well corrected for sun zenithal angles greater than 80°. The values r^t_{cloud} give the maximal value observed for r^t. For Weihenstephan, the greatest values of r^t do not reach r^t_{cloud} for the lowest zenithal angles. The analysis of the available measurements of the global hourly irradiation demonstrates that for this particular summer, there is no bright clouds for sun zenithal angles comprised between 25 and 40°. On the contrary, bright clouds are observed for greater angles and their values are close to r^t_{cloud}.

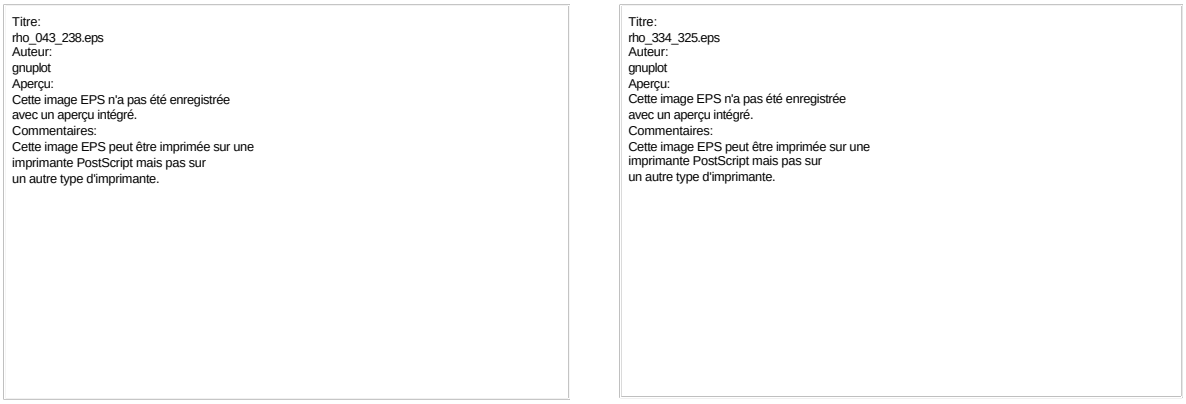

Figure 7.5. Values of $r^t(i,j)$ (points), $r_g(i,j)$ (diamond) and $r^t_{cloud}(i,j)$ (crosses) for Weihenstephan (left) and the ocean pixel (right) as a function of the sun zenithal angle.

8 THE RELATIONSHIP BETWEEN THE CLOUD INDEX AND THE GLOBAL HOURLY IRRADIATION

The hourly irradiation in the method Heliosat-I is computed as:

$$G_h(i,j) = KT_h(i,j)\, G_{0h}(i,j) = (-A\, n^t(i,j) + B)\, G_{0h}(i,j) \qquad (8.1)$$

According to Diabaté (1989), the coefficients A and B do not depend upon the geographical location but on the time of the day. Three sets of values were defined: one for the morning, one for mid-day and one for the afternoon. Several authors: Grüter *et al.* (1986), Michaud-Regas (1986) and Raschke *et al.* (1991) also use a linear relationship between KT_h and n in the method Heliosat-I. These independent studies show that a linear relationship leads to satisfactory results. However, Diabaté (1989) stresses that there is no explanation of the variability of the parameters A and B during the day while their variability along the year or with the latitude is negligible, and questions the validity of this relationship.

Beyer *et al.* (1996) underline that the parameter KT_h is not well describing the optical state of the atmosphere: a cloudy sky may have the same KT_h than a turbid clear sky though the radiative flux reaching the spaceborne sensor may be different because of the higher albedo of the cloud or the backscattering effects. They propose to use instead the clear-sky index K_{ch}, which is equal to the ratio of the hourly global irradiation at ground on an horizontal surface G_h to the same quantity but for clear skies G_{ch}:

$$K_{ch} = G_h / G_{ch} \qquad (8.2)$$

Doing so decreases the errors in the satellite-derived estimates. Furthermore, Beyer *et al.* show that the relationship may be simply written as:

$$K_{ch} = 1 - n \qquad (8.3)$$

with a negligible loss in accuracy. The gain in terms of operating the method is large since it is not necessary to use ground measurements to establish or correct the parameters A and B of the relationship.

However, this relationship has some drawbacks that need to be corrected. First, since the apparent albedo of the ground, ρ_g, is not the smallest value that can be observed, it happens that the cloud index n is negative. Equation (8.3) predicts a value of K_{ch} greater than 1, which is physically sound up to a limit of approximately 1,2 according to the observations. Secondly, the apparent albedo of the cloud, ρ_{cloud}, is not the greatest value that can be observed and the cloud index n may be larger than 1. Equation (8.3) predicts a value of K_{ch} negative, which is impossible. Actually, observations of the smallest clearness index in Europe for several years show that the minimal value is approximately 0,04 (ESRA, 1984 and 2000). Since

$$K_{ch} = KT_h\, (I_0\, \varepsilon \sin \gamma_S / G_{ch}) \qquad (8.4)$$

Using the model for clear skies of Perrin de Brichambaut, Vauge (1982), we find the minimal value of the clear-sky index, K_{ch}, of approximately 0,05, with an error of approximately 0,01.

Thirdly, a careful analysis of many comparisons between measured global hourly irradiations and cloud indices n made in the framework of the project Satel-Light (Fontoynont *et al.*,

1997) show that for overcast skies ($n \geq 0,8$), a linear relationship is inappropriate and underestimates K_{ch}. It is therefore proposed to use instead a quadratic relationship up to $n>1,1$ where the minimal value of K_{ch} of 0,04 is reached.

Taking into account these remarks and constraining the relationship and its first derivative to be continuous everywhere, except in $n = 0,2$, the new relationship is the following:

$$\begin{aligned} n^t < -0,2 \quad & K_{ch} = 1,2 \\ -0,2 < n^t < 0,8 \quad & K_{ch} = 1 - n \\ 0,8 < n^t < 1,1 \quad & K_{ch} = 2,0667 - 3,6667\, n^t + 1,6667 (n^t)^2 \\ n^t > 1,1 \quad & K_{ch} = 0,05 \end{aligned} \qquad (8.5)$$

Figure 8.1 exhibits this relationship, which is made of four parts. The continuity is ensured as well as that of the derivative, except in $n = -0,2$.

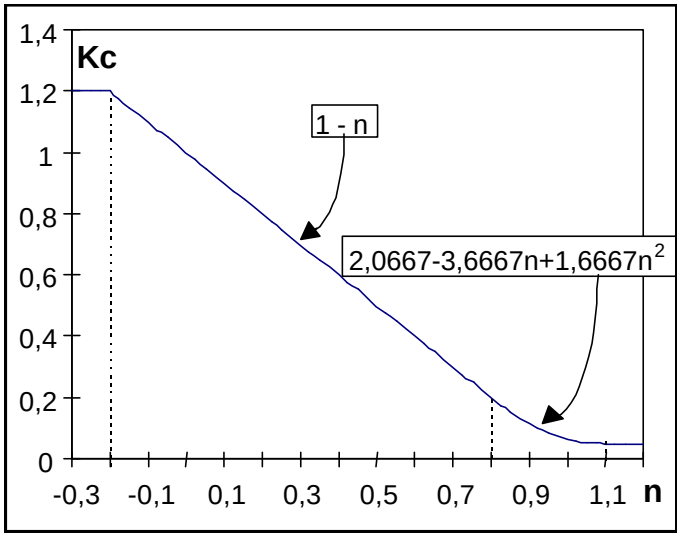

Figure 8.1. Relationship between the clear-sky index K_{ch} and the cloud index n

The University of Oldenburg adopted this model in their current version of the method Heliosat-I. Compared to the standard method Heliosat-I, it provides better results.

However, though this relationship is more satisfactory than the previous one, the limitation of the cloud index *n* to characterise the optical state of the atmosphere remains. The principle of the method Heliosat-I is that a difference in global radiation perceived by the method is only due to a change in apparent albedo, which is itself due to an increase of the radiation emitted by the atmosphere towards the sensor. This principle is not always verified. Other parameters may intervene, such as multiple cloud layers and dramatic changes in the ground albedo due to the snowfall or the shadow created by a neighbouring cloud.

9 THE COMPUTATION OF THE DAILY IRRADIATION

The computation of the daily irradiation $G_d(i,j)$ is based upon the N assessments of the hourly irradiation $G_h(i,j)$ made during the day. It follows the same principle that for Heliosat 1, using the clear sky quantities G_{cd} and G_{ch} instead of G_{0d} and G_{0h}. The equations are the followings:

$$G_d(i,j) = K_{cd}(i,j)\, G_{cd}(i,j) = G_{cd}(i,j) \sum_{h=1}^{N} w_h\, K_{ch}(i,j) \qquad (9.1)$$

where $w_h = \dfrac{G_{ch}(i,j)}{\sum_{h=1}^{N} G_{ch}(i,j)}$

It comes

$$G_d(i,j) = G_{cd}(i,j)\, \frac{\sum_{h=1}^{N} G_h(i,j)}{\sum_{h=1}^{N} G_{ch}(i,j)} \qquad (9.2)$$

10 COMPARISON BETWEEN RETRIEVED VALUES AND STATION MEASUREMENTS

A comparison is performed between irradiation values retrieved by the processing of Meteosat images and measured by ground stations is performed. It permits to measure the accuracy of the new method Heliosat II, remembering the discussion in Chapter 2.

Thirty-five stations were selected for the comparison. They were selected in flat areas, in order to avoid the specific errors encountered in mountainous areas. Table 10.1 lists these stations. The meteorological offices provided the global hourly irradiation values. These offices perform a screening for quality check. The formats and units were unified before comparison.

Measurements are performed in mean solar time or true solar time. The time of the meteorological measurements is that of the end of the measure. For example, the hourly irradiation at 11 hours is the integral of the irradiance from 10 to 11 hours. The satellite observations are performed in universal time (UT). Consequently, the initial time series of measurements are converted into other time series expressed in universal time. The time for the satellite observation depends upon the position of the site within the field of view; it can be computed exactly knowing the characteristics of the observing system and is expressed in UT. For each meteorological station, knowing its longitude, the universal time of the satellite observation T_{sat} is converted into local time. By weighting the two consecutive irradiation values centred on this local time t_{sat} and by assuming that the irradiance is constant within the hour, the estimated hourly value in universal time, $G^*_h{}^{meas}(T_{sat})$, was computed:

$$G^*_h{}^{meas}(T_{sat}) = G^*_h{}^{meas}(t_{sat}) = (t_1 - t_{sat} + 0{,}5)\, G_h(t_1) + (t_{sat} - t_1 + 0{,}5)\, G_h(t_1 + 1)$$

where t_1 and t_{sat} are local time expressed in hours, $t_1 = Round(t_{sat})$, and *Round* is the rounding operator (*Round(10,4)=10*; *Round(10,5)=11 etc.*).

The time series of estimated measurements $G^*_h{}^{meas}(T_{sat})$ are hereafter considered as actual measurements. Actually, more stations were acquired. Only were kept the thirty-five stations for which the Linke turbidity factor is known.

Only were used the measurements of hourly irradiation greater than 10 Wh m^{-2}. This value corresponds to the level of diffuse hourly irradiation for the sunset and sunrise under clear-sky at 60° N in Norway. For these hours of very low solar elevation, the measured irradiation is mainly of diffuse nature and is influenced by local conditions, including orography and the presence of nearby obstacles. By removing these values, we ensure better conditions for the validation process.

Station name	*WMO id.*	*Latitude*	*Longitude*	*Altitude*	*Country*
Aviemore	03063	57,20	-3,83	220	United Kingdom
Eskdalemuir	03162	55,32	-3,20	242	United Kingdom
Easthampstead / Bracknell	03763	51,38	-0,78	73	United Kingdom
Melle	06430	50,98	3,83	17	Belgium
Uccle	06447	50,80	4,35	100	Belgium

St. Hubert	06476	50,03	5,40	556	Belgium
Caen	07027	49,18	-0,45	78	France
St. Quentin	07061	49,82	3,20	98	France
Reims	07070	49,30	4,03	95	France
Bourges	07255	47,07	2,37	161	France
Macon	07385	46,30	4,80	221	France
Limoges	07434	45,87	1,18	396	France
Carcassonne	07635	43,22	2,32	130	France
Perpignan	07747	42,73	2,87	43	France
Valladolid	08141	41,65	-4,77	734	Spain
Hamburg - Sasel	10141	53,65	10,12	49	Germany
Bremen	10224	53,05	8,80	24	Germany
Seehausen	10261	52,90	11,73	21	Germany
Neubrandenburg	10280	53,55	13,20	73	Germany
Osnabrueck	10317	52,25	8,05	104	Germany
Braunschweig	10348	52,30	10,45	83	Germany
Potsdam	10378	52,37	13,08	107	Germany
Bocholt	10406	51,83	6,53	24	Germany
Kassel	10438	51,30	9,45	237	Germany
Dresden - Wahnsdorf	10486	51,12	13,68	246	Germany
Bonn - Friesdorf	10517	50,70	7,15	65	Germany
Weimar	10555	50,98	11,32	275	Germany
Trier	10609	49,75	6,67	278	Germany
Wuerzburg	10655	49,77	9,97	275	Germany
Coburg	10671	50,28	10,98	331	Germany
Saarbruecken	10708	49,22	7,12	325	Germany
Stuttgart	10739	48,83	9,20	318	Germany
Nuernberg	10763	49,50	11,08	312	Germany
Weihenstephan	10863	48,40	11,70	472	Germany
Budapest / Lorinc	12843	47,43	19,18	138	Hungary

Table 10.1. List of stations used for the comparison

The satellite data are high resolution images covering Europe and brought to the infrared resolution, that is 5 km at nadir. They are available every half-hour, from July 1994 to June 1995. We used only the images acquired for even slots (2, 4...). The satellite data were processed using the above-described algorithms. We use the values of the Linke turbidity factor read in the web site: *www-helioserve.cma.fr*. Estimates of the global hourly irradiation were thus obtained. Only the estimates, for which the sun elevation is greater than 12°, were kept for the comparison, as it has been said that the description of the physical processes is not valid below that limit.

Three months were used for the comparison: January 1995, April 1995 and July 1994. From each set of hourly irradiation, and for a given month, the daily irradiation was computed as follows.

For the station measurements, we sum up all the hourly irradiations greater than 10 Wh m^{-2}. The estimate is said valid if at least *N* hourly irradiations are used in the computation. *N* is equal to 6 in January and April and to 12 in July.

For the high resolution images, we use the above-described algorithm. The estimate is said valid if at least *N* hourly irradiations are used in the computation. For each hourly irradiation, the mean solar elevation should be greater than 12°. *N* is equal to 5 in January and April and to 8 in July.

Given the two time-series, and for all stations together, we compute the difference (measured - estimated) in several ways:

- for hourly irradiation for a given month, for all the hours,
- for the monthly mean of hourly irradiation for a given hour, for all hours,
- for daily irradiation for a given month, for all the days,
- for the monthly mean of daily irradiation,
- for the cumulative of the daily irradiation during 5 days (5-days irradiation). Only are kept 5-days estimates, which are made from at least 3 daily estimates (60 %),
- for the cumulative of the daily irradiation during 10 days (10-days irradiation). Only are kept 10-days estimates, which are made from at least 6 daily estimates (60 %),

For each parameter, the differences have been computed and are summarised in the table 10.2 below. The bias is usually useful for assessing the accuracy. For example, it ranges from 23 Wh m^{-2} in July 1994 to -10 in January 1995. However, it strongly depends upon the selected stations and the selected period and has no great statistical significance in this context because the field is not stationary. Consequently, only the RMSE is dealt with in the following. This parameter is more stable.

Information type	*Month*	*Mean value*	*RMSE*	*Correlation coefficient*	*Number of observations*
Hourly irradiation	Jan 95	137	62	0,83	5028
	Apr 95	361	96	0,90	8248
	Jul 94	569	103	0,87	8105
Daily irradiation	Jan 95	987	199	0,95	344
	Apr 95	3366	534	0,95	1044
	Jul 94	5817	566	0,94	887
5-days irradiation (at least 60 % of valid days)	Jan 95	4607	898	0,94	75
	Apr 95	16826	1794	0,96	209
	Jul 94	28736	2419	0,91	202
10-days irradiation (at least 60 % of valid days)	Jan 95	8788	1836	0,93	43
	Apr 95	33675	3285	0,96	104
	Jul 94	57680	3454	0,92	101
Monthly mean of hourly irradiation	Jan 95	142	41	0,91	160
	Apr 95	361	41	0,94	280
	Jul 94	568	48	0,93	272
Monthly mean of daily irradiation	Jan 95	891	215	0,88	20
	Apr 95	3367	243	0,97	35
	Jul 94	5776	307	0,92	34

Table 10.2. Differences between measured and estimated values in Wh m^{-2}. For high-resolution images

The results are very good, compared to objectives. The accuracy observed by comparison with ground measurements is better than the targets set up before the development. The correlation coefficient is high in all cases.

Table 10.2 shows a problem with the low sun elevations. This appears in the comparison of the hourly and daily irradiations. The method Heliosat-II does not behave well in these cases. It implies that the relative error is greater in January, when the frequency of low sun elevations is greater and the mean hourly irradiation is low, than in July. To assess better the influence of these cases, we introduce the estimates made for any sun elevation, without any constraint, in the comparison with ground measurements. The results are reported in the table 10.3 for the hourly and daily irradiations.

The satellite data we are using are only available between 0800 UT and 1500 UT. In April and July, and for the stations under concern, the sunrise and sunset are well outside this period: removing the constraint on the sun elevation does not add any value for the comparison. Accordingly, no difference can be evidenced for these months. Table 10.3 only reports on the month of January for hourly irradiation.

Information type	*Month*	*Mean value*	*RMSE*	*Correlation coefficient*	*Number of observations*
Hourly irradiation (for sun elevations greater than 12°)	Jan 95	137	62	0,83	5028
Hourly irradiation (for all sun elevations)	Jan 95	111	56	0,84	7546
Daily irradiation (for sun elevations greater than 12°)	Jan 95	987	199	0,95	344
	Apr 95	3366	534	0,95	1044
	Jul 94	5817	566	0,94	887
Daily irradiation (for all sun elevations)	Jan 95	851	318	0,91	1018
	Apr 95	3503	535	0,95	1086
	Jul 94	5999	579	0,93	895

Table 10.3. Assessing the influence of the constraint on the sun elevation. Comparison of the ground measurements and the satellite estimates, in Wh m^{-2}

In January, the number of values of hourly irradiation strongly increases when all elevations are taken into account. The RMSE decreases together with the mean value and the relative RMSE increases from 45 to 52 percent. This confirms that the quality of the assessment decreases as the sun elevation decreases. Higher errors are expected for the months of April and July if the hours of low sun elevation are included in the comparison.

As for the daily irradiation, the error strongly increases in January both in absolute and relative value. This is because the frequency of low sun elevation is large for this winter month. In April and July, the error slightly increases.

For the hourly and daily irradiation, this table show that it is possible to remove the constraint on the sun zenithal angle if necessary, still keeping an acceptable accuracy. Removing this constraint, or decreasing the threshold, leads to a larger number of estimates, which may be useful.

The role of the Linke turbidity factor is investigated for the hourly and daily irradiation. The actual values of the Linke turbidity factor are close to 3,5, the value usually adopted for Europe. Table 10.4 gives the mean value and the standard deviation of the Linke turbidity factor for the 35 stations. The mean value ranges from 3,0 (winter) to 4,5 (summer). The standard deviation is approximately 0,5 for the year.

	Mean value	*Standard deviation*
January 1995	3,0	0,4
July 1994	4,5	0,5

Table 10.4. Mean value and standard deviation of the Linke turbidity factors for the stations, for January and July

We assume a constant Linke turbidity factor equal to 3,5 for all stations and re-compute the satellite estimates. Table 10.5 reports the results of the comparison between the ground measurements and the satellite estimates, with and without the actual values of the Linke turbidity factor.

Information type	*Month*	*Mean value*	*RMSE*	*Correlation coefficient*	*Number of observations*
Hourly irradiation using known $T_L(AM2)$	Jan 95	137	62	0,83	5028
	Apr 95	361	96	0,90	8248
	Jul 94	569	103	0,87	8105
Hourly irradiation setting $T_L(AM2)$ to 3,5	Jan 95	137	63	0,83	5028
	Apr 95	361	96	0,90	8248
	Jul 94	569	103	0,87	8105
Daily irradiation using known $T_L(AM2)$	Jan 95	987	199	0,95	344
	Apr 95	3366	534	0,95	1044
	Jul 94	5817	566	0,94	887
Daily irradiation setting $T_L(AM2)$ to 3,5	Jan 95	987	197	0,96	344
	Apr 95	3366	540	0,95	1044
	Jul 94	5817	567	0,94	887

Table 10.5. Assessing the influence of the Linke turbidity factor. Comparison of the ground measurements and the satellite estimates, in Wh m^{-2}

The difference between the results is negligible. It confirms that a value of $T_L(AM2)$ of 3,5 is well adapted to Europe and especially to the Northern Europe since most of the measurements are for this area. The simulation of the hourly and daily global irradiations under clear sky shows a relative difference of approximately 5 percent in irradiation between a $T_L(AM2)$ of 3,5 and a $T_L(AM2)$ of 4,5. This is much higher than what is observed in the table 10.5 and can be explained by the fact that in this area, the skies are not often clear: the mean observed daily irradiation amounts to approximately 0,7 times the clear sky irradiation. Since the influence of $T_L(AM2)$ is limited to the clear skies, this explains the negligible differences.

Raschke *et al.* (1991) and Iehlé *et al.* (1997) reports larger differences that come from the difference in geographical area: Africa for the first authors, or from the special interest on the sunny days for the latter. For these authors, the knowledge of the actual values of $T_L(AM2)$ is preferable to a standard value of 3,5.

The partner EHF selected a standard value of 3,5 for the processing of the satellite data using an advanced version of the method Heliosat-I. The partner ENTPE adjusted regional empirical models on the values of the European database read in the web site: *www-helioserve.cma.fr*, for the server Satel-Light. The table 10.5 confirms the little influence of their approach onto the results.

11 ACCURACY OF THE RETRIEVAL OF IRRADIATION VALUES FROM METEOSAT IMAGES IN B2 FORMAT

The B2 data used by ENSMP for establishing a climatological database are characterised by the fact they are formed by pixels that are effectively pixels of original size (*i.e.*, 5 km) but with a sub-sampling of 6 in each direction. Knowing exactly how a B2 image is formed from the main stream of data, we were capable of simulating the B2 data from the high resolution. The images in B2 format are only available every 3 hours in universal time, starting at 0000 UT. Accordingly, only were kept the simulated images for these hours. The same comparisons as above but with now these B2 format were performed.

The satellite assessments are restricted to solar elevations greater than 12°. Comparisons of hourly irradiation are limited to ground measured values greater than 10 Wh m^{-2}. The values of the Linke turbidity factor are read in the web site: *www-helioserve.cma.fr*.

The same parameters than for the high resolution are computed. The construction of daily irradiation is as for the high resolution images, but the number *N* of hourly irradiations should be greater than or equal to 2 in January and April and 3 in July.

An additional problem for the comparison with ground measurements arises from the fact that a measuring station is not necessarily contained within a B2 pixel. An interpolation method is requested to estimate locally the irradiation from the irradiations computed at the surrounding B2 pixels. According to the results of Iehlé *et al.* (1997) who compared several methods, we select the nearest-neighbour technique. It should be underlined that the results strongly depend upon the relevance of the selected technique to the local spatial properties of the irradiation. The smoother the field, the better the assessment by the nearest-neighbour technique. In case of high spatial variations, the technique will be inappropriate as most of the standard ones. Given the properties of the areas under concern in this work, the results should be regarded as the typical accuracy that can be achieved. Lower accuracy will be find in cases of large variations in orography or juxtaposition of local climates etc.

The results are good, compared to objectives. The accuracy observed by comparison with ground measurements is better than or close to, the targets set up before the development (table 11.1). The correlation coefficient is high in all cases.

Of course, the accuracy is less than that observed for the high resolution images. The degradation of the accuracy comes from both the smaller numbers of images available for the B2 format, and the interpolation process.

We performed an analysis of the influence of the difference in the number of images used to compute the daily irradiation. For this purpose, we used only the high resolution images. The daily irradiation was computed by using the nine possible slots on the one hand, and the B2 slots taken every 3 hours (0000 UT, 0300 UT, 0600 UT ...) on the other hand. Of course, there are discrepancies, which are approximately half of the differences observed between the tables 10.2 and 11.1. The larger the number of images, the more accurate the retrieval.

Then, still using the high resolution images, we compare the satellite estimates of the daily irradiation for the true pixel and for the simulated B2 pixel. We observe that the gap in space

between the measuring station and the B2 pixel has as much influence as the weak number of images for computing daily irradiation.

Information type	*Month*	*Mean value*	*RMSE*	*Correlation coefficient*	*Number of observations*
Hourly irradiation	Jan 95	136	65	0,78	1767
	Apr 95	337	112	0,86	3097
	Jul 94	539	128	0,82	3059
Daily irradiation	Jan 95	984	291	0,89	345
	Apr 95	3401	730	0,91	1044
	Jul 94	5797	852	0,86	954
5-days irradiation (at least 60 % of valid days)	Jan 95	4559	907	0,93	76
	Apr 95	17001	2242	0,94	209
	Jul 94	28912	2914	0,86	203
10-days irradiation (at least 60 % of valid days)	Jan 95	8792	1717	0,93	42
	Apr 95	33983	3990	0,94	105
	Jul 94	57865	4862	0,84	101
Monthly mean of hourly irradiation	Jan 95	140	41	0,87	56
	Apr 95	338	52	0,94	105
	Jul 94	538	59	0,94	102
Monthly mean of daily irradiation	Jan 95	892	225	0,85	19
	Apr 95	3402	350	0,92	35
	Jul 94	5792	399	0,86	34

Table 11.1. Differences between measured and estimated values in Wh m^{-2}. For B2 images

These results clearly demonstrate that the method Heliosat-II may apply to the images in B2 format with a satisfactory accuracy, thus opening new avenues in the climatology of the solar radiation. The B2 images may even be used to assess the hourly irradiation. However, given the poor sampling in time of these images, it may be recommended to limit their use to the assessment of daily irradiation or to the irradiation for larger periods.

12 CONCLUSION

The method Heliosat-II meets the objectives set up before its development. It is more physically sound than the previous one. It also presents results that are more accurate. All parameters that needed to be tuned for each implementation of the method Heliosat-I have been removed, set up to constant values, or automatically determined. The method Heliosat-II has the capabilities to process any type of data from geostationary meteorological satellites, including large time-series of images taken by different sensors. It is applicable in real-time or on archives of images, whatever their resolution. By suppressing empirically defined parameters, the implementation is the same for all cases. It facilitates exchange of knowledge and further collective improvements of the method Heliosat-II. One may use now a single map of apparent ground albedo instead of having one per slot processed, which may amount to 18 maps for high latitudes in summer for assessing hourly irradiation and 36 in the case of half-hourly irradiation.

The accuracy observed by comparison with ground measurements is better than the targets set up before the development. The Table 12.1 exhibits the objectives set up for the root mean square error (RMSE) and the observed RMSE for the high resolution images and the ISCCP-B2 images. The values for July 1994 have been reported since they are the greatest. For the high resolution images, the errors are well below what was targeted. As for the ISCCP-B2 images, the RMSE is better than, or close to, the targeted values.

Type	*Objectives for RMSE*	*Observed RMSE (high resolution)*	*Observed RMSE (ISCCP-B2)*
Hourly irradiation	~ 130	103	128
Daily irradiation	~ 800	566	852
5-days sum of daily irradiation	~ 3000	2419	2914
10-days sum of daily irradiation	~ 5500	3454	4862
Monthly mean of hourly irradiation	~ 80	48	59
Monthly mean of daily irradiation	~ 400	307	399

Table 12.1 Accuracy objectives for the method Heliosat-II for a single pixel and accuracy observed in July 1994. In Wh m^{-2}.

It should be noted that no ground measurement was used for the development, contrary to the method Heliosat-I and others. This ensures a worldwide application of the method Heliosat-II.

Several authors developed methods using a set of measurements from meteorological stations. The assessment of the accuracy was made by comparing the estimates to the same set or another set of measurements taken in the same region in a similar or adjacent period. The results obtained by the method Heliosat-II compare favourably with such published results, presented in the Table 12.2. Note that the reported errors are computed after averaging values on several pixels, thus reducing the RMSE, while for the method Heliosat-II, a single pixel was used.

Type	*Period*	*RMSE*	*Comments*
Hourly irradiation	May 1979	120	Grüter *et al.* (1996) Western Europe
	June 1979	80	
	April 1982	~ 65	
	July 1983	77	Diabaté (1989), France
	July 1985	57	
	May-June 1993	95	Beyer *et al.* (1996), Germany
	Year 1983	64	Diabaté *et al.* (1988a), France
	Years 1983-1985	70	Diabaté (1989), France
Daily irradiation	June 1979	600	Grüter *et al.* (1996) Western Europe
	April 1982	560	
	Years 1983-1985	~ 370	Diabaté (1989), France
Monthly mean of hourly irradiation	June 1979	25	Grüter *et al.* (1996) Western Europe
	April 1982	24	
Monthly mean of daily irradiation	June 1979	250	Grüter *et al.* (1996) Western Europe
	April 1982	280	
Climatological averages of monthly mean of hourly irradiation	Winter	11	Maxwell (1998), 1981-1990 regional average, USA
	Summer	17	

Table 12.2. Errors (RMSE, in Wh m^{-2}) reported by authors developing a method and using measurements for tuning models and parameters.

The method Heliosat-II may be improved in several points. The clear-sky model does not take into account the diffuse part of the radiation that has been reflected once or more by the ground before impinging on the site under concern. It is known from previous works that this has a little impact for high sun elevations and large size of pixels. In any other cases, low sun elevation or pixel size smaller than approximately 1 km, this physical process should be taken into account. This implies a modification of the model and the knowledge of the surrounding albedoes, including their bi-directional properties. It would help in solving the problem of the sun elevations less than 12°. Another major point of improvement is likely the relationship between the clear sky index and the cloud index. Gains will be reached if superimposed cloud layers may be identified and separately modelled.

The snow covering periodically the ground as well as permanent cloud coverage over a site creates problems in preventing from accurate determining the apparent ground albedo. Another source of information is necessary for the daily knowledge of the snow coverage; there is presently no appropriate tool. As for the permanent cloud coverage, one may use a climatological knowledge of the typical ground albedoes that would be observed without the clouds. These drawbacks were present in the method Heliosat-I.

The method Heliosat-II, as well as all other known methods, cannot perform accurately in areas where the scales of variability of the irradiation are smaller than 2-5 times the size of the pixel. This holds for the mountainous areas, for example. The Swiss meteorological office

uses a combination of Heliosat estimates and a dense network of ground measurements for the valleys in the Alps.

The gains in accuracy obtained relative to the method Heliosat-I are not coming from an increase of the dimensionality of the inputs originating from the satellite images, which remain the same. They come from external knowledge, that is the elevation and the Linke turbidity factor for each pixel of the area to process and some properties of the sensor for the day under concern. Thus, the implementation of the method Heliosat-II requests such knowledge.

The calibration step is not necessarily implemented in the method Heliosat-II. The necessary information, *i.e.* the calibration coefficients for each day and the incoming extraterrestrial solar irradiance in the visible channel for the various Meteosat sensors I_{0met}, are publicly available from the server Helioserve (*www-helioserve.cma.fr/calibration*) for the satellites Meteosat from 1985 up to 1997 (Rigollier, 2000). Hence, the Heliosat II procedure may tap into this database through an encoded URL to get the necessary values. For the other years, one may use the Eumetsat server (*www.eumetsat.de*) that provides a couple of calibration values per year. For the other satellites, this information is not always available, depending upon the satellite.

Though we used a published method, there are several innovative aspects in the calibration of the Meteosat data. Firstly, we found several errors in the initial method and we proposed corrections or revisions, increasing the accuracy. Secondly, the calibration factors were computed for all days for the period 1985-1997 and signal processing techniques were employed to fill gaps and take into account the changes in sensor. Finally, a database was created that can be accessed by anybody using a standard browser. The knowledge gained in calibration during the development of the method Heliosat-II has strong generic aspects and may be used outside this specific application and likely for other series of satellites.

Several databases of terrain elevation are available in gridded format depending upon the requested size of the cell. The most known databases are ETOPO5 (5' of arc angle) and GTOPO30 (30" of arc angle) which are covering the whole world. Their owners have not made them accessible through a standard navigator or an encoded URL. Except for high elevations, neglecting the elevation is of second order on the result.

The value of the Linke turbidity factor is of primary importance in the Heliosat II method since it governs the clear-sky irradiation. It may be a problem, since it is known for a limited number of sites. Angles *et al.* (1998, 1999) set up a Web server of such values for several hundred of sites in Europe (*www-helioserve.cma.fr/Linke*). For Europe, one may use a value of 3.5. Some empirical laws help in assessing a value for any place in the world.

12.1 Benefits of the Heliosat-II development to the SoDa project

There is presently no operational implementation of the complete method Heliosat-II. This requests resources that are under discussion within the Consortium for the creation of long time-series of daily irradiation and will likely be approved. Beyond this and as initially expected, the development of the method Heliosat-II benefits to the project SoDa in several important aspects.

12.1.1 Assessing the clear-sky models of Meteotest and ENTPE

The work performed here on the clear-sky models compared the models used by the partners Meteotest and ENTPE in their commercial products (MeteoNorm) or near-commercial (server Satel-Light). They were compared to the model used in the commercial product ESRA. The baseline information was provided by long time series of quality-controlled measurements of irradiation. This has been detailed in the previous pages. The outcomes are that the clear-sky model of Meteotest should be slightly improved for low solar zenithal angles (high solar elevation), and that the model of ENTPE behaves very similarly to the ESRA model and does not need changes.

12.1.2 The ESRA clear sky models as a library and a simulation tool

The ESRA clear-sky models have been coded in language C as part of a library. This library will be made available through the web site Helioserve: *www-helioserve.cma.fr*, with some documentation still to be realised, based on the present document.

In this site, we have realised a simulator of the clear-sky irradiation based upon this library. The user can simulate the clear-sky hourly and daily irradiations, given the day, geographical site, the elevation and the Linke turbidity factor. Two options have been selected for the implementation of this simulation. They stem from user requirements. They offer several common properties in the selection of the day, which can be entered using either the georgian or the julian calendar. The latter has been introduced because it is that usually used in the simulation of Earth observation missions.

In the first option, links have been made to the database of the Linke turbidity factor, available through the same web site, and to a database of meteorological stations. This database has been implemented from the information provided by the ESRA, is accessible through the same web site but has not been publicised. The user may select a meteorological station in a given country in Europe from a list, which comes automatically with its properties: geographical co-ordinates, elevation, and Linke turbidity factor for each month. These parameters are fed into the simulation tool.

In the second option, the user enters all the parameters. The geographical co-ordinates may be entered using either the sexagesimal or the decimal system.. This tool is very helpful to study the impact of any of these parameters (latitude, elevation, and Linke turbidity factor) on the clear sky irradiation.

These tools are very often used for methodological development dealing with irradiation. They are very easy to use and permit an instantaneous knowledge of the irradiation under clear skies. This irradiation indicates the maximum value that is expected and is helpful for many applications.

12.1.3 The clear sky simulator as a resource for the SoDa service

An effort has been made within the WP 5.2 "advanced parameters" to benefit from the clear-sky simulator and to make this resource available through the SoDa service. Starting from the simulator code, a new code was written (in PHP), which now exploits the databases through the Internet. Only one option is presently available. The user enters/selects the geographical co-ordinates and the day through the GeoSearch and TimeSearch tools of the SoDa intelligent

system. The link to the appropriate web site in JRC permits to collect the elevation value. The user has still to enter the Linke turbidity factor because there is no database covering the whole world. These parameters are fed into the simulation tool and the user gets the simulated values.

This resource has been effectively used as one of the specific cases to set up the first elements of the 1st prototype and test several technologies for the interface between the resources and the intelligent system, especially because it is calling upon several other resources. It is therefore evolving and is not in its final version (before comments and request for changes made by users).

12.1.4 Improvement of the method for satellite image processing in operational use at the EHF (University of Oldenburg)

The EHF has implemented the method Heliosat-I with some improvements in the past years in order to predict the global irradiation in real time using images of the series of satellites Meteosat that are locally acquired by this team. The information is routed to several users for the management of large solar systems. The work accomplished for the development of Heliosat-II has confirmed this team in its replacement of the original model for clear-sky irradiation by a new model. This replacement was made in 1999. Rigollier *et al.* (2000) show that this new model offers similar properties to that of the ESRA, which is that recommended for the Heliosat-II method. The work performed in the SoDa project for the development of Heliosat-II on the clear-sky model shows that such models are appropriate for use in the Heliosat method. The current implementation adopts a Linke turbidity factor of 3.5 for Europe and does not take into account the elevation of the site. The present study demonstrates the low impact of these assumptions on the quality of the products provided by the EHF to its customers. This also holds for the web service Satel-Light.

The new relationship between the cloud index n and the clear-sky index K_c has already been implemented at the EHF and provides better results than the original one. The computation of the cloud index n is different from that in the Heliosat-II method: some empirical parameters remain but results are similar.

An important impact of the work accomplished for the method Heliosat-II has been to explain the discrepancies in irradiation between ground measurements and satellite estimates suddenly appearing when using the new Meteosat-7 satellite. The calibration activities demonstrate an important change in the incoming extraterrestrial solar irradiance in the visible channel of Meteosat-7 with respect to the previously published values for the satellites Meteosat-5 and 6. Later, Eumetsat has corrected the values for Meteosat-5 and 6. Owing to the Heliosat-II development, EHF was capable of correcting its procedures and capable of providing results as accurate as the previous ones.

Hence, the procedure implemented at EHF for the conversion of the Meteosat images into cloud index n and further into global hourly irradiation benefits from the achievements of the Heliosat-II project. These cloud indices n are archived at ENTPE for further use in several applications accessible through the SoDa intelligent system.

12.2 Benefits of the SoDa project to the development of the method Heliosat-II

The development of the method Heliosat-II is a strong component of the project SoDa. Reciprocally, even if the development of the method Heliosat-II was planned by the partner ENSMP before the decision of funding the project SoDa, its level of achievements and the rapid pace of development would have not been attained outside the framework of this project. The development clearly benefits from several resources not available at ENSMP, namely the simulator of atmospheric optics Modtran (EHF), very long-time series of detailed measurements available in the ESRA or within partners (EHF, ENTPE and some of their own partners), clear-sky models (J. Page as part of the ESRA and part of UMIST, EHF, ENTPE, Meteotest). The scientific advices are worth to be mentioned and are acknowledged for in the following section.

The achievements of this task pushed the partner ENSMP to investigate the implementation of the method Heliosat-II for climatological purposes. This was planned by ENSMP outside the framework of the project SoDa and in a longer term planning. Owing to the encountered help, it was possible to achieve the proof-of-concept and assess the accuracy of the satellite-derived estimates using the B2 format. Results are very satisfying. Given the fact that most of the information necessary for the operational implementation of the method Heliosat-II should be made available at the end of the year 2001, the partner ENSMP is encouraged to envision an operational exploitation in early 2002 of the Meteosat archives, starting from 1985. The images in B2 format have been already secured until 1999, pre-processed and quality-controlled. The implementation of an operational version of the method Heliosat-II will definitely demonstrate its role as an improved successor of the method Heliosat-I and will greatly enhance its dissemination worldwide.

Reciprocally, this implementation will demonstrate the benefits of the SoDa service by enhancing its role in providing the necessary information. Furthermore, operating the method Heliosat-II will benefit to the SoDa service and the SoDa project by providing an unique database of known quality, medium-scale (~ 15' of arc angle), covering Africa, Europe, Western Asia and the Atlantic Ocean, spanning over several years. The early implementation of the major achievements of the development of the method Heliosat-II in the operational chains of EHF and ENTPE ensures that this database will be consistent in terms of irradiation information and quality with the high spatial and temporal resolution database for Europe held at ENTPE and for Africa held at EHF for the five-years period overlap.

12.3 Benefits of the SoDa intelligent system to the implementation of the method Heliosat-II and its penetration

The project SoDa will benefit to the exploitation of the method Heliosat-II, its implementation and its penetration. As already seen, this method requests some information that are available through an encoded URL or not. The development of the SoDa intelligent system and its capabilities to access resources will help in the implementation by providing an easy access to the necessary information. Most of this information is already available in the form of databases.

Several databases for elevation are covering the whole world with a sufficient accuracy. Some parts of them have been made available through the SoDa Intelligent System, namely the ETOPO5 and the GTOPO30 but for Europe only. The quality of the database ETOPO5 is sufficient for the processing of satellite data as those of the Meteosat series. It is also intended to use this database in WP 5.1 "interpolation schemes" to develop an interpolation scheme for station measurements. Accordingly, the partner ENSMP should implement the database into one of its servers and make it available as resource in the SoDa service (presumably as an "internal use" resource not to be overwhelmed by requests having nothing to do with solar information). This action will cover the need for the elevation information.

The accurate calibration information is only available for the Meteosat images, if we do not consider the present generation of GOES satellites from the U.S.A. We do not have simple solutions to this problem. Either some institutions make an effort using e.g., our method to provide the calibration, or it is derived through the comparison of overlapping areas between calibrated Meteosat images and images from other satellites. In any case, this would request an important effort. Products from the next generation of meteorological satellites will be better calibrated.

The Linke turbidity factor is a necessary parameter. It is not known everywhere and an important effort is underway by the SoDa project to establish monthly maps of this factor with a sufficient spatial resolution and a sufficient accuracy (approx. 0.25). These maps will then be available as a resource of the SoDa service.

The B2 data used by ENSMP for establishing a climatological database are characterised by the fact they are formed by pixels that are effectively pixels of original size (*i.e.*, 5 km) but with a sub-sampling of 6 in each direction. It follows that the exploitation of this database will request an interpolation method. Iehlé *et al.* (1997) showed that the best results were obtained by the nearest-neighbour technique. It should be checked whether the interpolation scheme developed in the WP 5.1 provides better quality.

Once these Web tools and the necessary resources established, the implementation of the method Heliosat-II will become easy. Compared to the method Heliosat-I, the software is more complicated, because there are more formulas and more inputs are requested. Nevertheless, there are no more parameters to tune empirically, with more stable results consequently. As the method Heliosat-I, the method Heliosat-II can run in a fully automatic fashion on any kind of Meteosat visible data (Diabaté *et al*. 1989; Wald *et al*. 1992). A network of stakeholders, the Heliosat network, was established several years ago, gathering research institutes and companies. The network will welcome this new method, mostly for the processing in near-real time of the Meteosat images, including those of the future series of Meteosat second generation satellites, and other geostationary satellites, especially the GMS from Japan, Insat from India and GOMS from Russia. These stakeholders are mostly in Europe and in the domain of solar energy systems. Among those overseas, are the Food and Agriculture Organization for food problems in Africa and Asia and Meteo-France in New Caledonia for solar energy.

A side-product of the method Heliosat-I or -II is the map of the apparent ground albedo. Moussu *et al*. (1989) demonstrated the links between this apparent albedo and the actual ground albedo. This is more evident in the method Heliosat-II because of the calibration and

the explicit formulation of the atmospheric influence. Such maps of ground albedo have been employed to study the changes in vegetation in the Western Africa during the whole year 1984 (Diabaté *et al*. 1989) or the hydrological regime of Lake Chad during the past years, including the 1970's drought (Wald, 1990). The Australian Government presently uses them for sheep pastures concerns.

A significant improvement in accuracy is expected with the next generation of meteorological satellites, where more channels will be available to describe the atmosphere. A new method: Heliosat-III, will be developed, on new physical grounds, to take advantage of the series of the Meteosat Second Generation satellites to be launched in 2002. More parameters will be directly derived, such as the direct and diffuse component, while they are presently estimated from the global irradiation.

The method Heliosat-II has still a future for climatological purposes because Eumetsat will continue to produce the ISCCP-B2 images, which will be similar to those presently produced using the Meteosat Operational Programme (MOP series). It has also a future for the numerous organisations that purchased or will purchase a receiving station, because the information flow will not necessarily contains all the channels, which will be used by the Heliosat-III method. Finally, the method Heliosat-II will be easier to implement and offers accuracy, which is sufficient for many applications.

13 ACKNOWLEDGEMENTS

We are grateful to Hans-Georg Beyer, Dominique Dumortier, Annette Hammer, Detlev Heinemann, Pierre Ineichen, John Page, Christian Perrin de Brichambaut, Richard Perez, Corrado Ratto, Christian Reise, Antoine Zelenka for the numerous discussions we had on the method Heliosat and its various improvements. The EHF (University of Oldenburg) performed the atmospheric simulations by the model Modtran and the authors thank Annette Hammer for her precious collaboration.

Very fruitful discussions have been held with Eumetsat on several aspects: we particularly thank Yves Govaerts, for his help in the calibration activities and Richard Francis and the archives Department MARF for providing the B2 data at no or low cost and for helping us in better understanding the Meteosat system and the properties of the B2 format.

The meteorological offices from France, Germany, Hungary, Spain, The Netherlands and United Kingdom have kindly provided the measurements of global irradiation at no or low cost. They are thanked for their support.

The high resolution Meteosat data were kindly provided by the European Space Agency (ESOC). We especially thank Jean Le Ber.

14 REFERENCES

Angles J., Menard L., Bauer O., Wald L., 1998, A Web server for accessing a database on solar radiation parameters. In Proceedings of the Earth Observation & Geo-Spatial Web and Internet Workshop '98, Josef Strobl & Clive Best Eds., Salzburger Geographische Materialien, Universität Salzburg, Salzburg, Austria, Heft 27, 33-34.

Angles J., Menard L., Bauer O., Rigollier C., Wald L., 1999, A climatological database of the Linke turbidity factor. In Proceedings of the ISES Solar World Congress 1999, Jerusalem, Israel, July 4-9, 1999, volume I, 432-434.

Anonymous, 1995, Spatial interpolation of daily meteorological data. Report to Institute for Remote Sensing, Joint Research Center, Ispra, Italy.

Anonymous, 1996, *The Meteosat Archive, Format Guide No. 3, ISCCP Data Set (IDS) in OpenMTP Format*, February 1996, EUM FG3, Rev. 1.0, Published by Eumetsat, Darmstadt, Germany.

Blanc P., 1999, Développement de méthodes pour la détection de changement. Thèse de Doctorat, Ecole des Mines de Paris, Paris, France, 204 p.

Barnes R.A., Eplee R.E., Robinson W.D., Schmidt G.M., Patt F. S., Bailey S.W., Wang M., McClain C.R., 2000a, The calibration of SeaWiFS on orbit, *In* Earth Observing Systems V, W.L. Barnes Editor, Proceedings of SPIE, vol. 4135, 281-293.

Barnes R.A., Eplee R.E., Biggar S.F., Thome K.J., Zalewski E.F., Slater P.N., Holmes A.W., 2000b, SeaWiFS transfer-to-orbit experiment, *Applied Optics*, 39(30), 5620-5631.

Bauer O., 1996, Les échanges océan-atmosphère dans l'Atlantique subtropical nord-est : apports de Meteosat. Thèse de Doctorat, Université de Nice - Sophia Antipolis, 162 p.

Beyer H.G., Costanzo C., Heinemann D., 1996, Modifications of the Heliosat procedure for irradiance estimates from satellite images. *Solar Energy*, **56**, 3, 207-212.

Beyer H. G., Reise C. and Wald L., 1992. Utilization of satellite data for the assessment of large scale PV grid integration. In *Proceedings of 11th Photovoltaic Solar Energy Conference*, pp. 1309-1312, Hardwood Academic Publ., Switzerland.

Beyer H.G., Wald L., 1996, Merging ground-measurements and satellite-derived data for the construction of global radiation map. In Proceedings of the conference « Fusion of Earth data: merging point measurements, raster maps, and remotely sensed images », Cannes, France, February 6-8, 1996, Thierry Ranchin and Lucien Wald Editors, published by SEE/URISCA, Nice, France, 37-43.

Beyer H.-G., Czeplak G., Terzenbach U., Wald L., 1997, Assessment of the method used to construct clearness index maps for the new european solar radiation atlas (ESRA). *Solar Energy*, 61, 6, 389-397.

Brest C.L., Rossow W.B., Roiter M., 1997, Update of radiance calibrations for ISCCP, *Journal of Atmospheric and Oceanic Technology*, **14**, 1091-1109.

Cano D., 1982, Etude de l'ennuagement par analyse de séquences d'images de satellite. Application à l'évaluation du rayonnement solaire global au sol. Thèse de Doctorat, École Nationale Supérieure des Télécommunications, Paris, France.

Cano D., Monget J.M., Albuisson M., Guillard H., Regas N., and Wald L., 1986, A method for the determination of the global solar radiation from meteorological satellite data, *Solar Energy*, **37**, 31-39.

Colle S., Luna de Abreu S., Couto P., Mantelli S., 1999, Distribution of solar irradiation in Brazil derived from geostationary satellite data, In Proceedings of the Solar World Congress ISES 1999, Jerusalem, July 4-9 1999.

Costanzo C., 1994, Bestimmung der solaren Einstrahlung am Boden aus Meteosat-Daten-Untersuchung und Erweiterung einer empirischen Methode. Diploma thesis, Physic Dept., Carl von Ossietzky University, Oldenburg, Germany.

Delorme C., Gallo A., and Olivieri J., 1992, Quick use of Wefax images from Meteosat to determine daily solar radiation in France, *Solar Energy*, **49** (3), 191-197.

Desormeaux Y., Rossow W.B., Brest L., Campbell G.G., 1993, Normalization and calibration of geostationary satellite radiances for the Iinternational Satellite Cloud Climatology Project, *Journal of Atmospheric and Oceanic Technology*, **10**, 304-325.

Diabaté L., 1989, Détermination du rayonnement solaire à l'aide d'images satellitaires. Thèse de Doctorat en Sciences, École Nationale Supérieure des Mines de Paris, Paris, France.

Diabaté L., Demarcq H., Michaud-Regas N., Wald L., 1988a, Estimating incident solar radiation at the surface from images of the Earth transmitted by geostationary satellites: the Heliosat Project, *International Journal of Solar Energy*, **5**, 261-278.

Diabaté L., Moussu G., Wald L., 1988b, An operational tool for the fine-scale mapping of the incident solar radiation using satellite images : the Heliosat station. In : Proceedings of the 1988 annual meeting of the American Solar Energy Society, pp. 11-17.

Diabaté L., Moussu G., Wald L., 1989, Description of an operational tool for determining global solar radiation at ground using geostationary satellite images, *Solar Energy*, **42**, 201-207.

Dogniaux R., Lemoine M., 1983, Classification of radiation sites in terms of different indices of atmospheric transparency. In Palz W. (éditeur), Solar Energy R&D in the European Community, Series F, Vol. 2, Solar Energy Data. D. Reidel Publ. Co., Dordecht, 94-107.

Dumortier D., 1995, Modelling global and diffuse horizontal irradiances under cloudless skies with different turbidities. Final report JOU2-CT92-0144, Daylight II, Ecole Nationale des Travaux Publics de l'Etat, France.

Eplee R.E., Barnes R.A., Robinson W.D., Bailey S.W., Werdell P.J., Patt F.S., McClain C.R., 2000, SeaWiFS Calibration: Status after two years on orbit, *Journal of Atmospheric and Oceanic Technology*, IEEE, 3163-3165.

Eplee R.E., McClain C.R., 2000, MOBY data analysis for the vicarious calibration of SeaWiFS bands 1-6, *In* SeaWiFS Postlaunch Technical Report Series, Vol 9: SeaWiFS Postlaunch Calibration and Validation Analyses - Part 1, NASA/TM-2000-206893, vol. 9, pp. 43-50.

ESRA, *European solar radiation atlas*, 1984. Second and Extended Edition, Vols I et II. Edited by Palz W., Commission of the European Communities, DG Science, Research and Development, Report N° EUR 9344, Bruxelles.

ESRA, *European solar radiation atlas*, 2000. Fourth edition, includ. CD-ROM. Edited by J. Greif, K. Scharmer. Scientific advisors: R. Dogniaux, J. K. Page. Authors: L. Wald, M. Albuisson, G. Czeplak, B. Bourges, R. Aguiar, H. Lund, A. Joukoff, U. Terzenbach, H. G. Beyer, E. P. Borisenko. Published for the Commission of the European Communities by Presses de l'Ecole, Ecole des Mines de Paris, Paris, France.

Eumetsat, 1996, Annex to the Meteosat-5 calibration report. Meteorological Products Extraction Facility (MPEF), March 1996, Published by Eumetsat, Darmstadt, Germany, 25 pp.

Evans R.H., Gordon H.R., 1994, Coastal zone color scanner "system calibration": a retrospective examination, *Journal of Geophysical Research*, **99** (4), 7293-7307.

Fontoynont M., Dumortier D., Heinemann D., Hammer A., Olseth J.A., Skarveit A., Ineichen P., Reise C., Page J., Roche L., Beyer H.G., Wald L., 1997, Satel-Light, Processing of Meteosat data for the production of high quality daylight and solar radiation data available on a World Wide Web Internet server, Mid-term progress report JOR3 - CT 95 - 0041, Project Satel-Light, for the Commission of the European Communities, Ecole Nationale des Travaux Publics de l'Etat, Vaulx-en-Velin, France.

Govaerts Y.M., 1999, Correction of the Meteosat-5 and –6 radiometer solar channel spectral response with the Meteosat-7 sensor spectral characteristics, *International Journal of Remote Sensing*, **20** (18), 3677-3682.

Govaerts Y.M., Pinty B., Verstraete M.M., Schmetz J., 1998, Exploitation of angular signatures to calibrate geostationary satellite solar channels, In proceedings of the IGARSS'98 conference, 6-10 juillet 1998, Seattle, USA, **1**, 327-329.

Grüter W., Guillard H., Möser W., Monget J.M., Palz W., Raschke E., Reinhardt R.E., Schwarzmann P., Wald L., 1986, Solar Radiation Data from Satellite Images, Solar Energy R&D in the European Community, Series F, Volume 4, D. Reidel Publishing Company, 100 p.

Hammer A., Heinemann D., Westerhellweg A., 1997a, Normalisation of Meteosat counts - an investigation basing on ocean pixels, Satel-Light project for the Commission of the European Communities. Carl von Ossietzky University, Oldenburg, Germany.

Hammer A., Degner T, Heinemann D., Westerhellweg A., 1997b, Modifications of the Heliosat method coud index improvements, detection of snow cover and results of radiative transfer calculations, Satel-Light project for the Commission of the European Communities. Carl von Ossietzky University, Oldenburg, Germany.

Hay J.E., 1981, The mesoscale distribution of solar radiation at the Earth's surface and the ability of satellites to resolve it, In Proceedings of the First Workshop on Terrestrial Solar Ressource Forecasting and on Use of Satellites for Terrestrial Solar Resource Assessment, Washington D.C., February 2-5 1981.

Hay J.E., 1984, An assessment of the mesoscale variability of solar radiation at the Earth's surface, *Solar Energy*, **32**, 425-434.

Hay J.E., Hanson K.J., 1985, Evaluating the solar resource: a review of problems resulting from temporal, spatial and angular variations, *Solar Energy*, **34**, 151-161.

Heidt F.D., Teichmann C., Büchler P., Schulze-Kegel D., 1998, Satellite-based solar radiation data go Internet, In Proceedings of the second ISES-Europe Solar Congress, EuroSun'98.

Hulme M., Conway D., Jones P.D., Jiang T., Barrow E.M., Turney C., 1995, A 1961-90 climatology for Europe for climate change modelling and impact applications, *International Journal of Climatology*, **15**, 1333-1363.

Iehlé A., Lefèvre M., Bauer O., Martinoli M., and Wald L., 1997, Meteosat: A valuable tool for agro-meteorology, Final report for the European Commission, Joint Research Centre, Ispra, Italy.

Ineichen P., Perez R., 2000, Derivation of cloud index from geostationary satellites and application to the production of solar irradiance and daylight illuminance data, *Theoretical and Applied Climatology*, **64**, 119-130.

Justus C. G., 1989, An operational procedure for calibrating and assessing the stability and accuracy of shortwave satellite sensors. Final Report of the Georgia Institute of Technology, Atlanta, Georgia, USA, November 1989, 99 pp.

Kasten F., 1996, The Linke turbidity factor based on improved values of the integral Rayleigh optical thickness. *Solar Energy*, **56**, 239-244.

Kasten F., 1990, Höhenabhängigkeit der Globalstrahlung bei wolkenlosem Himmel, communication personnelle entre Kasten F., DWD, et Zelenka A., Swiss Meteorological Institute.

Kasten F. and Young A.T., 1989, Revised optical air mass tables and approximation formula. *Applied Optics*, **28** (22), 4735-4738.

Kneizys F. X., Abreu L.W., Anderson G.P., Chetwynd J.H., Shettle E.P., Berk A., Bernstein L.S., Robertson D.C., Acharya P., Rothman L.S., Selby J.E.A., Galery W.O., Cough S.A., 1996, The MODTRAN 2 / 3 Report and LOWTRAN 7 Model. Technical report, Phillips Laboratory, Geophysics Directorate, Hanscom AFB.

Kriebel K.T., 1981, Calibration of the Meteosat visible channel by airborne measurements. *Journal of Applied Optics*, 20 (1),11-12.

Kriebel K. T., Amann V., 1993, Vicarious calibration of the Meteosat visible channel. *Journal of Atmospheric and Oceanic Technology*, 10 (2), 225-232.

Kriebel K. T., Mannstein H., Amann V., 1996, Absolute calibration of the Meteosat-5 visible channels. In Proceedings of the 1996 Meteorological Satellite Data Users' Conference, EUM P 19, Published by Eumetsat, Darmstadt, pp. 31-40.

Lefèvre M., Bauer O., Iehlé A., Wald L., 2000, An automatic method for the calibration of time-series of Meteosat images, *International Journal of Remote Sensing*, **21** (5), 1025-1045.

Meteonorm, 2000, Remund J., Kunz S., Lang R., *Meteonorm version 4.0, Global meteorological database for solar energy and applied climatology*, Part I: Review and Software, prepared by Meteotest, Bern Switzerland, Swiss Federal Office of Energy.

Maxwell E. L., 1998, Metstat - The solar radiation model used in the production of the national solar radiation data base (NSRDB), *Solar Energy*, 62(4), 263-279.

Michaud-Regas N., 1986, Mise en oeuvre et validation d'une méthode opérationnelle et automatique pour l'évaluation d'atlas solaires en Europe à l'aide de mesures satellitaires Meteosat. Thèse de Doctorat, Université Paris VII, Paris, France.

Molineaux B., Ineichen P., Delauney J.J., 1995, Direct luminous efficacy and atmospheric turbidity – improving model performance, *Solar Energy*, **55** (2), 125-137.

Moulin C., Lambert C.E., Poitou J., Dulac F., 1996, Long term (1983-1994) calibration of the Meteosat solar (VIS) channel using desert and ocean targets, *International Journal of Remote Sensing*, **17** (6), 1183-1200.

Moulin C., Schneider X., 1999, Calibration of the Meteosat-5 sensor visible channel, *International Journal of Remote Sensing*, **20** (1), 195-200.

Möser W., Raschke E., 1983, Mapping of global radiation and of cloudiness from Meteosat image data: theory and ground truth comparisons, *Meteorologische Rundschau*, **36**, 33-41.

Möser W., Raschke E., 1984, Incident solar radiation over Europe estimated from Meteosat data, *Journal of Applied Meteorology*, **23**, 166-170.

Moussu G., Diabaté L., Obrecht D., Wald L., 1989, A method for the mapping of the apparent ground brightness using visible images from geostationary satellites, *International Journal of Remote Sensing*, **10** (7), 1207-1225.

Neckel, H., and D. Labs, 1984, The solar radiation between 3300 and 12500 Å. *Solar Physics*, 90, 205-258.

Obrecht D., 1990, Météorologie solaire et images satellitaires : cartographie du rayonnement solaire, détermination de l'albédo des sols et évaluation de l'ennuagement. Thèse de Doctorat en Sciences, Université de Nice- Sophia Antipolis, France.

Pastre C., 1981, Développement d'une méthode de détermination du rayonnement solaire global à partir des données Meteosat, *La Météorologie*, VI^{e} série N°24, mars 1981.

Perez R., Seals R., Zelenka A., 1997, Comparing satellite remote sensing and ground network measurements for the production of site/time specific irradiance data, *Solar Energy*, **60**, 89-96.

Perrin de Brichambaut C., Vauge C., 1982, *Le gisement solaire : Evaluation de la ressource énergétique*, Paris: Technique et documentation (Lavoisier).

Pinker R. T. and Laszlo I., 1991. Effects of spatial sampling of satellite data on derived surface solar irradiance. *Journal of Atmospheric and Oceanic Technology*, **8**, 1, 96-107.

Raschke E., Stuhlmann R., Palz W., Steemers T.C., 1991, *Solar Radiation Atlas of Afric*a. Published for the Commission of the European Communities by A. Balkema, Rotterdam, 155 p.

Rigollier C., 2000, Vers un accès à une climatologie du rayonnement solaire : estimation de l'irradiation globale à partir d'images satellitales. Thèse de Doctorat en Sciences et Technologies de l'Information et de la Communication, Université Nice – Sophia Antipolis, France, 194 p.

Rigollier C., Bauer O., Wald L., 2000, On the clear sky model of the 4th European Solar Radiation Atlas with respect to the Heliosat method, *Solar Energy*, **68** (1), 33-48.

Rossow, W. B., Desormeaux, Y., Brest, C. L. and Walker, A. (editors), 1992, International Satellite Cloud Climatology Project (ISCCP): Radiance calibration report. WMO/TD-No. 520, WCRP-77, World Climate Research Programme, International Council of Scientific Unions (ICSU) and World Meteorological Organisation (WMO), Geneva, December 1992, 104 pp.

Schiffer, R.A. and Rossow, W.B., 1983, The International Satellite Cloud Climatology Project (ISCCP): The first project of the World Climate Research Programme. *Bulletin American Meteorological Society*, 64, 779-784.

Schiffer, R.A. and Rossow, W.B., 1985, ISCCP global radiance data set: A new resource for climate research. *Bulletin American Meteorological Society*, 66, 1498-1503.

Stuhlmann R., Rieland M., Raschke E., 1990, An improvement of the IGMK model to derive total and diffuse solar radiation at the surface from satellite data, *Journal of Applied Meteorology*, **29**, 596-603.

Supit I., 1994, Global radiation. Agriculture series, EUR 15745, European Commission, Office for Official Publications, Luxembourg, 194 p.

Tanré D., Deroo C., Duhaut P., Herman M., Morcrette J.J., Perbos J., Deschamps P.Y., 1990, Description of a computer code to simulate the satellite signal in the solar spectrum: the 5S code, *International Journal of Remote Sensing*, 11(4), 659-668.

Taylor V.R., Stowe L.L., 1984, Reflectance characteristics of uniform Earth and cloud surfaces derived from Nimbus 7 ERB, *Journal of Geophysical Research*, **89**(D4), 4987-4996.

Vermote E., Tanré D., Deuzé J.L., Herman M., Morcrette J.J., 1994, Second Simulation of the Satellite Signal in the Solar Spectrum (6S), 6S User Guide, NASA-Goddard Space Flight Center - Code 923, Greenbelt, USA.

Wald L., 1989, Some examples of the use of structure functions in the analysis of satellite images of the ocean, *Photogrammetric Engineering and Remote Sensing*, **55**, 1487-1490.

Wald L., 1990, Monitoring the decrease of Lake Chad from space. *Geocarto International*, 5, 3, 31-36.

Wald L., 1998, In-flight interband calibration of the AVHRR data by a cloud-viewing technique. In Proceedings of the EARSeL Symposium 'Future trends in remote sensing', P. Gudmansen Ed., A. A. Balkema Publ., Rotterdam, pp. 453-459.

Wald L., Wald J.-L., Moussu G., 1992, A technical note on a low-cost high-quality system for the acquisition and digital processing of images of WEFAX type provided by meteorological geostationary satellites. *International Journal of Remote Sensing*, 13, 5, 911-916.

World Meteorological Organization (WMO), 1981, Meteorological aspects of the utilization of solar radiation as an energy source. Annex: World maps of relative global radiation. Technical Note N° 172, WMO-N° 557, Geneva, Switzerland, 298 pp.

Zelenka A., Czeplak G., d'Agostino V., Josefson W., Maxwell E., Perez R., 1992, Techniques for supplementing solar radiation network data, Technical Report, International Energy Agency, # IEA-SHCP-9D-1, Swiss Meteorological Institute, Krahbuhlstrasse, 58, CH-8044 Zurich, Switzerland.

Zelenka A., Perez R., Seals R., and Renné D., 1999, Effective accuracy of satellite-derived hourly irradiances, *Theoretical and Applied Climatology*, **62**, 199-207.